SPATIOTEMPORALLY PRECISE OPTICAL STIMULATION SYSTEM FOR CONTROLLING NEURAL ACTIVITY IN-VITRO

By

PERRY THOMAS TWYFORD

A DISSERTATION PRESENTED TO THE GRADUATE SCHOOL
OF THE UNIVERSITY OF FLORIDA IN PARTIAL FULFILLMENT
OF THE REQUIREMENTS FOR THE DEGREE OF
DOCTOR OF PHILOSOPHY

UNIVERSITY OF FLORIDA

2011

To my family, Loren, Stefani, Evan, Julie, and Jack

ACKNOWLEDGMENTS

I would like to thank Dr. Tom DeMarse for his support and inspiration throughout my time at the University of Florida. I thank the other members of my committee, Dr. William Ogle, Dr. Bruce Wheeler, and Dr. Arunava Banerjee for helpful feedback. I also thank Phil Barish for virus synthesis and general help with matters of genetic engineering. I thank the members of the Wheeler lab, Eric Franca for his long hours conducting cell culture preps, Sankar Alagapan, Kucku Varghese and Liangbin Pan for insightful and spirited experimental discussions. I would also like to extend my thanks to the J. Crayton Pruitt Family and the University of Florida Alumni Foundation for their financial support of this research. Finally, I thank my family and friends, without whose support this work would not have been possible.

TABLE OF CONTENTS

page

LIST OF TABLES

LIST OF FIGURES

LIST OF ABBREVIATIONS

AP	Action Potential
CamKIIa	Calcium/calmodulin-dependent kinase II alpha
ChR2	Channelrhodopsin-2
CTS	Cross-Trial Similarity
DBS	Deep Brain Stimulation
DIV	Days In-Vitro
DLP	Digital Light Processing
DMD	Digital Micromirror Device
GFP	Green Fluorescent Protein
GUI	Graphical User Interface
Halo	Halorhodopsin
HFS	High-Frequency Stimulation
LED	Light Emitting Diode
LFP	Local Field Potentials
MEA	Micro-electrode Array
MOI	Multiplicity of Infection
PSTH	Post-stimulus Time Histogram
SVM	Support Vector Machine
YFP	Yellow Fluorescent Protein

Abstract of Dissertation Presented to the Graduate School
of the University of Florida in Partial Fulfillment of the
Requirements for the Degree of Doctor of Philosophy

SPATIOTEMPORALLY PRECISE OPTICAL STIMULATION SYSTEM FOR CONTROLLING NEURAL ACTIVITY IN-VITRO

By

Perry Thomas Twyford

December 2011

Chair: Thomas B. DeMarse
Major: Biomedical Engineering

Optogenetics is an emerging field whose core technology enables optical, rather than the more traditional electrical, neural stimulation. What has yet to be addressed is the need for optical stimulation systems that are precise both temporally and spatially. Here we demonstrate an LED and Digital Light Processing (DLP) based system in conjunction with Multi-electrode Array (MEA) technology enabling simultaneous optical stimulation and recording of neural events, absent of electrical artifact, and capable of single neuron specificity. With this system we have achieved a spatial resolution of approximately 10 micrometers with millisecond temporal precision. Using this new stimulation system in conjunction with excitatory optogenetic channels, we have characterized the system for optimal culturing, infection efficiency, and neural photostimulation parameters including duration, timing, and spatio-temporal response from MEA recordings. The technology was then employed demonstrating burst suppression via photostimulation using high-frequency stimulation, spatial modulation, and mean-field feedback. The system described in this dissertation represents the frontier of neural stimulation and will eventually become a powerful mainstream tool within the MEA field and across neuroscience in general.

CHAPTER 1
INTRODUCTION AND BACKGROUND

Micro-Electrode Arrays

A relatively new tool for investigating the electrical properties of neural cultures at the network level is the Micro-Electrode Array (MEA), which was developed in the 1970's. These small arrays of electrodes lie inside a culture well, so that neural networks can be cultured directly on top of them. An example of a common 60 electrode MEA is shown in Figure 1-1, with a neural culture. While the 60 electrode version is by far the most common version, MEAs are now available that enable 256 (MCS, Ayanda Biosystems) or 4,096 (Berdondini el al., 2001; Gandolfo et al., 2010; Imfeld et al., 2008) electrodes for extremely high-density recording schemes.

Each electrode of the MEA measures the extracellular electrical activity from 0-3 surrounding neurons. This allows a far greater number of neurons to be examined than was previously possible through other methods (Gross et al., 1997; Pine et al., 1980; Potter et al., 2001). These MEAs allow us to see network events that are not captured through single cell patch clamps, such as local field potentials (LFPs) and network-wide bursts. The result is a more complete view of the network activity than is possible through any other method.

MEAs have been used to study a wide variety of topics in the field of neuroscience, including plasticity (Bakkum et al., 2008; Chiappalone et al., 2008; Eytan et al., 2003; Jimbo et al., 1999; Kerchner et al., 2008; Madhavan et al., 2006; Tateno et al., 1999), examination of burst patterns (Raichman et al., 2007; Tabak et al., 2003; Wagenaar et al., 2006), neural development (van Pelt et al., 2005), and formation of computer models of neural networks (Massobrio et al., 2008; Mongillo et al., 2007).

While recording neural activity from MEAs has proved useful, using MEAs to stimulate activity has suffered from significant problems. For one, electrical stimuli are non-specific, activating all cell types. Secondly, the fixed electrode locations of MEAs provide low spatial resolution. Perhaps the biggest problem with electrical stimulation using MEAs has been the stimulation artifact, in which the stimulation pulse saturates the neural signal for tens of milliseconds on the stimulated electrode, and several milliseconds on other electrodes in the array. This prevents examination of high temporal precision processes of the network within these first several milliseconds. What is needed is an alternative method of stimulating activity while still allowing electrical recording.

Photostimulation

Several methods have recently been developed in the scientific community that utilize light in order to stimulate neural activity. These methods have shown many advantages over traditional electrical stimulation, and have demonstrated neural control previously unachievable. The three primary methods of photostimulation are glutamate uncaging (see Callaway et al., 2002), chemically modified ion channels (see Volgraf et al., 2006), and naturally occurring photosensitive ion channels (see Deisseroth, 2011). Photosensitive ion channels, often referred to as "optogenetics", will be the primary focus of this dissertation.

Uncaging Methods

In the uncaging method, a neurotransmitter of interest is bound to a photosensitive bioactive molecule or “cage”, typically a nitrobenzyl group, which renders the neurotransmitter inactive. Upon application of ultraviolet light, the cage undergoes a conformational shape change, releasing the molecule into the extracellular environment.

This process is illustrated in Figure 1-2. A particularly popular molecule for use in caging experiments is glutamate, one of the primary excitatory neurotransmitters in the brain. Glutamate uncaging has been used to successfully investigate a number of questions including dendritic integration (Losonczy et al., 2006; Shoham et al., 2005), and mapping neural connectivity (Pettit et al., 1999; Yoshimura et al., 2005). Uncaging methods can evoke neural activity at temporal precision on the order of tens of milliseconds with a spatial resolution of approximately 50 micrometers. Unfortunately, because caged glutamate is released quickly and does not replenish itself, this method does not support sustained trains of precisely timed spikes (Shoham et al., 2005). It also requires the addition of exogenous caged glutamate, a property which increases the difficulty of using this methodology in-vivo. Additionally, this method is difficult to use in a cell specific manner due to the fact that nearly all cell types in the brain use similar neurotransmitters, particularly glutamate. In an attempt to increase the cell specificity of glutamate uncaging, Zemelman et al. produced a neural population that expressed two different receptors, the capsaicin receptor TRPV1 and the purinergic receptor $P2X_2$, which is sensitive to ATP. Then, by releasing either capsaicin or ATP from their molecular "cages" using different wavelengths of UV light, they were able to selectively activate one cell type or the other. This increase in cell specificity, however, came at the cost of decreased temporal control (Zemelman et al., 2003).

Chemically Modified Ion Channels

Sometimes referred to as the "ball and chain" method, this technique utilizes a molecule sensitive to ultraviolet light (UV) known as Azobenzene. Upon application of UV light, Azobenzene, a molecule normally 17 angstroms long, folds in half to a length of 10 angstroms (Banghart et al., 2004). This change in conformation was capitalized

on by attaching a desired molecule to the extracellular side of a transmembrane ion channel (Volgraf et al., 2006). For example, when in its native state, an ammonium molecule attached to the Azobenzene plugs an ion channel. When UV light is applied, the Azobenzene folds and the ammonium molecule is removed, unplugging the channel and allowing ions to flow (Figure 1-3). For example, Szobota et al. engineered ionotropic glutamate receptors both in culture and then introduced the receptors into sensory neurons in zebrafish. This group was able to produce precisely timed action potentials and sustained depolarization, and successfully blocked the escape response to touch in zebrafish (Szobota et al., 2007). Fortin et al. created an optically active potassium channel by introducing a photoswitch-able affinity label (PAL) that, due to a reactive electrophile, covalently attached to potassium channels that repolarize neurons. They demonstrated sustained light control of K^+ channels in culture with no observed negative effects (Fortin et al., 2008).

Similar to the uncaging method, this method requires the addition of exogenous chemicals. Because adding exogenous chemicals increases the difficulty of this methodology, and could potentially be toxic, this method is not ideal for use in-vivo. The time course of this method varies depending on which channel is used, ranging from milliseconds (Volgraf et al., 2006) to several seconds (Fortin et al., 2008). However, the ability to genetically target modifications (e.g. Volgraf et al., 2006) provides a distinct advantage over the uncaging method.

Photosensitive Ion Channels

Recently, an alternative has emerged known as optogenetics (Nagel et al., 2003), in which specialized light activated ion channels are inserted into a neuron's cell membrane, making the cell's electrical potential sensitive to light. This promising field

has recently witnessed extensive growth, particularly in the area of neuroscience, where the use of light mediated neural activation has demonstrated control that was previously unachievable by electrical stimulation alone. The use of these channels has also gained attention as a method of achieving neural control with extremely high temporal precision, while requiring no additional chemicals to be added to the culture. Most of the naturally occurring ion channels used by this method are derived from light sensitive algae, which use the channels to help them move within a water column toward light for photosynthesis. Once a gene for a channel is introduced into a live neuron, the neuron will produce the ion channels and distribute them to the cell membrane for the remainder of the life of the cell.

History

The first light-activated rhodopsin to be discovered was the haloarchael proton pump bacteriorhodopsin, a member of the microbial opsin family including both ion pumps and channels (Oesterhelt and Stoeckenius, 1971; Oesterhelt and Stoeckenius, 1973; Racker and Stoeckenius, 1974). Type I opsins are protein products of microbial opsin genes, and are only called rhodopsins when bound to a retinal molecule. Type II mammalian opsins are a system of two proteins, one that detects light and one that modulates ion flow (Yizhar et al., 2011). Today, the term “opsin” is used collectively for either the gene or the protein itself. At the time of their discovery, it was not well understood how opsins might be used in neuroscience research. Francis Crick, co-discoverer of the double helical structure of DNA, had noted the need for a new method of neural stimulation that could differentiate between cell types (Crick, 1979). Crick even hypothesized that light could be a possible solution to this problem, but the connection was not made until decades later. Throughout the ensuing years, more

opsins were discovered with different effects, spectral responsiveness, and efficiencies. These opsins included Halorhodopsin (Matsuno-Yagi and Mukohata, 1977), and Channelrhodopsin (Nagel et al., 2003), two of the primary optogenetic tools used today. Concurrently, state of the art technologies were being applied to better understand the mechanics and kinetics of the opsins, such as the identification of the retinal-binding site in Halorhodopsin (Lanyi and Oesterhelt, 1982), the structure of the cell envelope of halobacterium (Blaurock et al., 1976), and the mechanism of halorhodopsin's suppression of activity (Schobert and Lanyi, 1982).

It was not until 2005 that an opsin was successfully introduced into mammalian neurons simultaneously by several laboratories (Boyden et al., 2005; Li et al., 2005; Nagel et al., 2005). The most widely utilized channel today is Channelrhodopsin-2 (ChR2), a light gated cation channel found in the unicellular green alga *Chlamydomonas reinhardtii*. Unlike bacteriorhodopsin, ChR2 activity depends more on channel closing kinetics than retinal isomerization (Feldbauer et al., 2009). Upon application of light, the channel undergoes a conformational change to open the channel pore, allowing an inward depolarizing current within 50 microseconds. This allows the neurons to be controlled with extremely high temporal precision (less than 5 ms jitter), as well as generate highly reproducible spike trains (greater than 98% repeatability) (Boyden et al., 2005).

More recently, *Natronomonas pharaonis* Halorhodopsin (Halo), has been used to inhibit neural activity, providing an excellent complimentary opsin to ChR2. Halo is a photosensitive chloride pump, which causes hyperpolarization of a cell's membrane to suppress a neuron's ability to generate action potentials (AP). The reason that this tool

has been so successful in conjunction with ChR2 is that ChR2 and Halo have relatively unique activation wavelengths that are over 100 nm apart, ChR2 at ~470nm and Halo at ~580 nm (Zhang et al., 2007). As a result, each opsin can be expressed in the same cell and controlled independently using two light sources of different wavelengths. Because the kinetics of both channel types exhibit extremely high temporal precision, they provide a means for unprecedented control to both actively enhance or suppress activity of single neurons or neural populations.

Basic characterization

Characterization of optogenetic channels has primarily come from single electrode in-vitro experiments, which have demonstrated speed of activation and spatial control far superior to traditional electrical stimulation methods. While the ChR2 channel was originally developed by Nagel (Nagel et al., 2003) for use in neuroscience research, many of the basic characteristics of both ChR2 and Halo were further developed by the lab of Karl Deisseroth (Boyden et al., 2005; Zhang et al., 2007). For example, Boyden et al. examined the temporal control utilizing ChR2. These experiments were conducted using a lentiviral vector containing a ChR2-YFP construct, the same construct employed within experiments in this dissertation. Using patch clamp to monitor activity, they used a blue-filtered 300 Watt xenon lamp to apply light pulses of varying duration (5-15 ms) in an attempt to determine the minimum duration capable of producing an action potential 100% of the time. The results show that a 5 ms pulse consistently produces subthreshold activity, while a 15 ms pulse will reliably produce an action potential. They examined the electrical profile of neurons during stimulation, and determined that the time to spike using optical stimulation was an average of 10 ms.

Next they applied light pulses to simulate spike trains to individual neurons to determine the repeatability of neural action potential (AP) activation. Each train consisted of 45 light pulses (15 ms duration of each pulse) whose timing was based on a Poisson distribution. First, three identical pulse series were applied to a single neuron. The trial-to-trial repeatability of each train was 98%. Next, three identical pulse series were applied to three different neurons. The pulse trains produced were nearly identical, and the jitter (a measurement of the temporal variation in spike timing) between neurons was calculated to be about 1-3 ms.

This group also investigated the reliability of neuronal activation in response to stimulating trains of light pulses when the frequency of the light pulse delivery was increased. Their results showed a significant drop in reliability between 5 and 20 Hz (from ~95 to ~25%,respectively), likely due to the refractory periods of the individual neurons. Finally, they examined the basic electrical properties of the infected neurons, including membrane resistance, resting potential, and number of spikes evoked by current injection. They found no significant difference in any of these properties between transfected and normal neurons, meaning that both the ChR2 expression and the infection process produced no detectable side effects.

The relationship between the intensity of light needed for activation and spiking has been examined by several groups. In Boyden's original report, 8-12 mW/mm^2 of blue light was sufficient to elicit spiking responses in ChR2 expressing neurons, although they did not explicitly test the lower limits of this observation (Boyden et al., 2005). However, Degenaar et al. later determined that the minimum spiking irradiance of ChR2 with 470 nm light lies between 0.1 and 1 mW/mm^2 (Degenaar et al., 2009).

The light intensity is an important design consideration when selecting a light source, in that the light power density determines the temporal characteristics of the neural response. Current efforts using genetic methods are working toward altered forms of ChR2 to produce a channel with even stronger expression and activation at lower light intensities. For example, a genetically engineered bi-stable ChR2 molecule recently developed by Berndt can be activated at intensity levels as low as 0.01 mW/mm^2 (Berndt et al., 2009).

Next, Halo channels were added in combination with ChR2 by two groups simultaneously. This technique allows the ability to selectively activate or suppress neural activity at will. For example, Zhang et al. first suppressed naturally occurring spikes by applying persistent yellow light. The intensity of the light was correlated with the amount of suppression, with maximum suppression occurring at very high intensity levels of 21.7 mW/mm^2. In a simple demonstration of dual control, action potentials caused by blue light pulses were then inhibited in the presence of yellow light (Zhang et al., 2007). Even greater neuronal control was achieved by Han et al, where complex Poisson stimulation sequences were applied that involved both activation and suppression (Han et al., 2007). While Han's group showed potent inhibitory control at power levels of 10 mW/mm^2, the lower limit of intensity was not examined.

Together, these experiments have demonstrated the potential of optogenetics for extraordinary neuronal control that is capable of activation within 10 ms, can reproduce complex spike trains at frequencies of up to 10 Hz with a reliability of over 95%, and include both excitatory and inhibitory capabilities.

Opsin targeting

Perhaps one of the most significant advantages of the optogenetic paradigm is the ability to target transfection to specific cell types (e.g., excitatory or inhibitory, pyramydal, interneuron, or cells in a particular brain area where a cell type dominates). Several methods have already been developed to accomplish this goal including lipid transfection, electroporation, transgenic animals, and viral infection.

Lipid transfection, also known as lipofection, is a technique in which a gene of interest is housed in a lipid vesicle that, because it is constructed of a lipid bilayer, can easily merge with cell membranes. While this method is common for use in culture, its use in-vivo has been hindered by poor transfection efficiency, and instability in biological fluids (Audouy and Hoekstra, 2001). It generally has few ill effects on the neural population, and is known for its ease of use and high efficiency in culture. Lipofection has been successfully used in both primary hippocampal (Degenaar et al., 2009; Mutoh et al., 2010), and cortical cultures (Akemann et al., 2010)

Electroporation is a method of using a strong electric field to alter the permeability of the cell membrane, enabling insertion of DNA directly into the cytoplasm. It is primarily used as a gene delivery technique in-utero, known as IUE (Shimogori and Ogawa, 2008). Because different cortical layers are produced at different time periods during uterine development, electroporation at a specific time point will ensure the opsin is only expressed in that particular cortical layer. This technique has been harnessed successfully by several research groups (Adesnik and Scanziani, 2010; Gradinaru et al., 2007; Petreanu et al, 2007) to introduce opsins into specific cortical layers.

Creating transgenic mouse lines that express certain opsins under local promoter-enhancer regions is a more recent development. Despite the high cost and difficulty,

this technique has been used extensively to study cortical connectivity (Wang et al., 2007), inter-region connectivity (Arenkiel et al., 2007), cortical information processing (Sohal et al., 2009), and the circuitry of Parkinson's disease (Gradinaru et al., 2009).

Wang et al. used a transgenic mouse line expressing ChR2 to study cortical connectivity. They used a small laser spot to stimulate a ChR2 expressing neuron, while simultaneously monitoring post-synaptic response in a non-ChR2 expressing neuron. By scanning the laser light spot, they were able to effectively map the synaptic connections for a single neuron in a living cortex (Wang et al., 2007).

Arenkiel et al. also used a line of transgenic mice that express ChR2-YFP broadly throughout the entire nervous system. They utilized the Thy1 promoter, which is neuron specific. These mice were then used to map the neural circuitry between the olfactory bulb and the piriform cortex (Arenkiel et al, 2007). Perhaps the greater implication is the outline of a system for precise manipulation of any neural activity in the entire intact mammalian brain using light. As the entire nervous system expresses ChR2, each part can be activated independently, with high temporal precision, and absent of electrical artifact.

Sohal et al. expressed ChR2 and Halo in parvalbumin interneurons, thought to control synchronized neural oscillations, throughout the cortex. They found that suppressing parvalbumin activity suppressed gamma oscillations throughout the cortex, whereas stimulating these interneurons drove gamma-frequency activity. Further, modulating the frequency of excitatory input was found to enhance signal to noise ratio throughout the entire neural circuit (Sohal et al., 2009).

Another group attempted to examine optogenetics as a tool in Deep Brain Stimulation (DBS), as a replacement for traditional electrical stimulation. By using different stimulation techniques, as well as targeted transgenic ChR2 expression, Gradinaru et al provided insight into the DBS mechanism, as well as the disease circuitry that caused the disease state to begin with. They found that stimulation by ChR2 reduced seizure activity, while inhibition by Halo did not prevent further seizures. Additionally, it was found that DBS targeted to the subthalamic nucleus region was effective in reducing Parkinson's symptoms, which implicates this region as very important in the disease state (Gradinaru et al, 2009). These questions about both DBS mechanism and Parkinson's disease circuitry were unable to be answered by traditional electrical means, but were easily solved using optogenetics.

The most versatile method of gene delivery, and by far the most common, is the viral vector. These viral systems have a high speed of expression, versatility throughout experimental situations, excellent efficiency and potency, and are capable of a high level of customization based on choice of vector and promoter. The two most common viral vectors are lentivirus and adeno-associated virus (AAV). Together, they have been used successfully to induce opsin expression in the brains of mice (Adamantidis et al., 2007; Ciocchi et al., 2010; Haubensak et al., 2010; Kravitz et al., 2010; Lobo et al., 2010; Petreanu et al., 2009), rats (Aravanis et al., 2007; Gradinaru et al., 2009; Lee et al., 2010), and primates (Busskamp et al., 2010; Diester et al., 2011; Han et al., 2009). Furthermore, the use of cell-type specific promoters permits expression in only a certain population of neurons. For example, using the promoter Ca^{2+}/calmodulin-dependent kinase II alpha (CaMKIIa) will target only excitatory neurons in the cortex and

hippocampus (Dittgen et al., 2004), a very useful population. Using a hGFAP promoter will target exclusively astrocytes (Brenner et al., 1994; Gourine et al., 2010; Gradinaru et al., 2009; Jakobsson et al., 2003). The fSST promoter will target inhibitory neurons (Nathanson et al., 2009). Many more promoters exist, and more work in this field will undoubtedly continue to reveal useful promoters for targeted expression.

There are two notable problems to viral expression systems. The first is that the infection method can be a rather sensitive process. Delivery of too much virus can easily cause cytotoxicity, while too little produces levels of expression too low for utility. Secondly, the small size of the viral capsid restrains the potential size of the genome to be delivered. And because the promoters themselves can be relatively large, this must be factored into the total load size. Lentivirus can hold up to 9 kilo-base pairs (kb), or the length of 9000 neucleotides (Kumar et al., 2001). Adeno-associated virus (AAV) vectors can hold even less, approximately 4.7 kb (Dong et al., 1996). Adenovirus vectors can hold more, up to 27 kb, but consistency and toxicity are constant concerns with these vectors (Soudais et al., 2004). Some promoters can be up to 5 kb in length, so care must be taken to choose the correct viral vector to safely house the genetic load of choice.

Light delivery methods

Another important decision when designing an experimental paradigm is the choice of light source. Lasers are the primary choice particularly in-vivo due to their intensity and tissue penetration depth, but there are now a number of reports using commercial LEDs (Grossman et al., 2010) and incandescent sources (Boyden et al., 2005). In cases where multiple opsins are expressed in a single cell, whose opsins have

overlapping activation spectra, it is important for any light source to have a very narrow spectral emission band so as to only activate the opsin of choice.

Lasers typically have a narrow spectral bandwidth of less than 1 nm and can be precisely tuned to almost any frequency. Additionally, they can be controlled at kilohertz frequencies for extremely fast applications. The beams typically have a very low divergence, which makes them ideal for spatially precise applications (Schoenenberger et al., 2008). Lasers can also be coupled to fiberoptic cables for deep stimulation of brain tissue (Adamantidis et al., 2007; Aravanis et al., 2007), but are costly to build.

Light emitting diodes, or LEDs, are an attractive alternative because of their low cost, ease of use, and reliability, and typically have spectral width in the 10s of nanometers. While LEDs generally produce a substantial amount of heat, an important factor when considering in-vivo experiments, they have been used successfully in-vitro (Adesnik and Scanziani et al., 2010; Campagnola et al., 2008; Gradinaru et al., 2007; Ishizuka et al., 2006; Petreanu et al., 2007; Wen et al., 2010), and, coupled to fiberoptics, in-vivo (Gradinaru et al., 2007; Iwai et al., 2011; Petreanu et al., 2007). Because LEDs typically have a wide angle of divergence, spatial precision can be added by passing LED output through a lens (Grossman et al., 2010) or using a digital light processing device (Arrenberg et al., 2010; Farah et al., 2007; Wang et al., 2007a). These experiments are discussed in more detail in the Structured Light Application and DLP sections.

Incandescent light sources, also known as arc lamps, are attractive due to their high power and fast pulse modulation via a shutter (Boyden et al., 2005). These lamps

output white light, which can be controlled by applying a narrowband spectral band-pass filter to produce the desired wavelength. This provides spectral control that is unmatched in other light sources but difficult to switch rapidly between multiple spectral bands. Additionally, a graded filter can be added to control light intensity.

Other in-vivo work

The first use of optogenetics in-vivo was conducted by Aravanis et al. ChR2 was delivered to excitatory neurons within a rat motor cortex using a viral vector with a CamKIIa promoter. A cannula guide was then targeted to the light sensitive area, and a fiberoptic was inserted and coupled to a 20mW solid-state laser diode. They were able to drive excitatory activity and observe direct behavioral correlations in the motor output of the rodents (Aravanis et al, 2007).

Adamantis et al. infected specific cells within the lateral hypothalamus, hypocretin-producing neurons, with ChR2. Hypocretin has been shown to stabilize the awake state, and loss of hypocretin function has been implicated in narcolepsy. Then the hypothalamus was optically stimulated using an optical fiber at different frequencies. They found that stimulation at 5-30 Hz reduced time taken to transition from sleep to wake, but stimulation at 1Hz did not (Adamantis et al, 2007). This direct relationship between optical stimulation frequency and specific mammalian behavior demonstrates the viability of optogenetic techniques in the mammalian brain to modulate brain function and behavior.

Two groups have developed systems that track freely-moving worms, estimate the spatial location of neurons expressing optogenetic channels, and can stimulate activity from a distance, using either laser light through a Digital Micromirror Device (DMD) (Leifer et al., 2011) or an off-the-shelf liquid crystal display (Stirman et al., 2011). While

impressive, these techniques may not translate to mammals in that a skull and thicker skin would inhibit light transmission to the brain.

While most in-vivo stimulation techniques rely on fiberoptics for stimulation as well as an electrode array for recording, technologies that combine these two methods have begun to emerge. Zhang et al. developed an “optrode”, a tapered fiberoptic that forms an electrical seal with a cell, allowing it to essentially record electrical activity from the cell that it is stimulating in a manner similar to patch clamp (Zhang et al., 2009). Neuronexus (Ann Arbor, Michigan) has begun commercial production of optoelectrodes, a series of implantable devices that merge fiberoptics with recording electrode arrays.

Advantages over electrical stimulation

The use of naturally occurring photosensitive ion channels expressed in neural cultures for light mediated neural control provides a variety of advantages over traditional electrical stimulation. Unlike many other photostimulation techniques, the use of ChR2/Halo requires no exogenous chemicals to be added to the neural population, reducing the risk of problems or side effects, especially when used in-vivo. For this reason, opsins are often referred to as being “single-component tools” (Yizhar et al., 2011). Many naturally occurring photosensitive ion channels require the cofactor all-*trans* retinal to function. Indeed, the fear that this cofactor would need to be added to brain tissue in order for the opsins to function had prevented their development for some time (Yizhar et al., 2011). While retinoids are known to exist in mammalian tissues, it was unclear if there were sufficient quantities to allow for full opsin functionality. It has since been shown that levels of all-*trans* retinal are indeed sufficient in mature mammalian brains (Deisseroth et al., 2006, Zhang et al., 2006) and across all vertebrate tissues that have been examined (Douglass et al., 2008, Yizhar et al., 2011).

Additionally, primary neural cell cultures, used in the following dissertation, also produce sufficient all-*trans* retinal to allow optogenetic function without further addition of this chemical (Zhang et al, 2007).

Another advantage of optogenetics is the increased specificity over electrical stimulation. Using lasers, LEDs, optical focusing techniques, or other methods, we can apply light to the network in a variety of different ways. Specifically, by using focused light we can activate a very small region of cells, or change the focus to activate a larger region. It allows more freedom to activate specific neurons than with traditional electrical activation. For example, Schoenenberger et al demonstrated this specificity using a focused laser to activate single cells (Schoenenberger et al., 2008). To create multiple patterns of light simulation, a structured light method is needed, discussed further in the Structured Light Application section.

The use of these photosensitive molecules permits unprecedented cell specificity afforded by the use of a genetic delivery method. Usually a virus is used to deliver the ChR2 or Halo gene, and the gene can be expressed using a variety of promoters that will genetically target particular cells types. This quality has proven exceedingly useful for translational research into in-vivo platforms. For example, different disease states are often attributed to unusual electrical activity in specific areas of the brain, and stimulating these areas electrically has shown promise in restoring normal function. Khosravani et al. demonstrated that brief, low frequency (0.5 Hz) electric stimulations to the mossy fibers in the hippocampal region (often associated with temporal lobe epilespy) resulted in a stabilization of neural activity in the hippocampus (Khosravani et al., 2003). Similarly, high frequency stimulation (130 Hz) to the sub-thalamic nucleus

can also have antiepileptic effects (Benabid et al., 2002; Vercueil et al., 1998). While there are many different stimulation paradigms to address different types of epilepsies, nearly all of them suffer from lack of specificity. Because electrical stimulation activates all cell types within a certain radius, and current from these stimulations can travel in complex and sometimes undesirable pathways, it can often stimulate regions of the brain other than the area of interest, resulting in unwanted side effects. In contrast, it has been shown that viral vectors can be delivered stereotactically into discrete brain regions (Aravanis et al, 2007; Cetin et al, 2006; Zhang et al, 2007) and particular cell-types can be targeted by the choice of promoter (Chhatwal et al, 2007; van den Pol et al, 2004). With the increase in specificity afforded by these tools, it may be possible to increase the effectiveness, and potentially decrease the side effects, of brain stimulation therapies, including anti-epilepsy therapies. For example, Tønnesen et al expressed Halo in hippocampal excitatory cells and prevented epileptiform activity from occurring within these populations during optical stimulation (Tønnesen et al., 2009).

The use of light activated stimulation does provide us with a unique solution to a problem that occurs when a recording electrode is used for stimulation: the stimulation artifact. The recording electrode is the basic tool of neural acquisition, but to examine neural networks beyond native activity we often wish to stimulate activity. Currently, the primary way to do this is through the recording electrodes. The result is a devastating artifact that lasts 10 ms or longer on the stimulating electrode, and 1 ms on all other electrodes in the area. By stimulating the neurons with light, we can avoid this artifact and for the first time examine the first 10 ms of the recording. Due to the high speed

with which neurons communicate with one another, it is likely that the precise spike timing during this first 10 ms holds important information.

Disadvantages

A primary disadvantage of optogenetic tools is the need to insert the optogenetic channels into the neural membrane. Although this can be done in a number of ways, described in detail above, a method of producing 100% cell transfection with no side effects has yet to be found. This may represent a considerable hurdle as this technology is translated into the clinical setting, where the need for safety and stability is paramount. There are, however, several viral gene delivery methods currently in the late stages of clinical testing (Kaplitt 2007).

Another disadvantage of optogenetic methods in an in-vitro platform is the need to maintain infected cultures in a dark environment to avoid continuous stimulation and probable excitotoxicity. There has been little research on the effect of chronic stimulation of neural cultures over the course of their life (see Brewer et al., 2009), but persistent light activation should be avoided in order to keep the development of the cultures as similar to controls as possible.

A potential issue is the effects of heating of neural populations from the light source. This is particularly of interest for in-vivo experiments, where surrounding tissue often receives 100 times more light intensity than is required at the target site (Aravanis et al., 2007; Gradinaru et al., 2010). Again, this issue may become obsolete in the near future as more sensitive opsins require lower light power densities, decreasing risk of damage to the tissue.

It has been suggested that light activation using certain lighting methods (eg laser) can produce a steady stimulation artifact, likely produced by the thermal heating of

metal electrodes (Ayling et al., 2009; Cardin et al., 2010). These artifacts affect local field potentials (LFP) more often than unit recordings, and can be easily removed using a band-pass filter.

Other initial disadvantages, including inadequate control speed (Boyden et al., 2005; Gunaydin et al., 2010) and viral toxicity (Gradinaru et al., 2008; Gradinaru et al., 2010; Zhao et al., 2008) have since been solved using genetic engineering of the channels or modified channel insertion techniques.

Future of Optogenetics

New naturally occurring photo-responsive ion channels are constantly being discovered. Recently a new inhibitory proton pump archaerhodopsin-3 (Arch) was discovered that outperforms Halo in speed of activation, photocurrents produced, and recovery time (Chow et al., 2010). Further investigation will likely reveal ever more effective tools of photostimulation among the large diversity of naturally occurring microbial opsin genes.

Because optogenetics is such a new area of study, we are still beginning to understand the full potential of the field. One area being explored is the use of genetic engineering techniques to alter how these channels express and function. In one instance, ChR2 was modified at the molecular level by substituting mammalian codons for algal codons to achieve higher expression in mammals. This new ChR2 is called humanized-ChR2 or hChR2 (Adamantis et al., 2007; Aravanis et al., 2007; Zhang et al., 2006). In this particular case, the increase in expression and current density came at the expense of slower channel closing kinetics and thus temporal precision (Gradinaru et al., 2007). Modifying the glutamate residue 123 of ChR2 resulted in a 2.5x increase in channel closure speed, but caused a decrease in photocurrent magnitude (Gunaydin

et al., 2010). Two groups independently created a bi-stable Channelrhodopsin by making a single modification of ChR2 at the C128 position that had multiple functional effects. It extended the lifetime of the open state of the channel, and made it responsive to light at orders of magnitude lower intensity than normal ChR2, due to enhanced kinetic stability (Bamann et al., 2010; Berndt et al, 2009). It is clear that while the channels can be enhanced using genetic engineering techniques, care must be taken to assure that negative side effects are minimized. Regardless, this field is sure to provide researchers with new and improved optogenetic tools for the foreseeable future.

Much like ChR2, Halo has also been the focus of molecular modifications. Gradinaru et al. have taken significant steps in improving the Halo channel, dubbing the new version eNpHr3.0, or Halo3.0. They have altered the genetic code of the channels to cause increased membrane trafficking in the neural processes, instead of primarily being expressed in the soma. This new channel has photocurrents nearly 20 times those of Halo, allowing stimulation using far-red and even infra-red light (Gradinaru et al., 2010). This is beneficial because red light can penetrate biological tissue much more easily than other wavelengths, allowing increased photostimulation depth through brain tissue. This new channel has already been used in multiple studies, with excellent results (Tye et al., 2011; Witten et al., 2010).

Among other uses, these optogenetic techniques have the potential to improve therapies for any disease currently treated by deep brain stimulation (DBS). These include Parkinson's disease, depression, obsessive-compulsive disorder, chronic pain, and epilepsy. By increasing specificity, treatments for these and other disorders can

become more effective with fewer side-effects. Current optogenetic applications of DBS include depression (Covington et al., 2010), respiration (Alilain et al., 2008), epilepsy (Tønnesen et al., 2009), Parkinson's disease (Kravitz et al., 2010), addiction (Witten et al., 2010), and anxiety (Tye et al., 2011).

Outside of neuroscience, optogenetics has been employed for the study of a wide variety of fields, including cardiac function (Arrenberg et al., 2010; Bruegmann et al., 2010), muscle tissue control (Stirman et al., 2011), and stem cell differentiation (Stroh et al., 2010; Tønnesen et al., 2011; Weick et al., 2010).

Previous Work

This section will focus on previous work that has been done utilizing the tools used within this dissertation, including MEAs and structured light application.

Optogenetics on MEAs

Optogenetics is being studied widely in retina due to its potential to aid in retinal degeneration, either as a therapy or as part of a retinal implant system. Current retinal implant technology (see Zrenner, 2002) uses a grid of electrodes surgically implanted to the back of the retina. A camera then records an image, which is processed into electrical stimulations, and applied to an array of electrodes over the retina to simulate natural photo excitation. Problems with current generations of this technology include constraints on electrode density, image processing speed, and the need for surgical intervention. With an optogenetic retinal prosthesis, an intact retina could be infected with ChR2 and Halo, requiring a single injection. No other surgical intervention would be necessary. Then a simple image could be projected onto the eye, which would be capable of extremely high spatial resolution. This makes optogenetics extremely interesting to researchers of the retina and retinal prosthetics.

In 2006, Bi et al. infected ChR2 into mouse retina that had suffered from photoreceptor degeneration, and examined restored functionality using an MEA (Bi et al., 2006). When light was applied to the retinal slices, they observed robust activity across a large number of electrodes that was precisely time-locked with light application, and graded based on light intensity. In 2009, the same group performed a similar experiment but now infected retinas with both ChR2 and Halo (Zhang et al., 2009a) demonstrating complete silencing of endogenously active neurons with the application of 580nm yellow light. Both experiments were performed with gross light application with a 750 watt xenon lamp projected through a fiberoptic cable onto the entire array.

In 2010, Busskamp et al. attempted to restore light sensitivity to retina suffering from retinitis pigmentosa. In retinitis pigmentosa, the light sensitive rods of the eye degenerate first, leaving only the light-insensitive cones. By conferring light sensitivity on these remaining cones, it may be possible to give some basic vision to sufferers of this disease. Using Halo-expressing cones in ex-vivo human retina, the group was able to effectively restore light sensitivity. They showed an increase in cone induced current stronger than that seen in wild type rods or cones. Additionally, they infected the retina of live mice with induced retinitis pigmentosa and showed a restoration of light sensitivity, as proven by the performing of a simple task. The mice were placed in a box with a light compartment and a dark compartment. As the intensity of light in the light compartment was increased, mice expressing Halo spent significantly less time there, compared to those with induced retinitis pigmentosa, suggesting restoration of light sensitivity (Busskamp et al., 2010). This work demonstrates that optogenetics can be

used to restore light sensitivity in retina with certain types of degeneration, and an effective prosthetic interface may someday be able to restore color sensitivity, and perhaps full vision.

Structured Light Application

Various techniques have been proposed in order to achieve spatial precision for light application. These methods include arrays of LEDs (Grossman et al., 2010), two photon excitation (Andrasfalvy et al., 2010; Papagiakoumou et al., 2010; Rickgauer and Tank, 2009), lasers (Schoenenberger et al., 2008) and DLP devices (Arrenberg et al., 2010; Farah et al., 2007; Golan et al., 2009; Wang et al., 2007a)

A significant step toward spatial control of light application was taken by Grossman et al. with their construction of a micro-LED array (Grossman et al., 2010). An array of 64x64 blue micro-LEDs (20 micron diameter) was projected onto a neural culture using projection optics that allowed control of the LED spot size. The 1:1 configuration gave a spot size of about 30 micron diameter, while the 10:1 configuration gave a spot size of about 3 micron diameter. Each LED could be individually addressed, and the entire array could be shifted to align a certain LED with a particular neuron of interest. While providing great control, there are several drawbacks to this system. First is that the LEDs are single color, which would prevent multicolor optical excitation and inhibition. Another problem is the total size of the array. In the 1:1 configuration, the projected array covers an area of 3x3mm, but in the 10:1 configuration the area is only 0.3x0.3mm, a small portion of the total MEA area.

Digital Light Processing (DLP)

While the LED array discussed above represented significant progress toward a spatially precise light application system, the system had significant drawbacks that

would be difficult to overcome. Some of these drawbacks of the micro-LED array could be addressed with the use of a projector based on digital light processing (DLP) technology. A DLP is a system in which light is projected onto a set of digital micromirror devices (DMD), essentially an array of mirrors. Each mirror is digital, that is it can either be in the on or off position, as illustrated in Figure 1-5. If the mirror is on, it reflects the light onto the image. If the mirror is off, it reflects the light onto a collector, so that a pixel appears black. By cycling through red, green and blue light, the colors appear to mix on different pixels creating a complex color image with a high resolution. This technology is typically used in televisions and projectors.

Wang et al. constructed a system which projected the output of a DMD onto a neural culture containing light-activated ionotropic glutamate receptors (Wang et al., 2007a). They then used calcium imaging and a CCD camera to record where activity was occurring. They were able to evoke activity in areas stimulated by light, but their characterization of resolution was poor due to the nature of activating neural cultures via glutamate receptor channels. They simply said that they achieved a spatial resolution "at the micron scale", however a simple calculation shows that if they projected the entire DMD device of 800,000 mirrors onto the face of an MEA (1.4x1.4 mm), they could achieve a pixel size of approximately 1.56x1.56 micrometers. This is an extremely high resolution, and would allow precise control of the entire neural culture, as a neural soma is generally 10-30 microns in diameter and neural processes are roughly 1 micron wide.

Another group used a DMD-based device to control release of caged glutamate in cortical slices, using patch clamp to examine induced activity (Jerome et al., 2011). Because caged glutamate requires relatively high levels of light to be activated, they

could not use a commercially available DLP projector, but rather created their own using a commercial DMD device in conjunction with a UV laser. This greatly reduces the reproducibility of the system, and is a significant drawback. Still, they were able to achieve a pixel size of 2.7 μm^2 with 780,000 pixels, excellent resolution coupled with over 13 kHz speed.

Farah et al. also used a DLP device to stimulate retinal ganglion cells using both caged glutamate and ChR2 methods. They claim they were able to achieve resolution of 5 micrometers (Farah et al., 2007). The same group later abandoned DLP for a liquid crystal on silicon (LCoS) stimulation system. They constructed an efficient system as well as an impressive graphical user interface (Golan et al., 2009).

Arrenberg et al. used a simple DLP device to stimulate different areas of a zebrafish heart that had been genetically encoded with ChR2 and Halo in an attempt to locate and control cardiac pacemaker cells. They used the precision of this system to determine the exact size and number of cardiac pacemaker cells, something that could not be done using electrical stimulation (Arrenberg et al., 2010).

While several groups have utilized DLP systems in conjunction with optogenetics, none to date have applied DLP, MEA, and optogenetics to neural culture. This is rather surprising as this combination would significantly expand the capabilities of the MEA system and open new avenues for investigation previously impossible using standard electrical stimulation.

Objective

Optical stimulation via optogenetics in conjunction with MEAs will provide precise spatial control over single neurons or groups of neurons, as well as allowing recording directly after stimulation due to the absence of the stimulation artifact. Before this can

be accomplished, we must first demonstrate basic feasibility of inducing and expressing ChR2 and Halo mediated neural control in this system. We will then construct a light application system using a DLP with the spatiotemporal precision to fully exploit the possibilities of optogenetics.

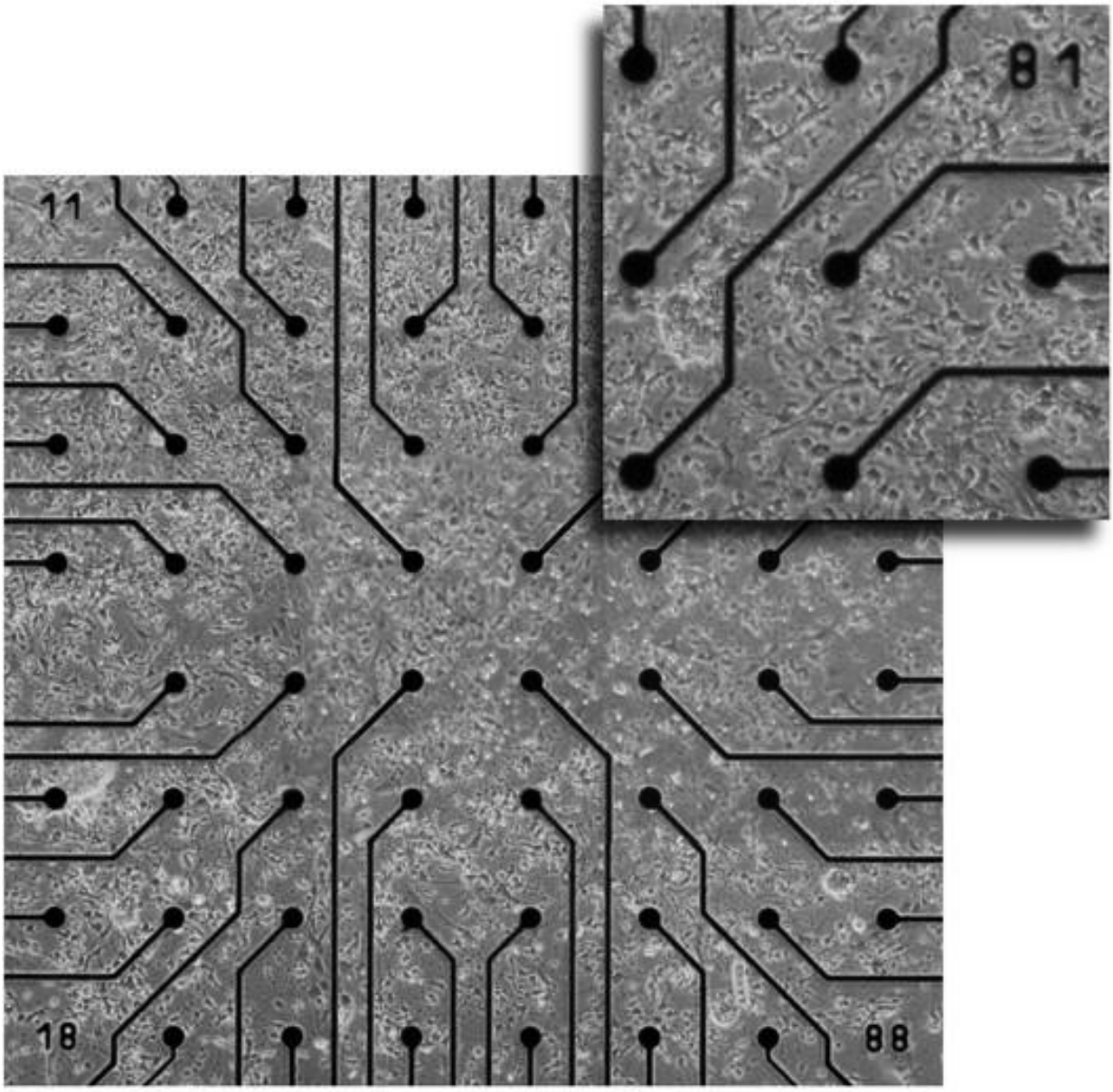

Figure 1-1. Multi-electrode Array (MEA). Microscopic image of a 60 electrode MEA and magnified portion of the array illustrating the network growth of E18 rat cortical neurons at 9 days in-vitro (DIV). Each 30µm diameter electrode is spaced 200 µm apart and can detect or stimulate neural activity (action potentials) from nearby neurons.

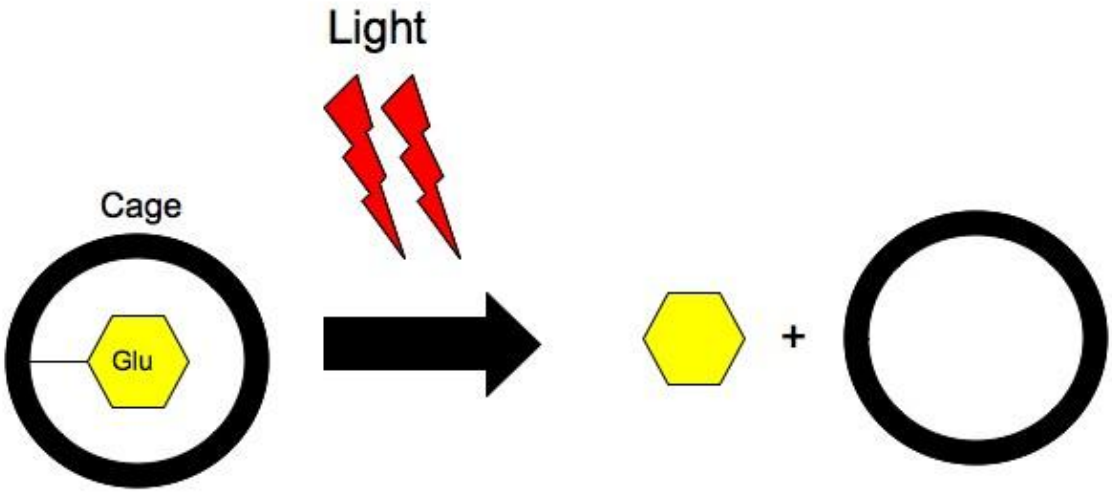

Figure 1-2. Glutamate uncaging. A glutamate molecule is bound to a light sensitive nitrobenzyl cage, which renders it inactive. Upon application of UV light, the cage changes conformation, releasing the glutamate to stimulate neural activity.

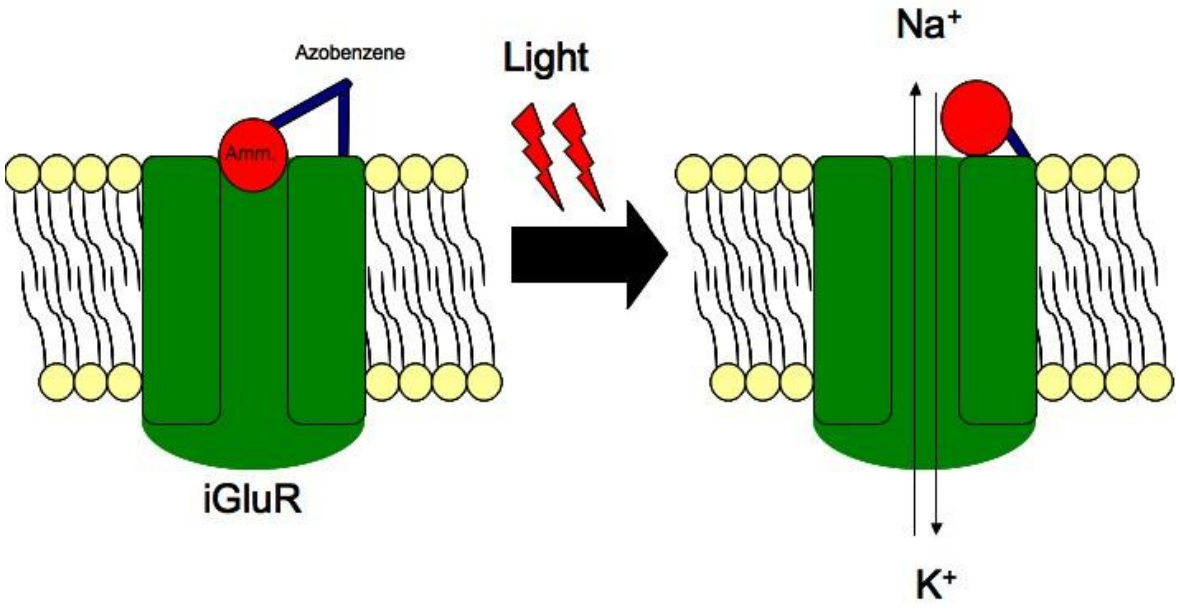

Figure 1-3. The “Ball-and-Chain” method. An ammonium molecule blocks an ionotropic glutamate receptor, and is held in place by a photoactive molecule, azobenzene. When light is applied, the azobenzene folds in half removing the ammonium from the channel pore and allowing ions to flow, causing depolarization.

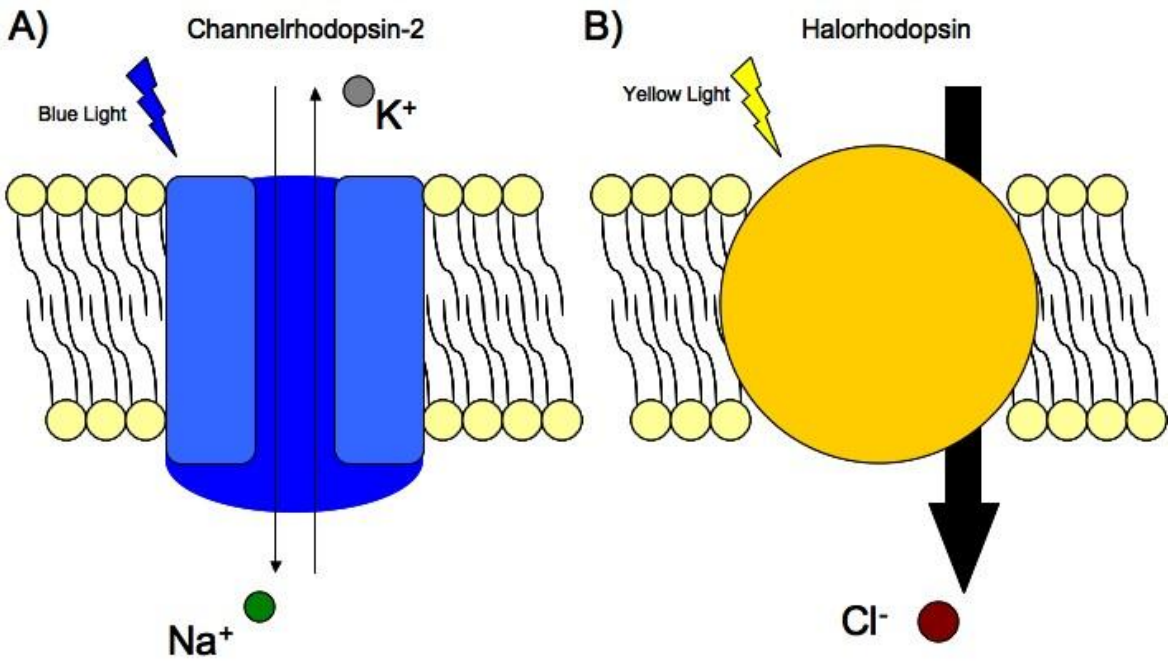

Figure 1-4. Naturally occurring photosensitive ion channels. A) Channelrhodopsin-2 (ChR2) is an excitatory cation channel. When exposed to blue light, the channel rapidly opens and causes cell depolarization. B) Halorhodopsin (Halo) is a yellow-light sensitive chloride pump, causing strong and sustained hyperpolarization.

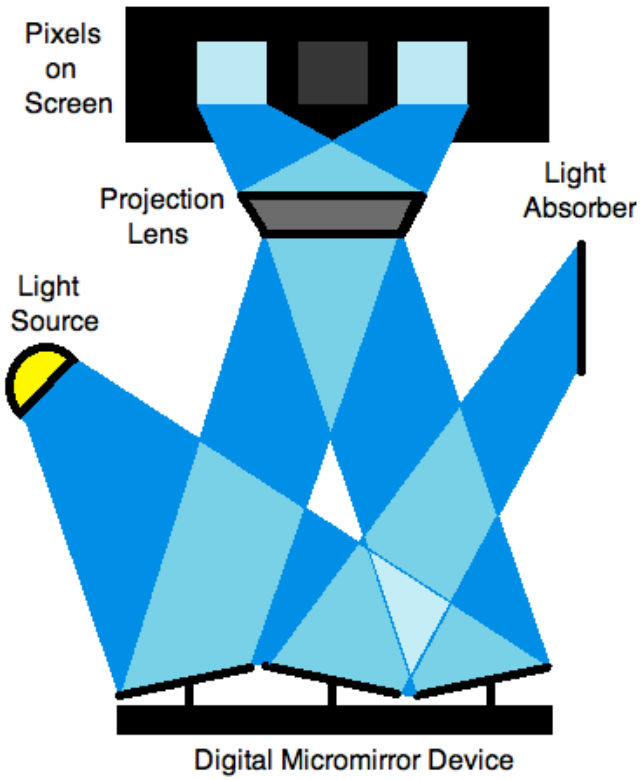

Figure 1-5. Digital Light Processing (DLP) Theory of operation. Light is projected from a light source onto an array of Digital Micromirrors, each of which is either in the 'On' or the 'Off' position. When off, the mirror deflects the light into an absorber. When on, the mirror reflects the light through a lens and into a pixel on the created image. By using a color wheel or separate colored LEDs, multiple colors can be created in a complex, high-resolution image.

CHAPTER 2
EXPERIMENTAL METHODS

Neural Cultures

Cell Culture

Embryonic rat cortical hemispheres obtained from Brain Bits at 18 days of gestation (E18), and were dissociated by enzymatic digestion with papain and mechanical trituration to produce a suspension of neurons and glia (Potter et al., 2001). These cells were randomly seeded onto the surface of an MEA composed of an 8x8 grid of 60 electrodes (Multichannel Systems, Reutlingen Germany). The surface of each MEA was pre-treated with 0.01% polyethylene-imine (PEI) (Sigma- cat #9002-98-6) and laminin (Sigma- cat #114956-81-9) to promote cell adhesion and growth in a uniform monolayer. Twenty micro-liters of the neuron/glial suspension was then added to the center of the array, containing an approximately 60,000 cells, producing a typical cell density of approximately 9,000 cells/ mm^2. An additional 1 ml of culture media was then added consisting of 90% Dulbecco's modified Eagle's medium (DMEM) (Gibco cat# 10569-010) supplemented with 10% Equine Serum (Hyclone cat# SH30074.03). The culture was rinsed once the following day with media and media replaced. Cultures were stored in an incubator at 37˚C and 5% CO_2, and covered with Fluorinated ethylene propylene (FEP) membrane lids to eliminate infection and reduce changes in osmolarity (Potter et al., 2001). Media was exchanged once per week.

Viral Infection

Twenty-four hours after plating, a lentiviral suspension with a Channelrhodopsin-2 – YFP Fusion (ChR2) was added as a bolus to each culture. The Yellow fluorescent protein (YFP) allows visualization and identification of infected cells, and thus cells

expressing ChR2. Viral concentration produced a multiplicity of infection (MOI) of approximately 5000 viral particles per neuron. Cultures were rinsed and media was exchanged 24 hours after infection. Cells that expressed the opsin would begin to fluoresce approximately 3 days after infection, and fluorescence increased until about 10 days in culture. Cultures expressing ChR2/YFP are shown at 14 DIV (days in vitro) in Figure 2-1 through Figure 2-3. Cultures were typically responsive to light within 7 days after infection, provided that the culture was old enough to exhibit endogenous activity. Infection efficiency for the cultures used in these experiments was visually estimated at about 90% by comparing bright-field cell counts with fluorescent cell counts.

Natural Activity

The spontaneous activity of the cultures was examined regularly during development, to ensure that the infection procedure did not produce any adverse effects on normal activity. The electrical activity of neurons in a network differs considerably from that of a single neuron, namely by the exhibition of bursting. Bursting is an extended period of network-wide, synchronized activity that typically lasts for several hundred milliseconds (Gross et al., 1999; Kamioka et al., 1996). Our cultures developed normally, beginning with very little asynchronous activity starting around 3 DIV. This lead into extended periods of bursting that lasted several seconds, known as “superbursts” (Wagenaar et al., 2006) followed by long periods of quiescence. Superbursts generally occur starting at 7-11 DIV, and can continue up to 30 DIV. After 30 DIV, bursts shorten to a few hundred milliseconds, becoming more frequent and representing the mature and stable state of the network (van Pelt et al., 2004). Raster plots of these different activity stages are shown in Figure 2-4. Unless otherwise

indicated, the majority of the following experiments were conducted at 30DIV with burst durations ranging from 130 to 250 ms (mean= 175 ± 52 ms) and inter-burst interval ranging from 5 to 14 seconds (mean= 9.00 ± 4.15 s). Spike rates ranged from 3.86 to 8.2 spikes per channel per second (mean = 6.25 ± 1.89).

Experimental Setup

Recording Suite

An MEA1060 system (MCS, Multi Channel Systems) was used to record neural activity (sampling rate 25 kHz, bandwith 300-10kHz). Real-time examination of electrical activity was made possible by internally developed software (T. DeMarse) built on the Open Source MEABench suite. Putative action potentials (spikes) were detected using a threshold detector set at 5 times the standard deviation of estimated electrode noise and the SUMMUX method was used to detect spontaneous burst events (Wagenaar et al., 2005). Experiments were conducted in custom temperature and CO_2 controlled environment to match conditions in the incubator. The chamber was also darkened to prevent interference from ambient light.

Bath Light Application

For bath light experiments described in Chapter 3, cortical cultures expressing ChR2 were stimulated using a blue high-power LED (λ =470 nm, 15mW) (CREE #C503B-BAS-CY0C0461) placed 1cm from the bottom of the MEA producing an illuminated area with a 5 mm radius. This corresponds to a light power density of 0.19 mW mm^{-2} measured with a Newport 1936-C Optical power meter. This is toward the lower limit of the reported minimum spiking irradiance for ChR2 of 0.1 to 1 mW mm^{-2} (Degenaar et al., 2009). The LED was controlled with a MultiChannel Systems STG1008 8-channel stimulator, a programmable stimulus generator that produces

square wave pulses whose duration, amplitude, and current or voltage can be precisely controlled. The warm-up time of LEDs is on the order of nanoseconds (Benavides and Webb, 2005), and was considered negligible for these experiments.

Control cultures on MEAs were also created that were not infected with ChR2 and stimulated with blue light, or cultures that were infected with ChR2 and stimulated with amber LED illumination under identical parameters. Neither illumination produced any evidence of photoactivation of neural activity.

DLP Light Application

The specifics of the DLP system are discussed in detail in Chapter 4.

Data Analysis

This section describes common metrics and data analysis techniques used in the following chapters. All data analysis was performed on either raw data (sampled at 25 kHz and band-pass filtered at 300-10000 Hz to remove LFPs) or spike files, a file of spike objects containing information about each individual spike, such as time, channel, and context. Spikes were determined by a threshold detector set at 5 times standard deviation. This data was then loaded and analyzed in Matlab V.7 (The MathWorks, Inc). General metrics are described below.

Spike rate

There are a number of methods that can be used to estimate the rate of neural activity. Perhaps the simplest is to divide the total number of spikes by the duration of the recording. However, this method may be inaccurate when comparing across cultures due to differences in the number of active electrodes. The solution is to calculate the rate of firing on active electrodes and take the average rate across electrodes. These rates, however, can be problematic when natural activity in culture

consists of a small number of short intense bursts followed periods of quiescence. An alternative is to divide each channels spike train into small bins (e.g., 5 ms), counting the number of times a spike occurred and dividing by bin duration to obtain an instantaneous rate over time.

Bursts

Burst detection consisted of found local maxima in the spike count histogram over all active channels. These maxima were then visually inspected and a culture-unique threshold was set. For maxima that were over the threshold (designated bursts), burst start and stop times were determined as the time when spike count crossed 5% of the maximum. Burst stats, such as duration and inter-burst-interval, were calculated using these start and stop times.

Input-Output Separability

The separation or discriminability of outputs (multichannel evoked patterns of activity) based on inputs (e.g. different stimulus locations, durations, etc.) was quantified using a support vector machine (SVM) classifier (Cortes and Vapnik, 1995). SVM finds a linear separating hyperplane with maximized margins in the hyperdimensional space. The classifier is trained from exemplars from the data set paired with the correct classification. A subset of the data is then tested (classified) and compared to the correct identities of the test set to determine correct classification performance. Higher separability among outputs would result in a higher percentage of correct classification.

Consider a study in which the array is sequentially stimulated at 5 different electrodes, repeated 10 times. Each stimulus evokes spikes that create a spatial (by electrode) and temporal response that can be classified. Spike times produced from each stimulus is binned over a window and combined for each channel to form a vector

that represents the features to be classified. This step is then repeated for each stimulus to form a matrix that can be used for training and testing SVM.

Cross-Trial Similarity

Cross-trial similarity (CTS) (Jimbo et al., 2000) is a metric that measures the similarity of electrical responses within a trial population. That is, if a culture is stimulated in a specific manner 10 times, CTS measures the similarity between those responses. This helps us quantify the reliability of response. First we must calculate the similarity coefficient (SC), shown in Eq. 2-1. The SC measures the degree to which two spatial electrical responses (P_1 and P_2) share the same active sites.

$$SC(P_1, P_2) = \frac{\mu(P_1 \bigcap P_2)}{\mu(P_1 \bigcup P_2)} \tag{2-1}$$

where the numerator is the number of sites active in both patterns and the denominator is the number of sites active in either pattern. We can then find the mean value of this similarity coefficient between different trials to determine the CTS, shown in Eq. 2-2.

$$CTS(t, t+\Delta t) = \frac{1}{S}\sum_{s=1}^{S}\left\{\frac{1}{R(R-1)/2} X \sum_{h=1}^{R}\sum_{k=h+1}^{R} SC[P_h^s(t, t+\Delta t), P_k^s(t, t+\Delta t)]\right\} \tag{2-2}$$

where $(t + \Delta t)$ represents the shifting time window, P is the spatiotemporal electrical pattern, R is the total number of repetitions, h and k are the repetition counts of the stimulation s, and S is the total number of stimulations.

Plots

Several plots are commonly used within this dissertation, and will be explained here. A raster plot is a common way to visualize multichannel spike activity across the entire array. Time is displayed along the x-axis and the electrodes are displayed along the y-axis. Each spike that is detected is represented as a black dot or vertical line on

the plot. Raster plots are useful to quickly display the network pattern of activity, or changes in these patterns over time. For example, periods of network wide bursts appear as semi-synchronous vertically aligned strips of points, whereas asynchronous activity occurring outside of bursts appear as randomly placed black dots throughout the plot. Shown in Figure 2-4 are raster plots of neural activity during various stages of maturity, consisting of asynchronous activity (A), mature bursting (B), and superbursting (C).

Another commonly used plot is the post-stimulus time histogram (PSTH). This is a method to examine the evoked response of a culture to stimuli. Neural activity is recorded for an interval after either electrical or optical stimulation. Spike data is then temporally binned into a histogram for each channel and displayed as separate plots representing each electrode, or combined across channels to portray the overall response. These histograms can then be displayed as simple line plots or converted to heatmaps. In general, a PSTH shows a fast onset of activity in response to stimulation, a peak where firing rate is maximal, followed by a gradual decay and then inactivity. Examination on a channel-by-channel basis shows the difference in activity levels in different areas of the array and identification of noisy or inactive channels. The spatial emphasis of this plot provides a useful method for this project, where spatial precision is a goal.

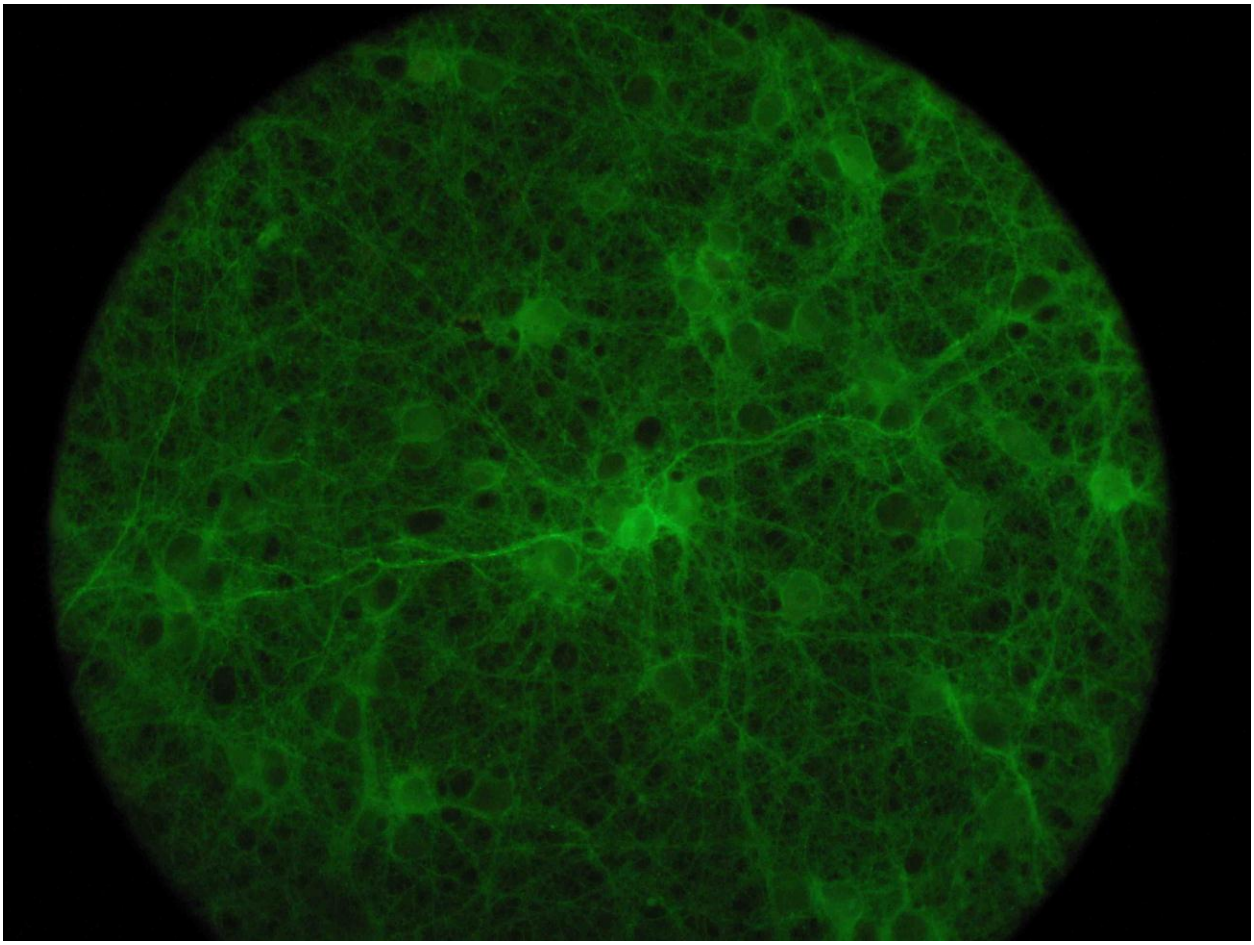

Figure 2-1. 40x image of ChR2 expressing neurons. Cultures were infected with a lentiviral Channelrhodopsin-2 – YFP Fusion (ChR2) and CamKII promoter that selectively targets excitatory neurons. Each cell fluoresces in areas of the cell where ChR2 is present. While ChR2 expression is substantial in neural soma, it is also visible in the neural processes.

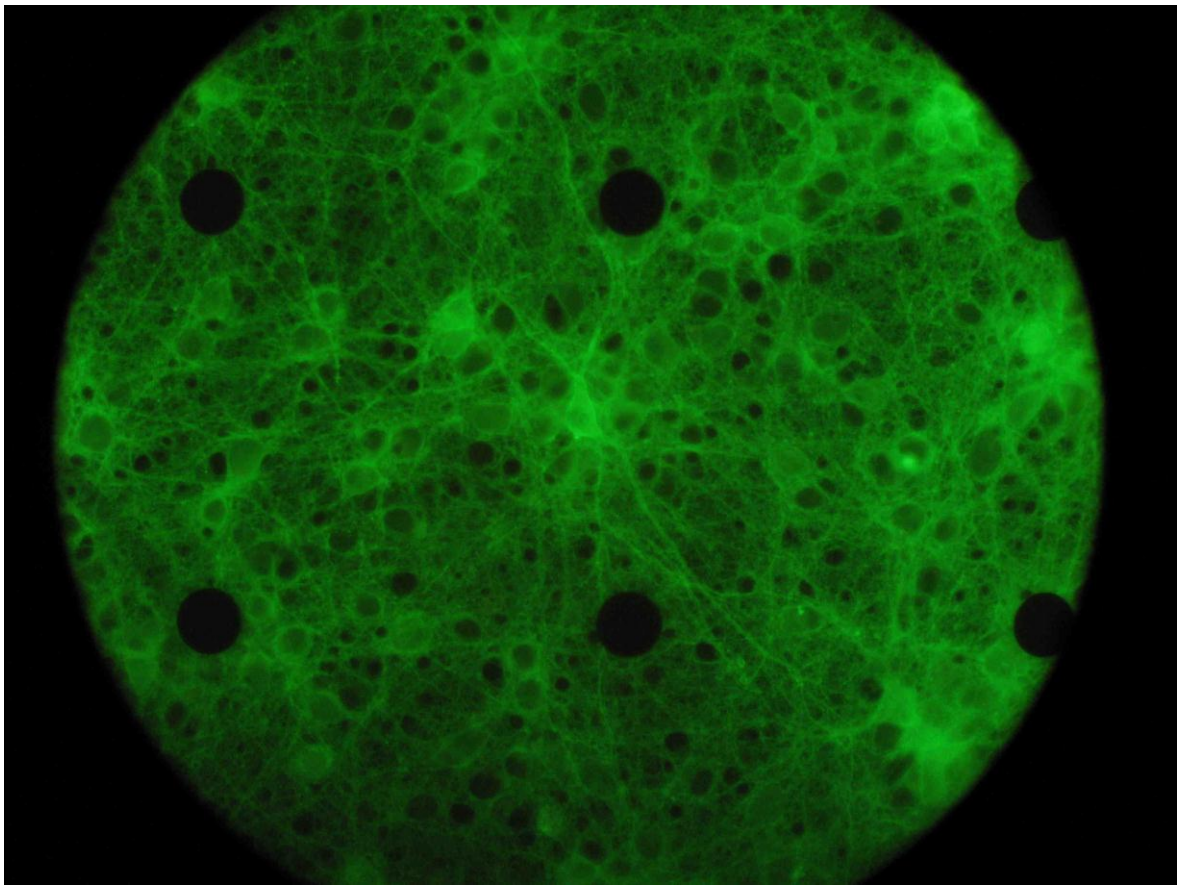

Figure 2-2. 40x image of ChR2 expressing neurons on an MEA. Taken from a different culture than Figure 2-1, this picture shows ChR2 expressing photosensitive neurons over a section of an MEA. The dark large circles are the electrodes on the array spaced 200 μm apart.

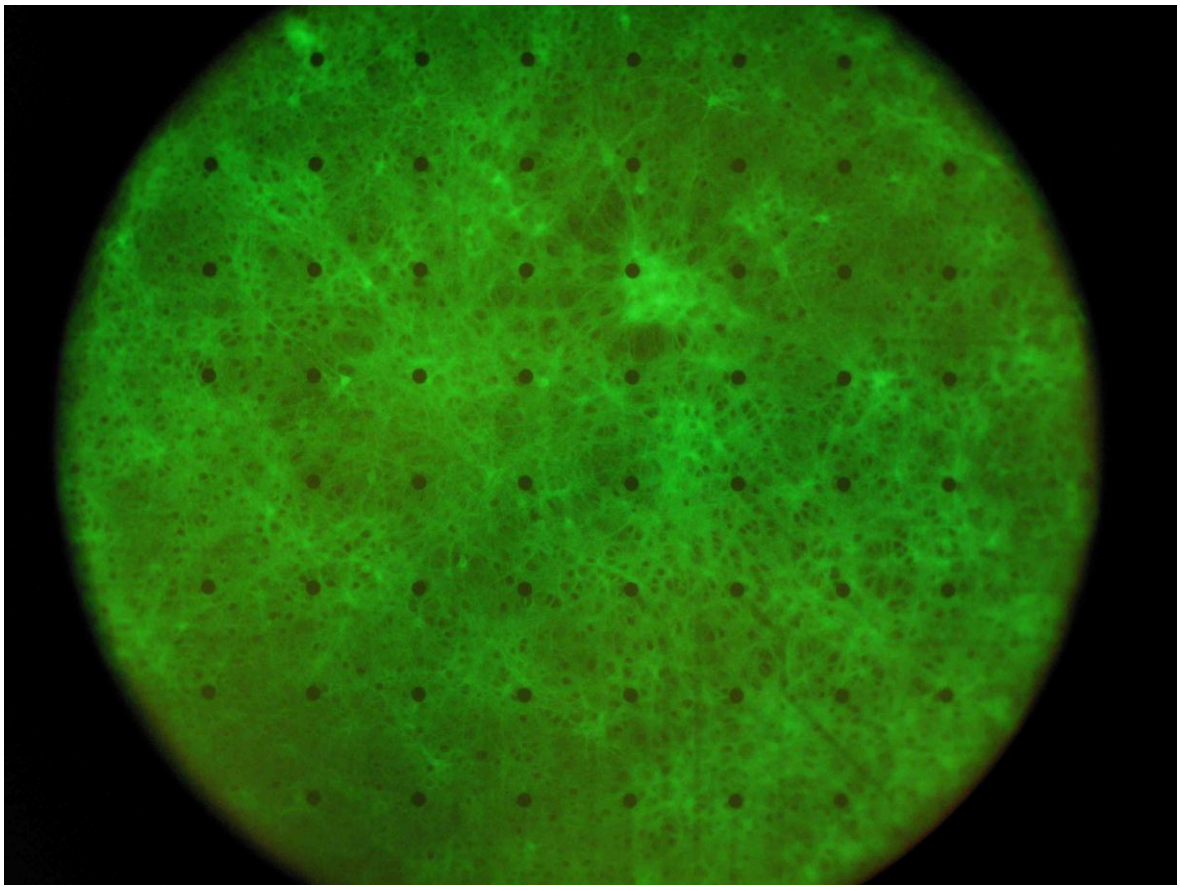

Figure 2-3. Full culture fluorescent expression of ChR2/YFP. 10x view of a cortical culture expressing ChR2/YFP fusion over the entire 60 channels of an MEA (black dots in figure). In a fusion, the ChR2 channel is fused to the YFP marker, so that the ChR2 channels themselves appear green. A dense green network, seen here, indicates robust infection efficiency within soma and the neuron's processes.

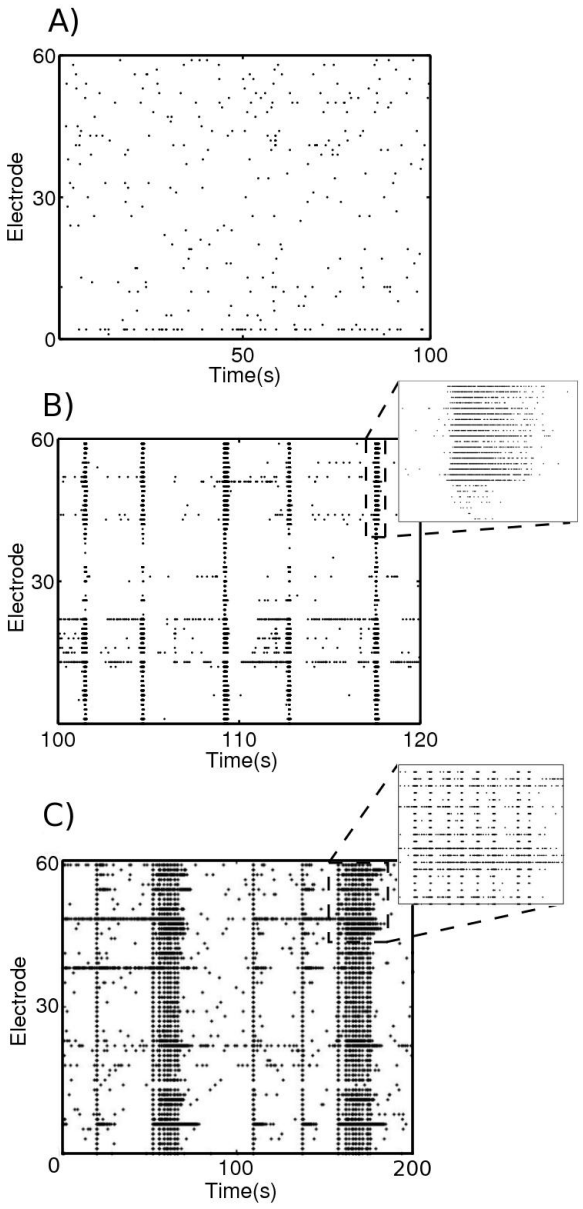

Figure 2-4. Raster plots during the various developmental stages of a single culture's activity. Note the difference in timescales between panels. A) Isolated asynchronous neural activity is common during early development (3-7 DIV), appearing as relatively independent firing with little evidence of synchronization. B) Mature neural activity after 30 DIV. Cortical cultures exhibit bursts consisting of short periods of culture-wide, synchronized activity distributed across the network appearing as vertical bands in the plot. Bursts typically occur every 3 to 4 seconds. Inset shows a 500 ms magnified view of a mature burst. C) From ages 7-30 DIV, cultures exhibit so called superbursts in which networks may burst for several to tens of seconds punctuated by long periods of relative inactivity. Inset shows a (25 sec) magnified view of a superburst that consists of a rapid succession of smaller bursts

CHAPTER 3
BATH LIGHT APPLICATION

Background

A number of traditional approaches have been developed to stimulate neuronal activity including electrical and pharmacological methods. Each technique presents many important features but also significant shortcomings. A novel method has recently appeared known as optogenetics (Banghart et al., 2004; Boyden et al., 2005; Nagel et al., 2003) that represents a major shift in neural stimulation technology. The field of optogenetics capitalizes on naturally occurring light-activated algal ion channels that are inserted into a neuron's membrane via viral carrier, rendering the neuron sensitive to light. Perhaps more importantly, the type of ion channel used can be varied to determine whether photostimulation will be excitatory, producing action potentials, or inhibitory, suppressing neural activity. For example, Channelrhodopsin-2 (ChR2) is a commonly used excitatory channel (Nagel et al., 2003) that has been shown to stimulate action potentials with remarkable precision and latencies less than 10 ms (Boyden et al., 2005). Conversely, the inhibitory channel Halorhodopsin has been shown to suppress neural activity, also with extremely high temporal precision (Han et al., 2007; Zhang et al., 2007). Hence, this novel technological achievement now permits almost complete control over each neuron's activity among a neuronal population, and is now rapidly being deployed in neuroscience for studies as a dynamic clamp (Wen et al., 2010), to delineate neuronal connectivity (Arenkiel et al., 2007; Petreanu et al., 2007), retinal prosthetics (Farah et al., 2007; Golan et al., 2009; Grossman et al., 2010), and applied as a method for seizure suppression (Tønnesen et al., 2009).

The ability to control the electrical activity of neural networks would also be extremely useful in conjunction with current multi-channel microelectrode array (MEA) technology that can simultaneously record network activity. MEA technology employs a grid of electrodes embedded within a glass substrate to provide an extracellular measure of neural activity (Gross et al., 1977; Pine et al., 1980; Thomas et al., 1972), and over the years has grown from 60 electrodes (Jimbo et al., 1998) to over 4096 (Imfeld et al., 2008; Gandolfo et al., 2010). These arrays have enabled the study of a number of important network phenomenon such as bursts (Raichman et al., 2008; Wagenaar et al., 2006), local field potentials (Egert et al., 1998), and plasticity (Cadotte et al., 2008; Chiappalone et al., 2008; Jimbo et al., 1999; Maeda et al., 1998; Madhavan et al., 2006). While recording neural activity from MEAs has proved useful, using MEAs to stimulate activity has suffered from significant problems. First, electrical stimuli are non-specific, activating all cell types, their axons, and perhaps even dendrites (Mcintyre et al., 2001; Nowak et al., 1998; Rattay et al., 1993). Electrode locations are also fixed providing low spatial resolution and little control over selectivity other than adjusting the magnitude of current or voltage applied. Perhaps the most troublesome problem with electrical stimulation has been the electrical artifacts that are generated during stimulation and recording that often completely obscure neural activity for tens to hundreds of milliseconds following even the most brief stimulation pulse. Recent advances in MEA stimulation have attempted to address this issue, but the problems have been only partially alleviated (Nam et al., 2009; Brown et al., 2008; Jimbo et al., 2003). The stimulation artifact prevents examination of high temporal precision processes of the network within these first several milliseconds. All of the problems with

current MEA stimulation techniques can be addressed through the use of optogenetics, by creating a system that can apply light in both a spatially and temporally precise manner.

Recent work has been reported to determine effective stimulation parameters for a single optically active neuron (Boyden et al., 2005; Li et al., 2005; Zhang et al., 2007), typically utilizing arc lamps (Boyden et al., 2005; Han et al., 2007; Li et al., 2005; Zhang et al., 2007; Zhang et al., 2009) or high power lasers (Chow et al., 2010; Schoenenberger et al., 2008) to achieve the high levels of irradiance necessary to activate ChR2. However, there are few reports studying the effects of photostimulation upon a network of neurons. In this paper we describe experiments in which a small population of rat cortical neurons have been made photoactive via ChR2, stimulated with a high intensity blue LED varying pulse duration and stimulation frequency, and examined electrically using MEA technology. Besides basic stimulation of activity, a potentially useful application of this technique could be burst suppression in culture, extending to seizure suppression in-vivo. We explore burst suppression here, and demonstrate this as a viable method of control.

Experiments

We measured each culture's response to photostimulation while manipulating two variables independently: the duration of each light pulse and the frequency with which that pulse was applied. In the first experiment, cultures were stimulated 10 times, with pulse durations of 1, 2.5, 5, 7.5, 10, 12.5, 15, and 20 ms (n=4 cultures). One pulse was delivered every 10 seconds to avoid any impact of network refractory periods (Blankenship and Feller, 2010) or induction of plasticity. Next, each culture was stimulated by varying both the frequency (inter pulse interval (IPI)) and duration of

stimulation. Frequencies tested were 0.2, 0.33, 1, 5, 10, 20, and 50 Hz, each at light durations of 5, 7.5, 10, and 15 ms (n=8). For any frequency under 5 Hz, 20 stimulations were applied and for any frequency faster than 5 Hz, 5 min of stimulation was performed.

Control cultures on MEAs were also created that were not infected with ChR2 and stimulated with either blue or amber LED illumination under identical parameters. Neither illumination produced any evidence of photoactivation, and data are not reported.

Results and Discussion

Under the optimal stimulation parameters, these cultures can exhibit highly reliable responses and precise spike timing. Figure 3-1B shows a raster plot of activity during 15 ms pulses of blue LED light delivered every 10 seconds, indicated by the blue bars. Natural bursting activity is shown in Figure 3-1A for comparison. Stimulation by the blue LED reliably evoked network-wide bursts of activity with high temporal precision.

Duration Modulation

Figure 3-2A shows the post-stimulus time histogram (PSTH), covering 1000 ms after a stimulation pulse is delivered. Histograms are averaged over all 10 stimulations for a single culture, where the beginning of each box represents the beginning of the blue light pulse. The duration of each stimulus is depicted as a different shade line. Figure 3-2B depicts the magnified view of the response at a single electrode denoted with an asterisk in panel A. Figure 3-2C shows the average response across all electrodes and cultures (N=4). As the duration of each light pulse increased, the latency to peak activity was smaller, and a larger evoked response was produced.

The pattern of evoked activity also changed across the 60 channels while manipulating pulse duration. We observed three distinct patterns, which were defined as insignificant activity, mild activity, and bursting. Bursting was defined as significant observable activity on 50-100% of the electrodes. Mild activity was defined as significant observable activity on 10-50% of electrodes. This signified activity that was produced by photostimulation but not strong enough to cause a full burst. Insignificant activity is activity on fewer than 10% of electrodes, which cannot be confirmed as being caused by the photostimulation.

We examined the ability of stimulation pulses of varying duration to evoke either mild activity, or full bursting activity. Figure 3-3 plots the percentage of trials that evoked activity (panel A), and percentage that evoked bursts (panel B) versus stimulus duration. Stimulus durations as short as 7.5 ms produced a reliable response in 97.5 ± 5.0 percent of trials (panel A). While pulse durations as short as 1 ms did sometimes evoke activity, the response was often only a few action potentials and was highly unreliable (only two of the four cultures responded to pulses of 1 ms). There appeared to be no specific threshold for duration at which a burst was reliably produced at 100% probability, seen in Figure 3-3B. Stimulus durations longer than 7.5 ms that reliably evoked activity (panel A) would also tend to evoke bursts on 80 ± 27 percent of trials. However, durations as short as 1 ms would also occasionally evoke a burst (< 10% of trials). This broad range of effective durations may be due to the refractory period following network bursts. Following each burst event, the network enters a refractory period due to depletion of synaptic resources, primarily intracellular calcium (Streit et al., 2006), that makes it very difficult to induce another burst (Tabak et al.,

2003). Hence, while strong pulses (pulses with longer durations) may be able to overcome this refractory period, shorter pulses may sometimes elicit a burst if the pulse occurs during periods when the refractory period has decayed and the network is more sensitive to input.

We also examined the effect of stimulus duration on burst properties, including burst length and time to onset of burst following a stimulus. Figure 3-4 plots burst length (panel A), latency to the first spike of a burst (panel B), and latency to the peak of a burst (panel C) versus stimulus length. While there were differences between cultures in terms of burst length across durations (ANOVA $F(3,5)= 249.923$, $p < 5.55\ e^{-16}$) there was no change in burst length within cultures by stimulus duration. This is surprising given that increasing the voltage/current or duration of electrical pulses delivered to a single electrode are known to evoke significantly larger bursts with different patterns (Jimbo et al., 2000), and shorter latencies (Wagenaar et al., 2004). With single electrode stimulation, increasing voltage or current levels results in increasing the area of tissue affected by the stimulus. In contrast our stimuli were presented across the entire network simultaneously, hence theoretically recruiting a majority of neurons to respond regardless of duration.

Analysis of the time to the burst start did show a small effect of stimulus duration, shown in Figure 3-4B. Burst start was determined as when spike count increased over 5% of maximum spike count in a burst. Although there was little difference between cultures in terms of latency to burst start ($F(3,5)=6.004$, $p < 0.0043$), there was a trend toward shorter latencies with increasing stimulus duration. In Figure 3-4B, 3 cultures showed a very slight decreasing trend toward decreased latency as stimulus duration

increased, while one culture had a very significant downward trend. The pattern of spontaneous activity in that culture was, however, somewhat different than the others. Namely, it exhibited a much longer inter-burst interval (14.6 vs. 5-8s) and longer average burst duration (250 vs. 150 ms) than the other cultures. This suggests that this culture was in a slightly earlier developmental stage, which is often characterized by a slower reaction to stimuli. This may explain why this particular culture was slower to respond to weak stimulation than other cultures. Panel C shows the time to peak elicited activity as duration was modulated. Again, three cultures showed a slight downward trend while one culture (the same outlier as above) showed a sharp decrease, attributable to its immaturity.

Next we determined if the number of spikes produced after each stimulus was affected by stimulus duration. Each culture was stimulated 10 times at durations of 1, 2.5, 5, 7.5, 10, 12.5, 15, and 20ms. For each stimulus that evoked activity, the total number of spikes was summed across the entire culture up to 50 ms after each pulse. The results are shown in Figure 3-5, which plots the normalized spike count by stimulus duration for each culture (points in figure) and overall average (line). As the duration of each stimulus increased, more spikes were evoked during the first 50ms of stimulation. In effect, bursts produced by longer stimulation pulses were denser than those produced by short pulses.

Electrical stimulation of single electrodes produces patterns of evoked activity across the MEA electrodes that vary by the location of the stimulating electrode (Dockendorf et al., 2009; Kermany et al., 2010; Pinato et al., 1999). Bath application of light could be considered to be an equivalent of a single stimulation location. To

determine if different patterns were produced from different stimulus durations, we measured the electrode location at which the first spike had occurred following each stimulus. For this analysis, spike times during the first 20 ms following stimuli for each duration were sorted into 1 ms bins and averaged across the 10 stimulations for each duration. From this we constructed a probability plot, represented as a heatmap, with channels on one axis and time after stimulus onset on the other. If activity on a given electrode tended to lead the response to a stimulus (i.e. first spikes occurred on this electrode) it would appear as a dark region for that channel during the early phase of the response. The results of one representative culture, shown in Figure 3-6, show that there are particular neurons that fire first when light is applied, prior to activity propagating to the entire network. In fact there are several electrodes shown in Figure 3-6 that consistently fire at the same time within this 20 ms time period, notably electrodes 10 and 11, at 7-8 ms, and electrode 40, at 8 and 9 ms (arrows) following the stimulus. All stimulations of 5 ms or longer produced considerable activity at these times, suggesting that these electrodes had one or more neurons surrounding them that expressed ChR2.

Figure 3-7 and 3-8 plot the average cross trial similarity (CTS) metric for one of the subjects for each of the stimulus durations presented. This metric measures the similarity, or reliability, of the evoked pattern of activity across trials. Overall cross trial similarity showed a rapid peak within the first 10-25ms followed by a decline then a sharp rise in similarity, peaking in magnitude within 50-100 ms, before once again decreasing. The result from the initial 10-25 ms is understandable since that period typically represents the direct activation of neurons from the stimulus before activity

begins to propagate outward across the culture. It is also consistent with results from electrical stimuli showing a similar time frame. During electrical stimuli, the CTS during the latter portion of the response often declines to baseline. By contrast, photostimulation produced a second peak of maximal similarity, occurring 50 to 100 ms after the stimulus onset. The duration of the stimulus also affected peak similarity (Figure 3-8). The maximum peak similarity occurred during the 7.5, 15, and 20 ms stimulus durations while shorter durations produced peaks that were delayed, particularly at 5ms durations.

This reproducibility is consistent with electrical stimulation where the early phase of the response (up to 20 ms) is characterized by high precision spike timing, and is theorized to correspond to direct activation by stimulation, whereas the late phase (after 20 ms) is far more chaotic, and thought to correspond to synaptic activation (Jimbo et al., 2000). It is also reminiscent of data suggesting the presence of so-called “trigger networks” or “leader neurons” in which spontaneous bursts in culture are shown to originate from a select few neurons in the network (Eckmann et al., 2008; Pan et al., 2009).

Frequency Modulation

We then determined the effects of manipulating the frequency of stimulus delivery in conjunction with stimulus duration. Previous studies have shown that stimulated activity in MEAs will change markedly at different stimulation frequencies (Chiappalone et al., 2008; Eytan et al., 2003; Jimbo et al., 1999). Particularly, high frequency stimulation to random electrodes has been shown to disrupt bursting in cortical cultures (Dockendorf et al., 2009; Wagenaar et al., 2005) and actively suppresses seizure-like activity in brain slice preparations (Albensi et al., 2004). Figure

3-9 depicts the number of spikes counted within a 50 ms interval after stimulation as both frequency and duration of photostimulation were varied. Spiking significantly decreased as the interval between stimulations decreased or the duration of each stimulus decreased. Notably, stimulation at frequencies faster than 10Hz showed a considerable decrease in activity, even at longer stimulus durations. This is similar to previous reports that have employed high frequency electrical stimulation with MEAs (DeMarse et al., 2005; Eytan et al., 2003).

Burst Suppression Using Bath Light Application

Burst suppression has been demonstrated successfully using distributed electrical stimulation (Wagenaar et al., 2005), in which electrodes are individually stimulated cyclically at high frequency. We attempted to duplicate these results using bath light application at high frequency. In this experiment the frequency (10, 20, and 50 Hz) and duration (5, 10, and 15 ms) of blue LED pulses was varied in order to determine the degree to which bursts could be suppressed.

Figure 3-10 shows a typical example of burst suppression. Panel A shows a spike count histogram (100 ms bins) of the spontaneous activity of a culture. Large spikes in the figure represent bursts. That same culture was then stimulated with 15 ms light pulses at 50 Hz (Panel B). We can see that the spike counts per bin are significantly reduced, and there are much fewer bursts. Some bursts still occur, and one is indicated by the arrow. The raster plot of this burst is shown in Panel C, where network-wide activity temporarily increases. These bursts are termed “escapes” and represent cases where the network escapes control.

Figure 3-11A shows a spike time binned histogram of a network response to typical low frequency stimuli (15ms duration, 0.1 Hz), aligned to the light application period (blue bar in figure). These responses, discussed earlier, have a fast onset and are extremely dense for an extended period of time (up to 1000 ms). During high frequency stimulation, however, the duration of these bursts temporally contract, becoming significantly shorter as the frequency of stimulation increases. Figure 3-11B shows the same analysis during high frequency stimulation (15ms duration, 10Hz) for a single representative subject. With this stimulation paradigm, a very small, short burst of activity was created after each stimulus was delivered. Note the difference in axis scales between Figures 3-12A and 3-12B. The mechanism behind the burst suppression process, electrically or optically, is not fully understood. It is hypothesized that each stimulus directly activates neurons, but is not strong enough to propagate activity throughout the network. Because the stimuli are applied at such a high frequency, the cells' synaptic resources are constantly being depleted and therefore do not recover enough to allow a burst to propagate. Our results support this hypothesis, in that each stimulus produced a short burst of activity likely representing the direct activation of neurons expressing ChR2. Due to synaptic depletion, large network-wide bursts were entirely suppressed for an extended time. For the stimulation paradigm shown in Figure 3-11B bursts were suppressed for the length of the experiment.

We wanted to further examine the theory that the activity caused by high frequency stimulation represents direct optogenetic activation, with an absence of synaptic propagation. We looked at the spatiotemporal activity caused in the first several milliseconds after stimulation, and averaged it over multiple stimuli, shown in

Figure 3-12. Figure 3-12 shows the average response to 1000 high frequency stimulations (15ms, 10Hz), expressed as the probability of a single channel firing within a 1 ms bin. This analysis reveals distinct areas that fire with near 100% probability, meaning that similar activation patterns were produced following each stimulus. Typical direct activation time with ChR2 is between 5 and 10ms (Boyden et al., 2005). Due to the length of the evoked response (~40 ms), it is likely that this response is not purely the result of direct activation, but some propagation of activity as well. However, there is still significantly less propagation than we see during low frequency stimulation, where bursts can last 400-600ms.

To quantify and compare the degree of burst suppression between the different frequencies and durations, we calculated the suppression ratio of each level. A suppression ratio represents the square root of the ratio of variability in binned spike counts (variance) during spontaneous activity, including bursting, divided by the variability during high frequency stimulation (Rosenblum et al., 2004). The burst suppression ratio equation is shown in Eq. 3-1.

$$SuppressionRatio = \sqrt{\frac{VAR(Spont)}{VAR(HFS)}} \tag{3-1}$$

Bursting represents periods of high rates of activity over 10 to hundreds of milliseconds. Dividing spike trains in 5 ms bins, irrespective of channel location, would result in a higher variance of spike counts among those bins compared to periods when activity is relatively stable. Hence a reduction in bursting would result in a decreases variance and the suppression ratio would increase. Figure 3-13 shows the suppression ratio for each photostimulation value of duration and frequency. Increasing either frequency or duration increased the degree of burst suppression using bath light illumination. The

highest level of suppression was seen at 50 Hz and 15 ms pulses. Though we did not test durations or frequencies beyond those shown in Figure 3-13, it is likely that longer pulse durations or higher frequencies would produce similar results, and could be optimized in future experiments to maximize suppression.

Different stimulation protocols produced markedly different burst control effects. By varying photostimulation duration and frequency, as well as other variables such as brightness, it may be possible to suppress bursting for an indefinite amount of time using optical stimulation. The bath light presentation for burst suppression we investigate here may be applicable to current in vivo efforts to suppress seizure activity in epilepsy, such as those currently treated using high frequency electrical stimulation (see Durand and Bikson, 2001).

Delayed Feedback

In this experiment, we explore the effect of feedback upon the pattern of neural activity. Specifically, we wished to know whether feedback can be used to suppress intrinsic bursting. In a neural simulation composed of 230 neurons, Batista et al. recently showed that feeding the mean membrane potential of a small pool of neurons back into the network following a delay (τ) would significantly reduce synchronization among those neurons. Values of τ were based on the intrinsic burst rate of each simulated network. While the domain of control versus τ was wide, values of τ near the intrinsic burst frequency had little effect on suppression ratios, while values from 1-25% produced substantial suppression (Batista et al., 2010).

For this experiment, mean-field activity was calculated every 10 ms as the mean spike rate across all channels. This value was then linearly transformed into an LED

intensity value via custom-built hardware with a combination USB interfaced microcontroller and Voltage DAC to drive LED output. In this experiment, τ was equal to 1000 ms based on intrinsic spontaneous burst rates observed before the experiment began. Figure 3-14 shows instantaneous spikes rates during a 60 second recording of spontaneous activity (without feedback, Panel A) and activity following application of delayed feedback (Panel B). Engaging feedback control rapidly attenuated the emergence of bursts resulting in a higher suppression ratio than that observed in the absence of feedback, shown in Figure 3-15.

Conclusions

Here we have demonstrated the ability of a single high-power blue LED to reliably evoke robust bursts of activity in dissociated cortical cultures at stimulus durations as short as 10 ms and limited asynchronous activity as low as 1 ms. While we can produce activity with short light pulses, temporal precision is increased as photostimulation duration increases. We saw light pulses of 15 ms or higher result in a faster onset of activity, and a faster time to reach peak activity. Optimal duration for producing bursts occurred near values of 15 ms at which bursts were reliably produced while maximizing temporal precision. This stimulus duration was optimal for both low and high frequency stimulations, however this parameter may change with different light intensities.

The pattern of activity within the network during photostimulation was similar to that reported using single electrode stimulation, where patterns of activation include consistent sites of burst origin. If a stimulus generated a burst, the spatiotemporal

pattern of spiking during that burst appeared to remain relatively consistent, regardless of stimulus duration.

At higher stimulation frequencies, photostimulation can also begin to suppress intrinsic bursting. The burst suppression ratio was maximized with photostimulation applied for 15 ms at 50 Hz. However, because these parameters are at the outer limits of what we employed, there are likely even more effective burst suppression parameters that could be used. A more rigorous parametric approach would be necessary to determine ideal stimulation parameters to maximize this effect.

While the temporal precision of this system is high, what we now require is a light application system that has both temporal and spatial resolution. While some work has been done in this area (Golan et al., 2009; Grossman et al., 2010; Wang et al., 2007a), it has generally been geared toward retinal prosthetics and clinical applications. A system such as this for use in stimulating in-vitro cultures on MEAs would be a great improvement on current electrical stimulation techniques. The ability to produce activity in a specific area of the network, potentially with single-neuron precision, could vastly enhance our understanding of the electrical properties of neural cultures, and how these cultures work in a network environment to perform computation.

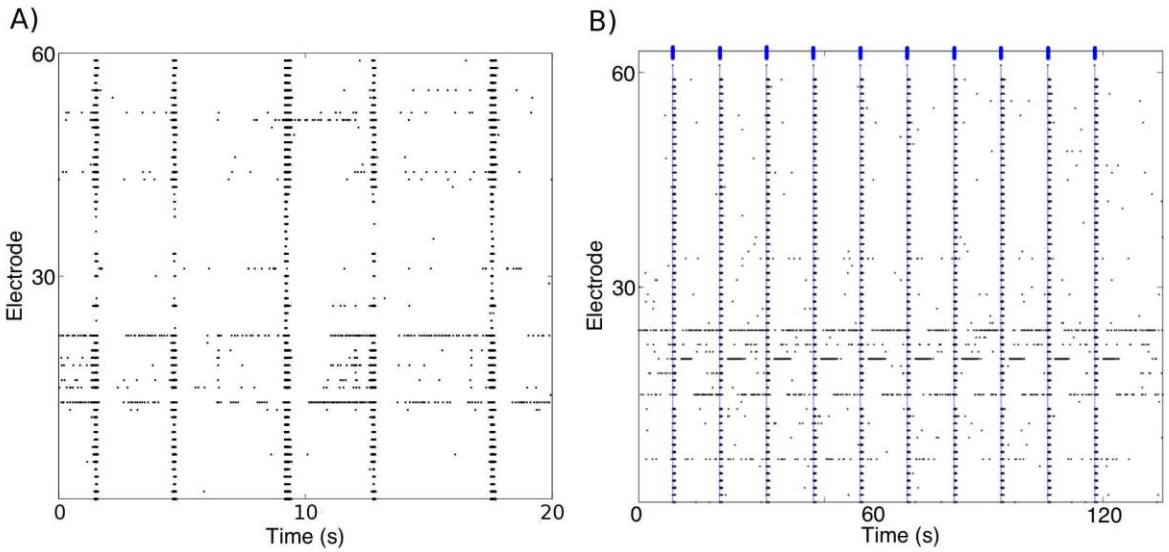

Figure 3-1. Raster plots of spontaneous and evoked activity. A) The raster plot shows 20 seconds of spontaneous activity in an infected culture at age 30 DIV. Each point represents one spike detected on a particular channel (vertical axis). Some asynchronous activity appears as single dots, but the majority of activity is contained in the spontaneous network bursts, which appear as vertical clusters of activity that are typical for cultures at this age. Mean burst duration for this culture was 130 $\pm$50 ms, and mean time between bursts was 5.06$\pm$4.02 seconds. Mean burst duration across all cultures was 175$\pm$52 ms, and mean time between bursts 9.00$\pm$4.16 seconds. These data agree with previously found average values for a healthy culture (Wagenaar et al., 2006), indicating that the infection procedure had no adverse effects on culture activity. B) Evoked activity every 12 seconds by a 15ms pulse of blue LED light (indicated by blue lines at the top of the figure). Each light pulse produces a brief period of network-wide activity, with 100% reliability.

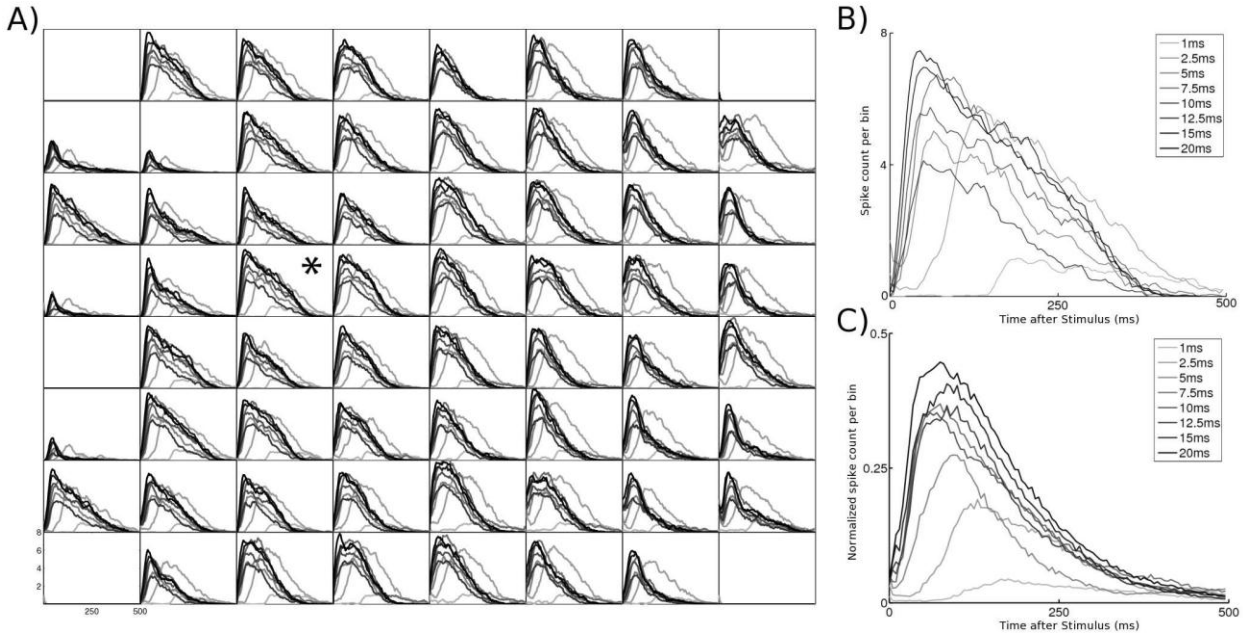

Figure 3-2. Post-Stimulus Time Histograms (PSTH). A) PSTH shows the activity of one culture as it is stimulated with blue light, averaged over 10 stimulations at 0.1 Hz for each stimulus duration (1, 2.5, 5, 7.5, 10, 12.5, 15, and 20 ms, represented by the different shade lines). Each box represents a histogram of the electrical activity of one electrode, in MEA layout, starting at the onset of the stimulus and lasting for 500 ms using 5ms bins. Legend is shown in B). Observe a fast onset of activity across the entire culture, followed by a slow decline over time. B) Close up view of asterisked electrode. Each line represents the average over 10 trials of that electrode's response to varying stimulus durations. C) Normalized average of stimulus response over all cultures (n=4) and all electrodes. As stimulus duration increases, the response becomes stronger and onset becomes faster.

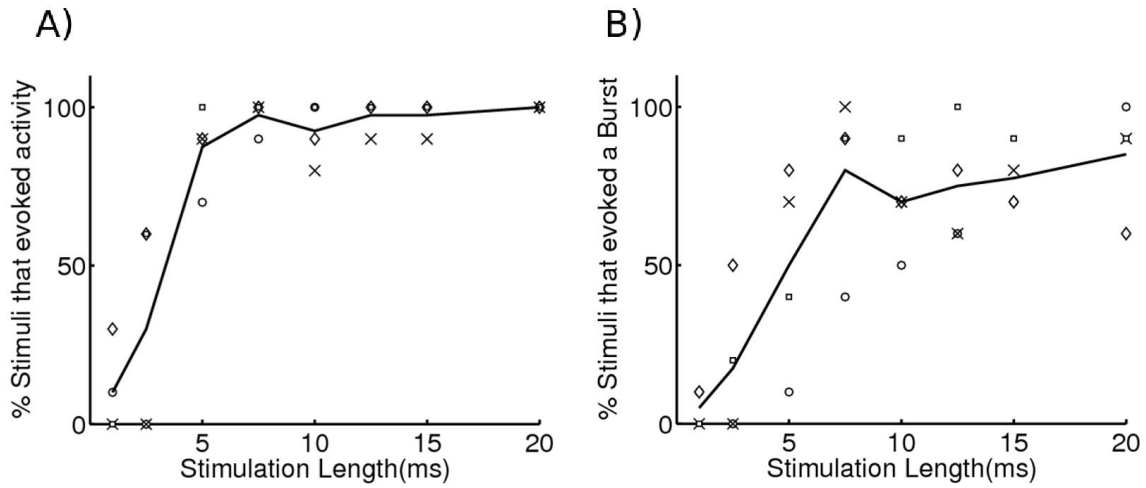

Figure 3-3. Ability of light pulses of different duration to produce activity. Cultures were stimulated at durations of 1, 2.5, 5, 7.5, 10, 12.5, 15, and 20 ms. Each light line represents a single culture (n=4) and the dark line shows the mean. A) Percentage of 10 light pulses at each duration that produced mild activity, defined as activity on at least 10% of the electrodes. At durations of 7.5 ms and higher, close to 100% of stimulation pulses produced some distinct amount of activity. B) Percentage of light pulses (10 total) at each duration that produced a burst, defined as significant activity on at least 50% of the electrodes. As the duration of stimuli increased, there was a general upward trend of the percentage of stimuli that produced a burst. The lack of a threshold at which all stimuli produced a burst may be attributed to the burst refractory period, discussed in the text.

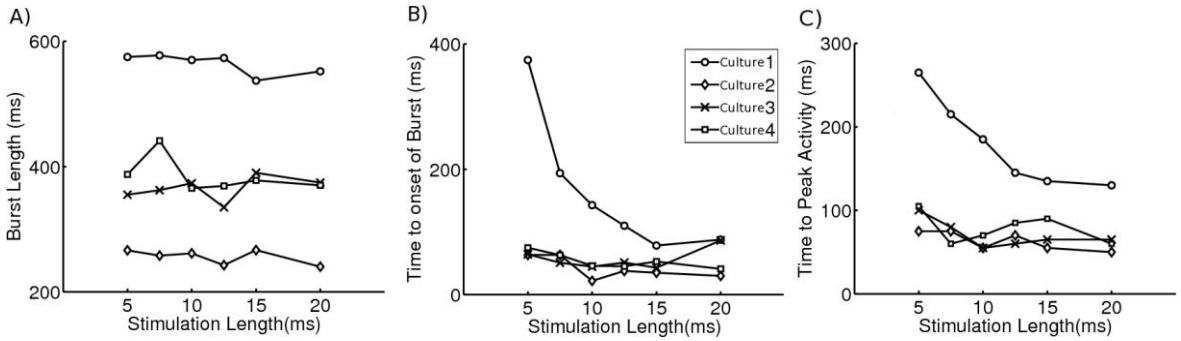

Figure 3-4. Effect of stimulation duration on burst properties. A) Effect of stimulus duration on the length of evoked bursts. The duration of bursts typically varies between cultures, ranging from 250 to 600 milliseconds in the figure, but this value was independent of stimulus duration. B) Mean time to burst onset following a stimulus of each duration. Three of four cultures show latencies to burst onset with a mean of approximately 50 ms, while the fourth subject had extremely high latencies until stimulus duration was above 15 ms. This culture was highly variable, possibly due to the network being in an earlier developmental stage than the others and characterized by a longer natural inter-burst interval and burst durations. In three of the four cultures there is a slight downward trend. C) Time following stimulus onset to peak activity. As stimulus duration increased the time to peak activity decreased gradually moving closer in time to stimulus onset. The same outlier in B also showed greater variation, for the same reasons described above.

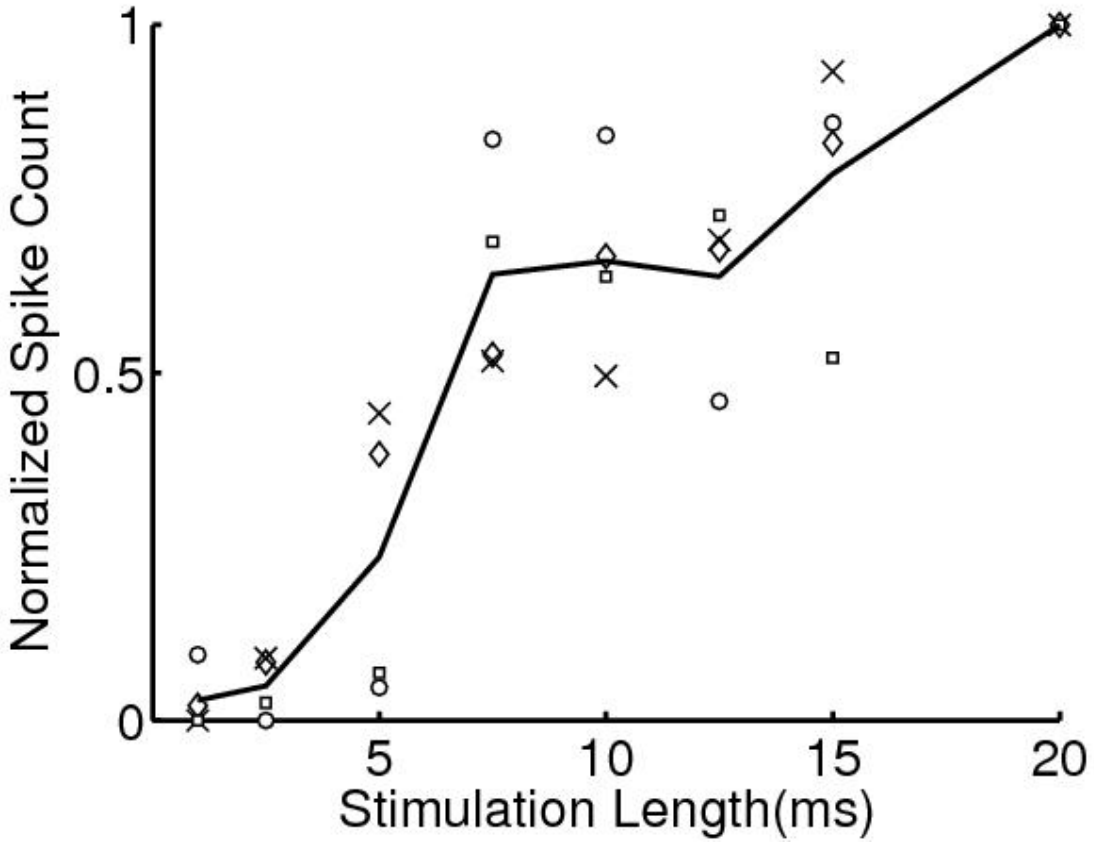

Figure 3-5. Normalized spike count in a 50 ms window after stimulation. For each photostimulation that produced a burst, the number of spikes for 50 ms after stimulation were counted, averaged over stimulations, and normalized. As length of stimulus increases, more spikes were counted in the 50 ms window, suggesting denser bursts. Markers used are same as those in Figures 4 and 5, and the line represents the mean.

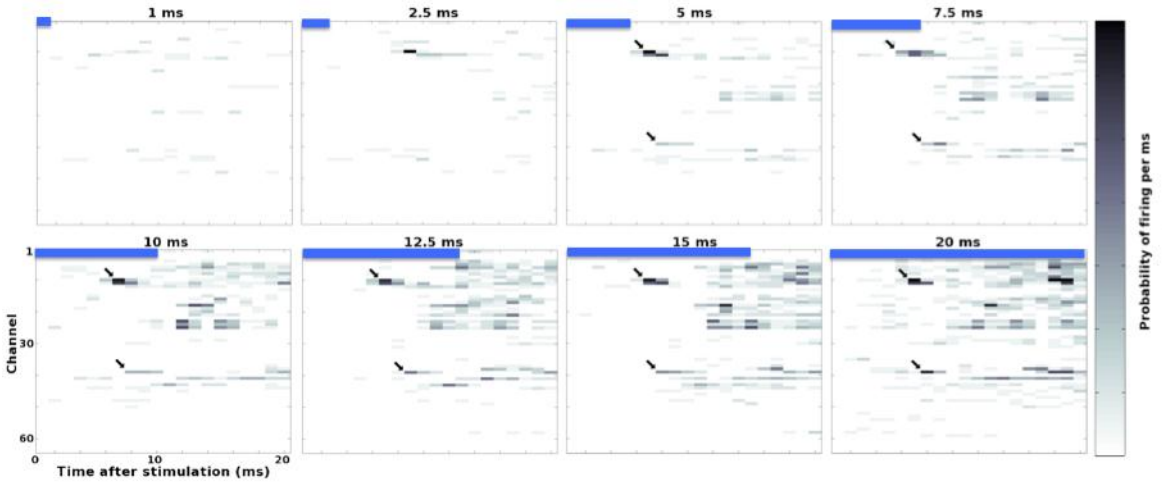

Figure 3-6. Spatiotemporal representation of burst propagation. Each subpanel depicts the probability of firing for each electrode during the first 20 milliseconds of activity evoked by bath illumination. For all stimulus durations greater than 2.5 ms, there are two locations that consistently fire early in the burst and are demarcated by arrows. This highly precise response pattern likely represents the direct activation of neurons expressing ChR2 whose activity then propagates to the rest of the culture. Increasing the duration of the photostimulus increased the likelihood of a response and increased the probabilities of firing overall. However, the pattern of activation during the course of the burst remained the same. This indicates that bath illumination may have effects similar to results seen with single electrode stimulation, where the response is dependant on stimulus location (e.g., Dockendorf et al., 2009).

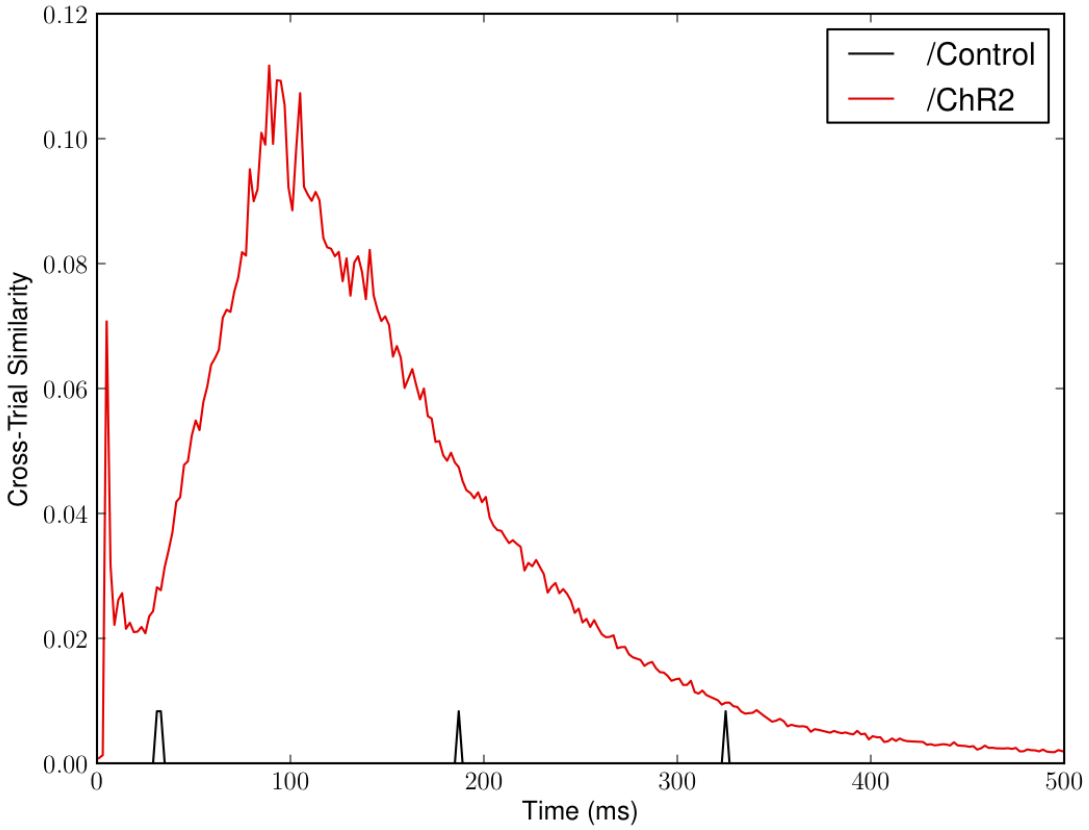

Figure 3-7. Mean Cross-Trial Similarity for LED stimulation. Cross-trial similarity (CTS) is a measure of spatiotemporal reliability of an evoked response pattern across trials. This figure depicts the CTS score by time after stimulus onset averaged across durations. During the LED duration experiment the similarity of the evoked response produced a sharp peak during the first 10-25 ms followed a sharp increase with maximum similarity peaking at approximately 100 ms before declining to baseline. The shape of the CTS is consistent with findings from electrical stimulation showing differences between the early and late phase of evoked responses (Jimbo et al. 2000).

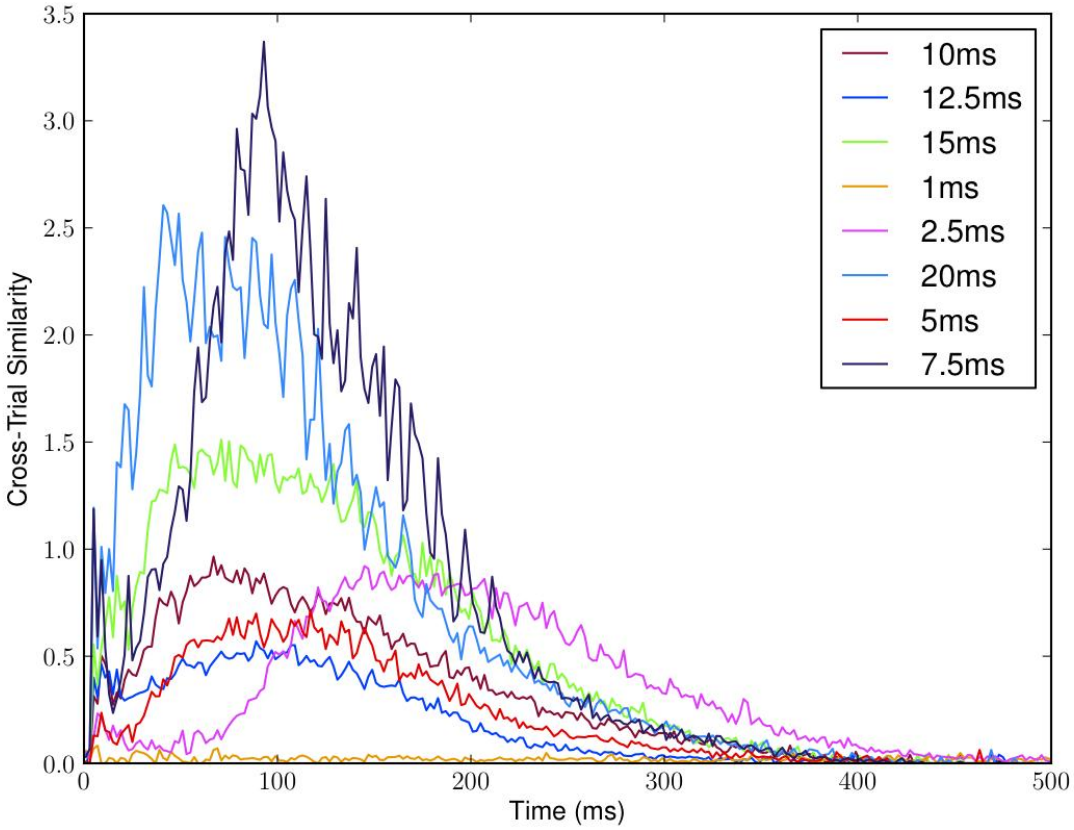

Figure 3-8. Cross Trial Similarity by stimulus duration for one culture. This plot depicts the cross trial similarity for each LED stimulus duration. Maximum peak similarity occurred similar during the 7.5, 15, and 20 ms stimulus durations. Stimulus durations shorter than 5ms produced peaks at times that were delayed relative to longer durations. This suggests that increasing stimulus duration increased the amount of similarity across trials while weaker stimuli delayed the onset of peak similarity later in time.

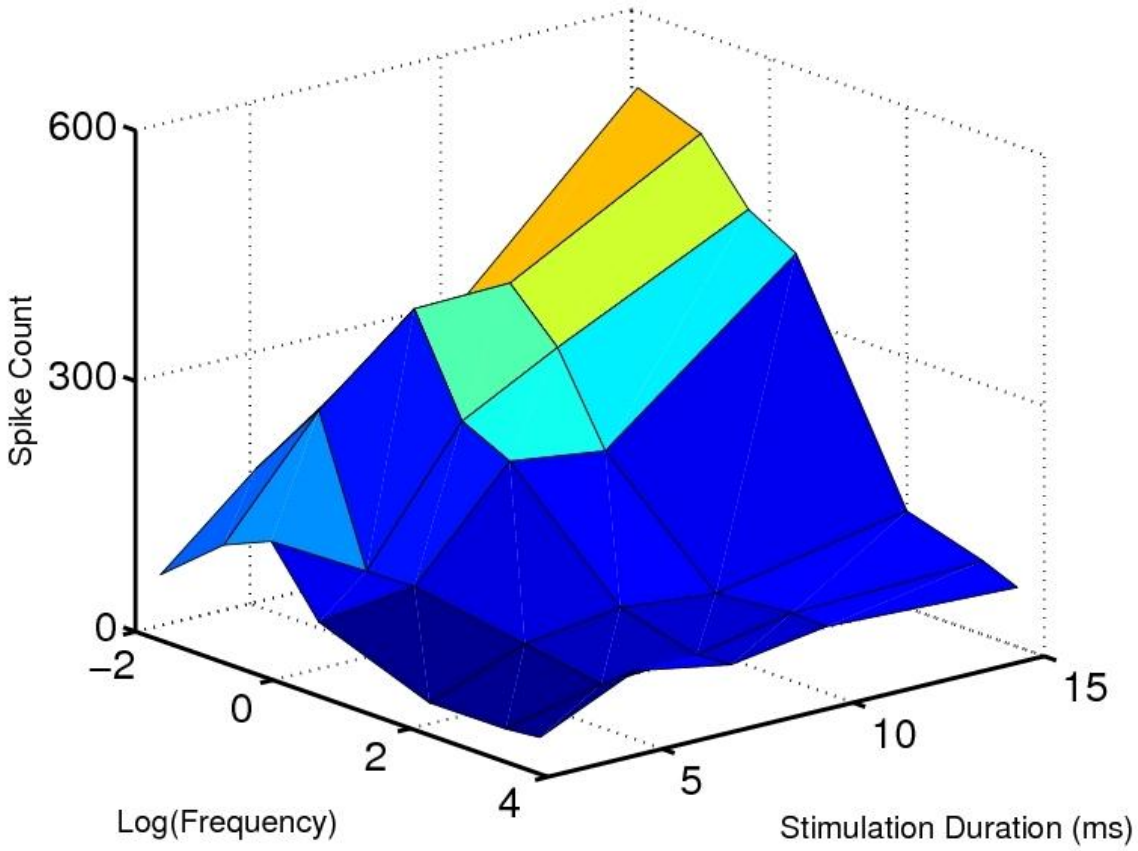

Figure 3-9. Number of spikes produced in a 50 ms window after stimulation for stimuli of varying duration and frequency. Stimulation durations tested were 5, 7.5, 10, and 15 ms, and frequencies were 0.2, 0.33, 1, 5, 10, 20, and 50 Hz. The amount of activity produced by stimulation can be increased by increasing the stimulus duration or decreasing the frequency at which stimulation is delivered. Notably, stimulation at frequencies higher than 10 Hz produce a strongly suppress bursting. A log scale was used to allow better visualization of the high frequency range.

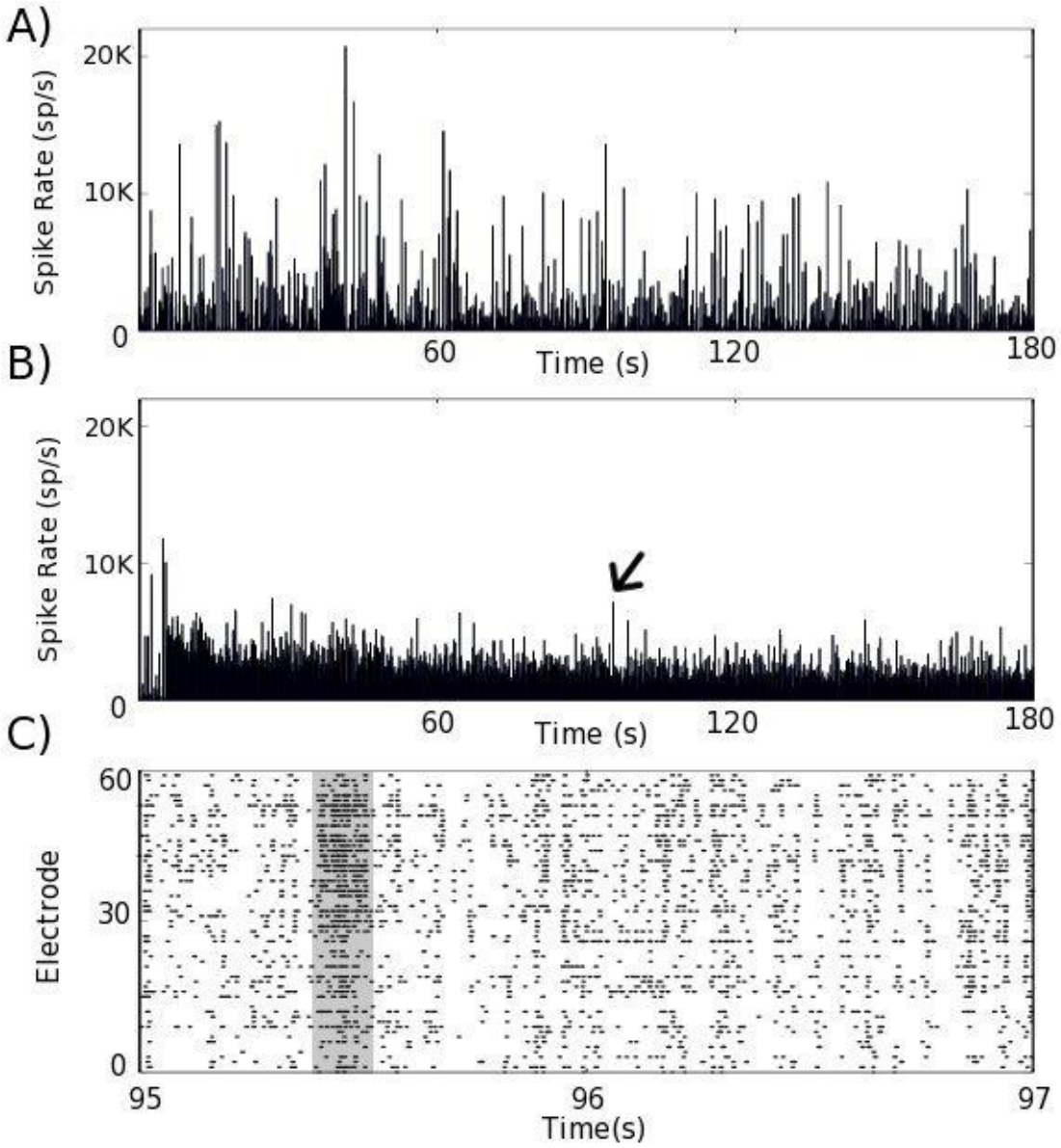

Figure 3-10. Burst suppression using bath LED light. A) Instantaneous spike rates during spontaneous activity of a culture over 3 minutes (100 ms bins). Large positive reflections represent network-wide bursts. B) Burst suppression LED application (15 ms light duration applied at 50 Hz), starting after about 5 seconds, produced significantly reduced bursting activity. Bursts still occur occasionally (arrow). C) Raster plot of indicated burst (shaded area). The surrounding activity is representative of burst suppression activity, where the majority of channels fire regularly but there is very little synchronization.

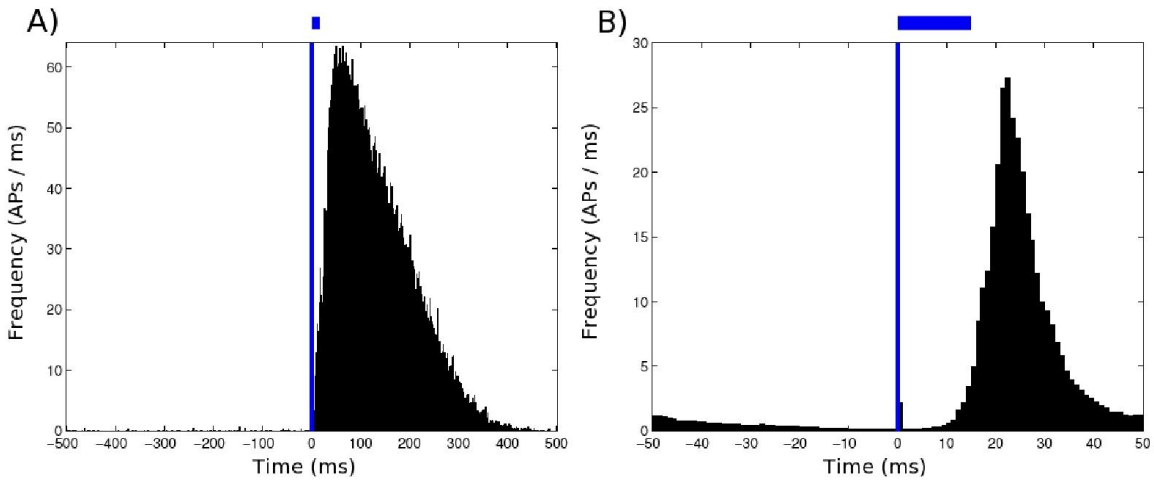

Figure 3-11. Photostimulation applied at high frequency has burst control effects. A) Low frequency (0.1 Hz), 15ms light pulses were applied and the average response was taken, aligned to the time of the triggered light stimulus. The average burst produced is extremely strong and lasts up to 400ms. B) High frequency (10 Hz) stimulation at the same duration produces much smaller, shorter bursts of activity. Response was averaged over 1000 stimulations, taken from the middle of the recording period. Notice the large change in scale from A) on both axis. Very little activity occurred outside of these triggered responses. Out of eight cultures tested, 6 exhibited these strong burst control effects, with different stimulation protocols (frequency and duration) having varying effectiveness.

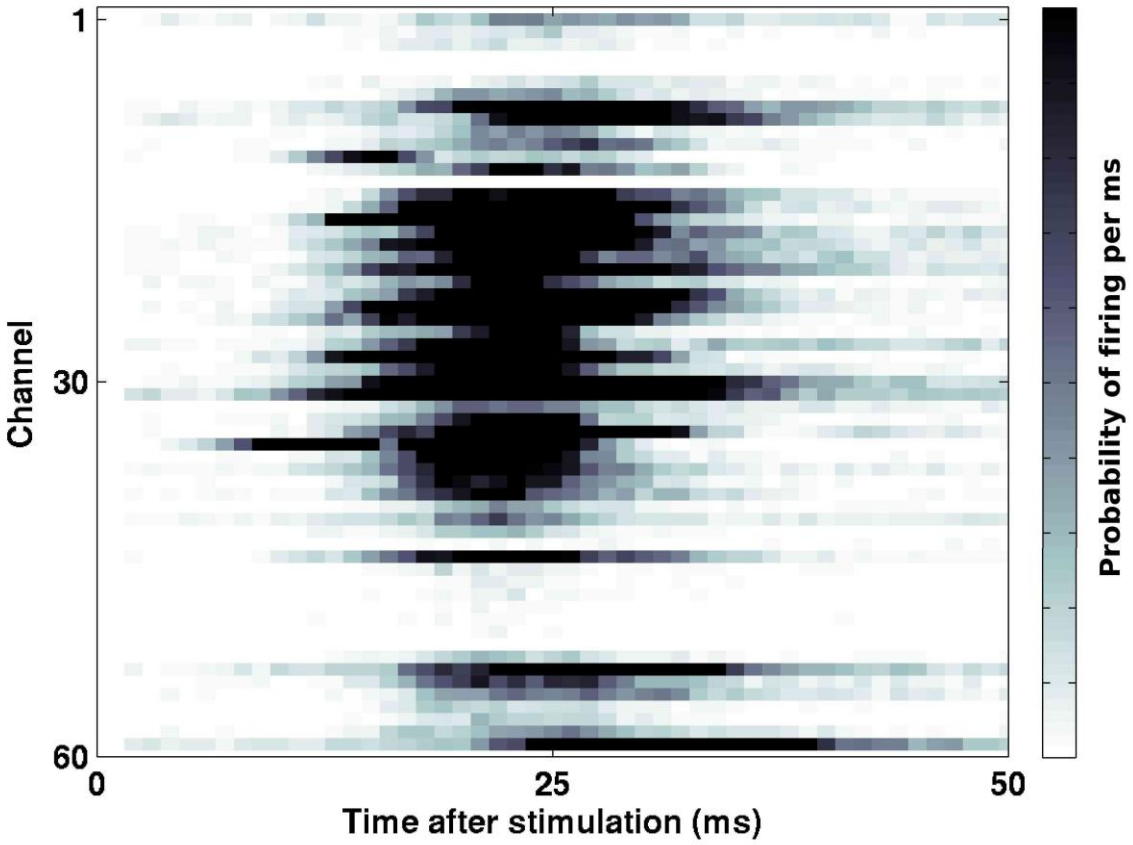

Figure 3-12. High frequency stimulation produces highly reproducible responses. Firing probability of channels as a function of time after stimulation. Color bar ranges from 0 to 1, and responses are averaged over 1000 stimulations (15ms, 10Hz) taken from the center of the recording period. High probability areas represent reproducible activity patterns, with far less network propagation than bursts produced by low frequency stimulation.

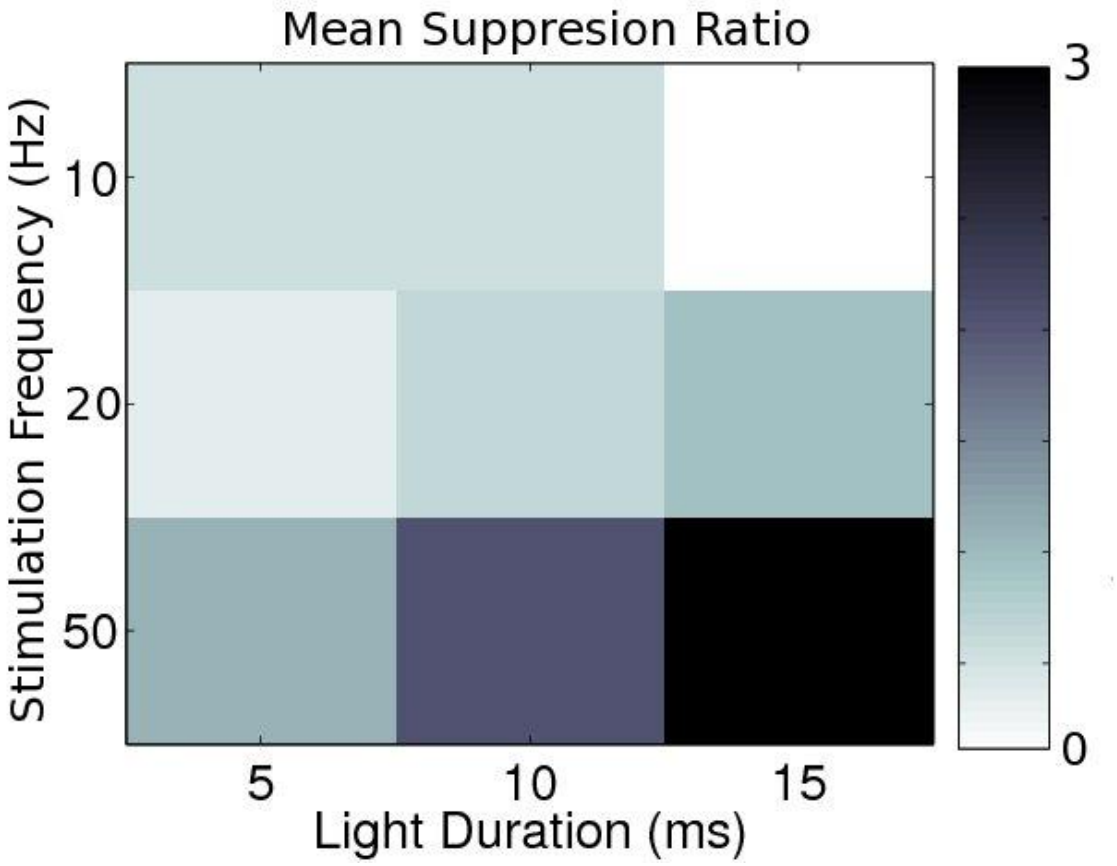

Figure 3-13. Suppression ratio during various levels of high frequency stimulation. Higher suppression of burst appears as progressively darker shades of grey. In this experiment the frequency of photostimulation (10, 20, and 30 Hz) and duration of each blue LED stimulation pulse (5,10,15 ms) was varied. Increases in either frequency or duration produce greater suppression of bursting with the most suppression seen with 50 Hz pulses at 15 ms in duration.

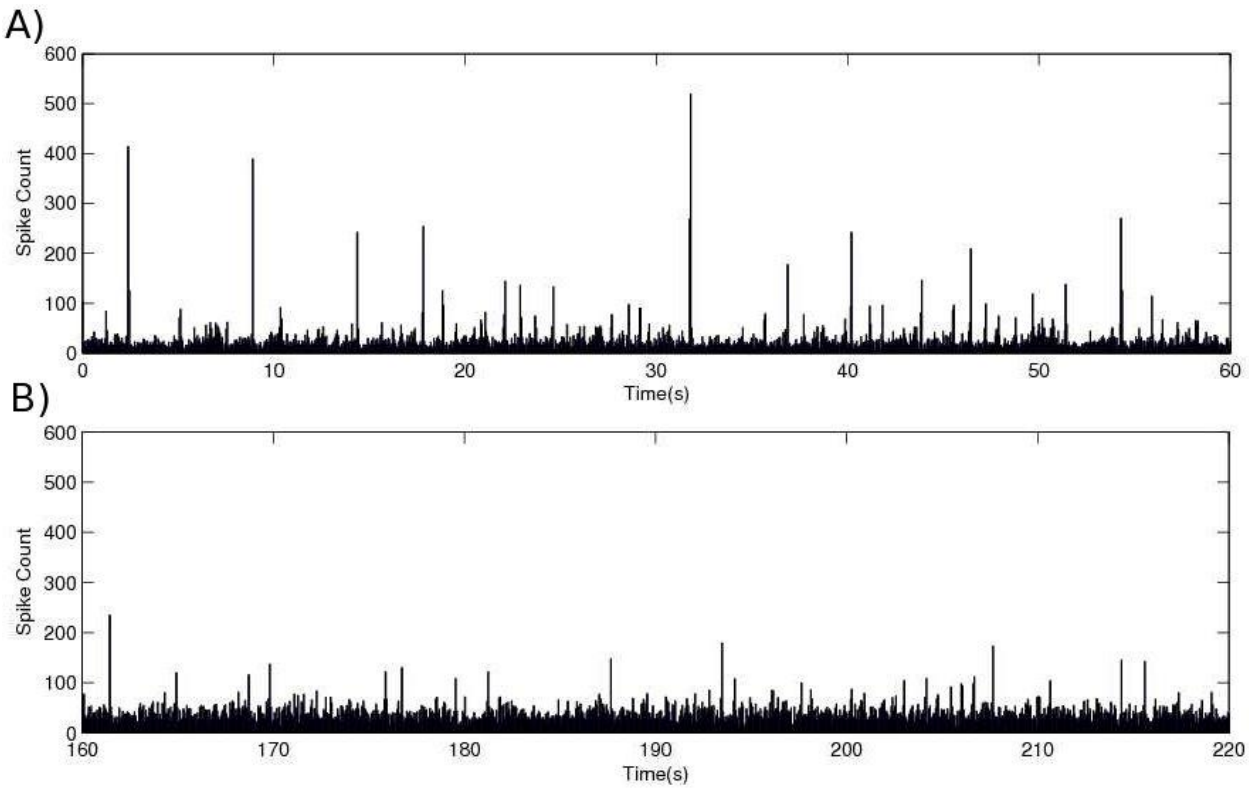

Figure 3-14. Meanfield feedback control for burst suppression. Instantaneous spike rates of activity during spontaneous activity (A), in which activity consists of spontaneous bursts followed by asynchronous activity, and after delayed mean-field feed-back control was applied (B). In this suppression method (based on Batista et al., 2010) activity levels across the network (meanfield) is fed back into the network after a delay (τ = 1000 ms) suppressing intrinsic bursting. Meanfield estimates consisted of the mean spike rate continuously calculated in a sliding 10 ms window. The mean spike rate was then linearly transformed into an intensity of a blue LED that illuminated the entire network of neurons. Application of delayed meanfield feedback successfully suppressed the bursting observed earlier.

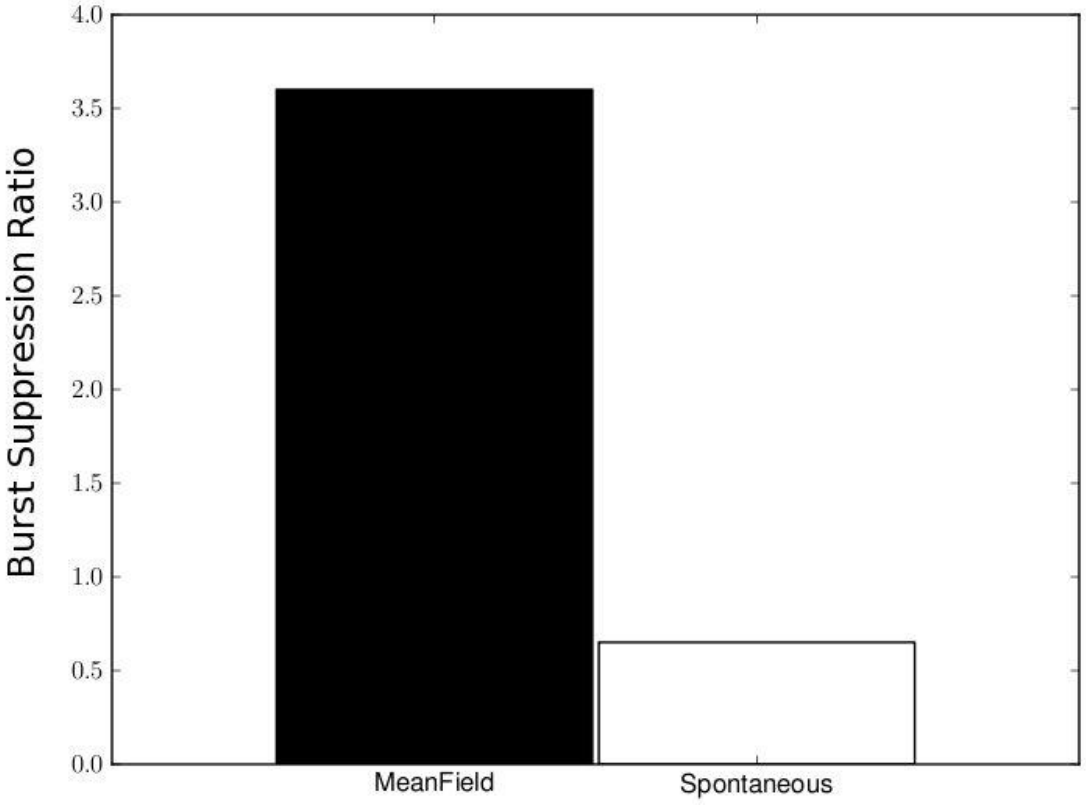

Figure 3-15. Suppression ratio during delayed meanfield feedback versus spontaneous baseline recordings. Application of mean-field based LED feedback into the neural network attenuated bursting and resulted in a higher suppression ratio compared to spontaneous levels. Variance estimates were calculated over 60 seconds of spontaneous and 120 seconds of feed back control (N = 1).

CHAPTER 4
DLP SYSTEM

DLP Operation

In the prior chapter we demonstrated that a simple high intensity LED could successfully evoke neural activity. However, perhaps one of the most exciting features of optogenetics is its potential to enable independent optical control of each and every neuron in a network. For the first time in neuroscience, researchers would have complete control over a network, opening new frontiers in the study of neural computation (Adesnik et al., 2010), learning (Huber et al., 2008; Jones, 2011; Rolls et al., 2011; Sohal et al., 2009; Tsai et al., 2009), structure-function or circuit mapping (Arenkiel et al., 2007; Gradinaru et al., 2009; Luo et al., 2008; Petreanu et al., 2007; Petreanu et al., 2009; Wang et al., 2007). The technology also has immediate applications to the field of retinal prosthetics (Busskamp et al., 2010; Farah et al., 2007), stem cells (Dottori et al., 2011; Tønnesen et al., 2011; Weick et al., 2010), and applications to neurological disorders such as epilepsy (Halassa et al., 2011; Tønnesen et al., 2009) or schizophrenia (Peled, 2011). In order to reach that milestone a device is needed with five primary characteristics: 1) It must be bright enough to activate the CHr2 or NpHr opsin, 2) It must be able to create relatively arbitrary light patterns, 3) The resolution (pixel size) should at least be near or smaller than the size of a typical soma (10 - 30 μm), 4) It should be able to stimulate rapidly with a minimum duration of 1 ms, 5) It should also be capable of projecting at least two colors, blue light for ChR2 and yellow/red light for Halo.

The majority of work in this field to date simply shines a spot of light onto tissue using a mercury arc or Xenon lamp with mechanical shutter (Arenkiel et al., 2007;

Banghart et al., 2004; Boyden et al., 2005; Gunaydin et al., 2010; Li et al., 2005) or laser with digital control (Aravanis et al., 2007; Han et al., 2009; Tønnesen et al., 2009; Wang et al., 2007a), limiting the ability to create structured light patterns. Recently a number of methods have been developed approaching this milestone. For example, fiberoptic cables have been used to transmit coherent (laser) light to mechanically create patterned light known as structured light.

In fact such a device has been in operation in our living rooms for over 10 years. This device, known as a digital light projection television, or DLP, uses a densely packed array of individually addressable mirrors known as a digital mirror device (DMD). A schematic of a DLP system is shown in Figure 1-2. A light source, typically a metal halide lamp, halogen lamp, or LED illuminates the surface of DMD. These mirrors are "digital" as they can be in either the 'On' or 'Off' position, with a switching speed of less than 30 microseconds. In the 'On' position, the mirror reflects the light through a projection lens, and becomes a pixel in the projected image. In the 'Off' position, the mirror reflects the light off to the side onto a light absorber, and that pixel appears black on the image. Furthermore, the intensity of the light source can be modulated in some systems (e.g. those that use LEDs), creating a wide variety of shades of gray. To create colors, three separate light sources are used, which are red, green, and blue. By cycling through these light sources at a very high speed, the three primary colors can be mixed at different ratios create the perception of millions of different colors.

A number of DLP based devices for optical stimulation have been reported (Arrenberg et al., 2010; Farah et al., 2007; Golan et al., 2009; Jerome et al., 2011; Wang et al., 2007a). For example, several groups have applied this technology, or

employed LED arrays, combined with MEA technology to study cardiac function (Abilez et al., 2011; Arrenberg et al., 2010; Jia et al., 2011). Optogenetics is particularly promising in the field of retinal prosthetics, where arrays of LEDs (Grossman et al., 2010) and DLPs (Golan et al., 2009; Farah et al., 2007) have been employed in vitro to study activation of isolated retina. LED arrays have also been used to stimulate dissociated hippocampal neurons and isolated retinal explants. Grossman et al (Grossman et al., 2010) fabricated a 64x64 grid of blue LEDs (50 μm spacing) to simulate visual stimuli and could reliably evoke activity when stimuli were presented at a rate up to 20 Hz. Reliability then declined to 50% at 40 Hz, compared with a patch electrode which was reliable up to 70 Hz. This reduction in fidelity at higher frequencies is primarily due ChR2 expression and channel kinetics (Arenkiel et al., 2007; Boyden et al., 2005; Ishizuka et al., 2006; Li et al., 2005; Wang et al., 2007; Zhang et al., 2006). In addition, they showed that increasing the intensity of light from 0.1, 0.2, and 0.3 mW/mm^2 increased the firing rate of a single unit (neuron) during 500 ms stimulation pulses but could still drive bursts of activity when stimuli were delivered at 10 and 20 Hz. Surprisingly, although there are reports using DLP in isolated retina (Farah et al., 2007; Golan et al., 2009), cardiac (Arrenberg et al., 2010), hippocampal cells (Wang et al., 2007), and brain slice (Jerome et al., 2011), this technology has not been combined with MEA technology in neural culture. Application of this technology to MEA based recordings would significantly enhance this technology and open new avenues for the in vitro study of computation and plasticity.

This chapter describes the development of a DLP based system whose light source consists of red, green, and blue high intensity LEDs, whose output is powerful

enough to activate ChR2. The system can create arbitrary light patterns with maximum resolution of 480 x 320 pixels, with a pixel size of approximately 10 μm, and can present stimuli at 1KHz while rapidly switching between red, green, and blue light channels for photostimulation of ChR2 or Halo. Performance of the system is characterized including minimum pixel size to elicit a response, and relationship between the amount of evoked activity and stimulation parameters, including spot size, stimulus duration, and frequency.

DLP Device – First Generation

Construction

We first constructed a device that was able to project an image onto the face of an MEA with a target resolution of 10 μm (roughly the size of a single soma). For the DLP projector, we used an Optoma Pico PK102, a small handheld projector (often referred to as a micro projector) measuring 17.8 x 50.8 x 106.7 (H x W x D). Technical specifications of the PK102 are listed in Table 4-1. To achieve the proper image magnification, the integrated lens was removed from the projector and the image was directed through a light collimator taken from a Nikon Biophot microscope (Nikon, Sendai Japan). The resulting device is shown in Figure 4-1, with the projector and lens assembled with sheet acrylic. When an image from this device was projected onto an MEA, it produced a single pixel size of approximately 10 μm, our target resolution. An example of the display is shown in Figure 4-3 in which an image of the University of Florida Gator (University of Florida, Gainesville Florida) mascot was projected directly onto the face of an MEA.

Issues

While this first generation of our device accomplished our first primary goal in terms of pixel size, there were significant shortcomings. First, the DLP device has no analog output, such as a sync out, with which we can sync light presentation with neural recordings on the MEA. Secondly, the speed of light application was not ideal. It was determined that the minimum light application for a single pixel was about 15 ms. While this is quite fast and approaches effective stimulation durations, faster stimuli are desirable for plasticity or HFS studies, where minimum duration between pulses should be on the order of 1 ms. Finally, the DMDs must cycle through the red, green, and blue LEDs (color output is interlaced) during projection. This results in very brief (< 10KHz) periods where no energy can delivered. Higher temporal precision is required.

DLP Device – Second Generation

The second generation of the device was considerably more complex than the first. It is based on a customizable embedded Linux system controlling a small DLP projector via HDMI output. The output is then passed through a 4x objective lens to demagnify the image, and presented directly onto the face of the MEA.

Hardware

The BeagleBoard embedded Linux system is a single board computer produced by Texas Instruments (Texas Instruments, Dallas Texas). It is specifically designed for open source development projects, and is an attractive option due to its low cost and low power. The heart of the system is an ARM Cotrex-A8 CPU running Linux (commonly used in cell phones, PDA, etc), and includes DVI/HDMI, S-Video, 2 USB, Ethernet, MicroSD, RS-232, and 2 stereo ports. It runs at 600 MHz and has an internal

memory of 128MB. It only requires 5V (2W) to run, and can therefore be run off of a USB connection or external 5V supply, without a heat sink.

The DLP that we used is the Texas Instruments DLP® Pico™ Projector Development Kit Version 2.0 (Texas Instruments, Dallas Texas) that has been designed for development projects. It uses the miniature DLP 0.17 HVGA DMD chipset, which has a 0.17 inch diagonal DMD array where each mirror is 7.56 micrometers^2, and has an HDMI input that can be connected directly to a computer, or in our case the HDMI output of the BeagleBoard. The device has a refresh rate of over 1.2 kHz, which corresponds to structured light application of less than 1ms. This is compared to 60Hz (~16ms) of the first generation device. Technical specifications are listed in Table 4-2. Due to a high level of electrical noise that was observed from the projector, it was housed in an aluminum enclosure (Box Enclosures, Lake Bluff Illinois) with a small hole drilled for the light path, which eliminated electrical noise during recordings on the MEA.

The computer that we used to control the system is an Intel Pentium 4 - 2.4 GHz processor running Ubuntu, an open source Linux operating system. This computer communicated directly with the BeagleBoard through a serial RS-232 protocol. The images were then processed on the BeagleBoard, and the output was sent through the HDMI cable directly to the DLP projector, where it was demagnified through the lens onto the MEA. Additionally, a custom BNC connector was added to the BeagleBoard to serve as a sync pulse that would tell us precisely when we were applying light, which we could then compare to the neural activity to determine if it was stimulated or endogenous.

Software

The software to control the DLP is a command-line program written in C with a python (Python Software Foundation) graphical user interface (GUI). In the command line portion, individual commands can be entered which will be queued into the DLP program. These commands include setting light color, setting pixel/square size, and setting the duration for light application. A full list of available commands is shown in Table 4-3. Additionally, you can load prewritten programs into the queue on the Linux system to conduct complex photostimulation patterns.

The python GUI is an extremely intuitive and useful addition to the software package, shown in Figure 4-3. It consists of an image of an MEA layout on the left, and a list of previous commands on the right. There are buttons for “Image”, “Immediate Mode”, “Help”, and “Upload”, as well as a toggle switch to change between pixel mode and rectangle mode. These will be described in more detail later.

Upon starting the program, an alignment routine is run. During this process, a crosshair is projected through the DLP onto the MEA. Looking at the output through the microscope camera, the user is asked to pick four distinct locations by moving the crosshair and clicking (e.g. four of the electrodes), followed by the escape key. The user then selects the same four locations on the MEA layout for florescence image within the GUI to create the coordinate transformation between image and MEA coordinate systems. Now, by clicking a single point on the image in the GUI, that location is translated into DLP coordinates, which can be loaded into the command line. The “Image” button allows the MEA image in the GUI to be changed. For example, one could load a fluorescence image of a particular array to identify opsin-expressing cells, then easily point and click on those cells to stimulate or create a program for later

download. When “Immediate Mode” is on, any command entered into the GUI will be sent to the DLP immediately. If immediate mode is not selected, commands will be accumulated in a text buffer displayed in the right-hand column of the interface that can be downloaded, saved, or cut and pasted into a text. The program defaults to pixel mode, where clicking on the MEA image will project a single pixel onto the culture. When rectangle mode is selected, one can click and drag on the MEA image to define the coordinates of the rectangle and a large rectangle the size of the selected region will be stimulated, rather than a single pixel. Finally, the “Help” button will provide help with the interface, and upload allows a list of commands to be uploaded directly into the command-line queue for execution.

Assembly

In addition to the light application, there were several other crucial parts to the system. The first is that the device had to be mounted on a microscope. Because the resolution of the light being applied is so small, a microscope is needed to visualize light patterns, as well as for the alignment process. We used an American Optical Biostar microscope (American Optical, Now out of business), with the eyepiece removed and replaced with an Apple iSight (Apple Inc., Cupertino California) webcam with a dark filter to prevent camera CCD saturation.

The second crucial element is an environmental chamber. These chambers maintain the temperature (37˚C) and CO_2 (5%) levels to create an environment similar to the incubator. This is critical to maintain stable recordings over long periods and ensure culture health for repeated sessions. We accomplished this with a box made of 7/16 inch clear sheet acrylic, covered in space blanket for insulation. The setup is shown in Figure 4-4, with important elements highlighted with white arrows. The top of

the environmental box is removed to provide a better view the recording system and DLP photostimulation device. The bottom of the environmental box (3) keeps temperature and CO_2 constant, which is pumped in via tubing (1). Commands entered on the computer are translated by the BeagleBoard (2) and sent to the DLP projector (4) housed in a blue aluminum case. This output is passed through a lens (7) onto the MEA (5). Electrical output of the MEA is read by the recording rig (6) and sent to a different computer. A webcam (8) is used to monitor light application in real time.

Figure 4-5 shows the view of the MEA through the camera, as a 4x4 pixel square is presented to a random site on the MEA. This blue spot is roughly 40 square micrometers.

Power

The projection intensity of light was measured with a ThorLabs S121C optical power meter, and read with a ThorLabs PM100D (Thorlabs LTD, Cambridgeshire UK) energy meter. The power was read at 473 nm (blue light) for squares of varying sizes. Pixel size was considered 10 micrometers for power density calculations. Because the projected area is not completely dark when the LED is on, the background light was measured at 11 μW, and subtracted from all measurements. Power resolution was 0.1 μW.

Total power and power density for each size pixel block is shown in Figure 4-6. The x-axis represents the length, in pixels, of a side of the applied square. A 1x1 pixel square showed no measurable increase in light power over background, likely because the power produced was below the minimum power resolution of the detector, 0.1 μW. A 3x3 pixel square showed a 0.1 μW increase, which translates to 0.11 mW/mm^2. Recall the minimum spiking irradiance of ChR2 as 0.1 to 1 mW/mm^2. (Degenaar et al.,

2009). Square sizes of 7x7 to 60x60 pixels all showed over 0.25 mW/mm^2 power density, well within the lower levels of activation. After this point, power density decreases with any further size increase. We hypothesize that further increases in square size produces the same total power, but spread out over a larger area, thus a lower light power density.

Table 4-1. Technical specifications of the Optoma Pico PK102

Technical Specification	Value
Size (mm)	17.8 x 50.8 x 106.7 (H x W x D)
Brightness	11 ANSI Lumens
Contrast Ratio	2000:1
Resolution	800 x 600
Internal Memory	4 Gb
Video Input	Composite, Component, VGA
Horizontal Sync	31.5 kHz
Vertical Sync	60 Hz

Table 4-2. Technical specifications of the DLP Pico Projector Development Kit V.2

Technical Specification	Value
Size (mm)	44.8 x 67.4 x 14.2 (H x W x D)
Brightness	7 ANSI Lumens
Contrast Ratio	1000:1
Resolution	480 x 320
Vertical Refresh	1440Hz during single 1-bit color mode
Internal Memory	4 Gb microSD card
Video Input	DVI-D RGB888, VGA

Table 4-3. List of commands available in ndlp

Command	Result
SETPX x y	Set pixel block size (default 4)
SETCLR r g b	Set draw color in rgb values
SETDURMS ms	Sets stimulus duration in ms(max 1000) (default 200)
SPIX x y	Draw pixel (of setpx size) at x y location (for stimdur)
SRECT x y w h	Draw rectangle at center x y with width and height
SLINE x1 y1 x2 y2	Draw line from start point x1 y1 to end point x2 y2
DLYMS ms	Set delay between commands in milliseconds
REPEAT n	Repeat current command stack n times
TESTP n ms	Test random location pixels, n times with ms delay
CROSS x y	Draw crosshair at coordinates
EXEC	Execute current command stack
Backlight w/r/g/b	Turns on/off backlight of color white/red/green/blue
GRID on/off	Turns grid on/off for alignment purposes
RESET	Clear current command stack
CLR	Clear current command prompt
SHOW	Show current command stack
SETMODE 0/1/2/3	Set color mode to RGB/R/G/B

Figure 4-1. First generation DLP device. The DLP projector was mounted on a piece of 7/16” sheet acrylic with 2 screws to adjust the angle of the projector. The lens is held in place directly below the DLP projector by an acrylic housing. This system can project a 640x480 pixel image but is limited in terms of the frequency at which stimuli can be presented.

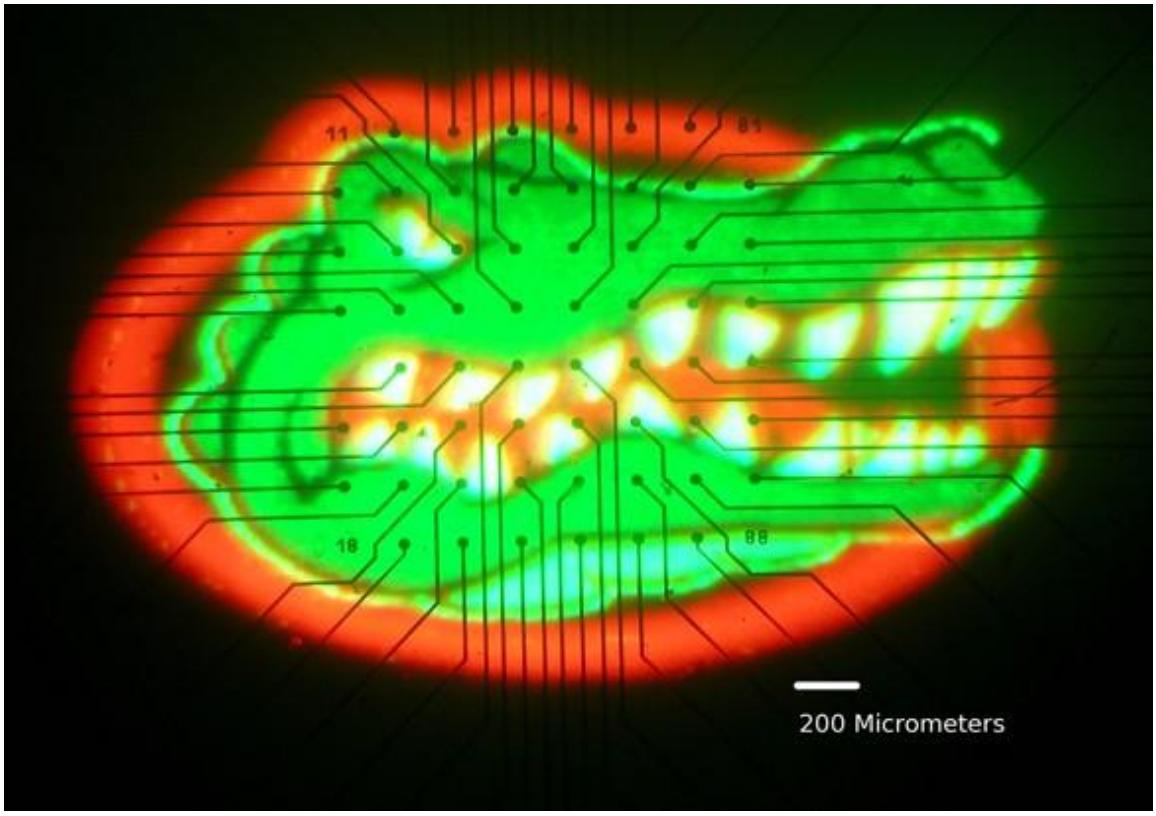

Figure 4-2. Image projected onto an MEA from first generation device. An image of the University of Florida Gator mascot (University of Florida, Gainesville, Florida) was projected through the device onto the face of an MEA. This image produced pixel size of approximately 10 μm, our goal size as this is roughly the size of a single neuron soma. The MEA electrodes are 30 μm in diameter with 200 μm between each electrode.

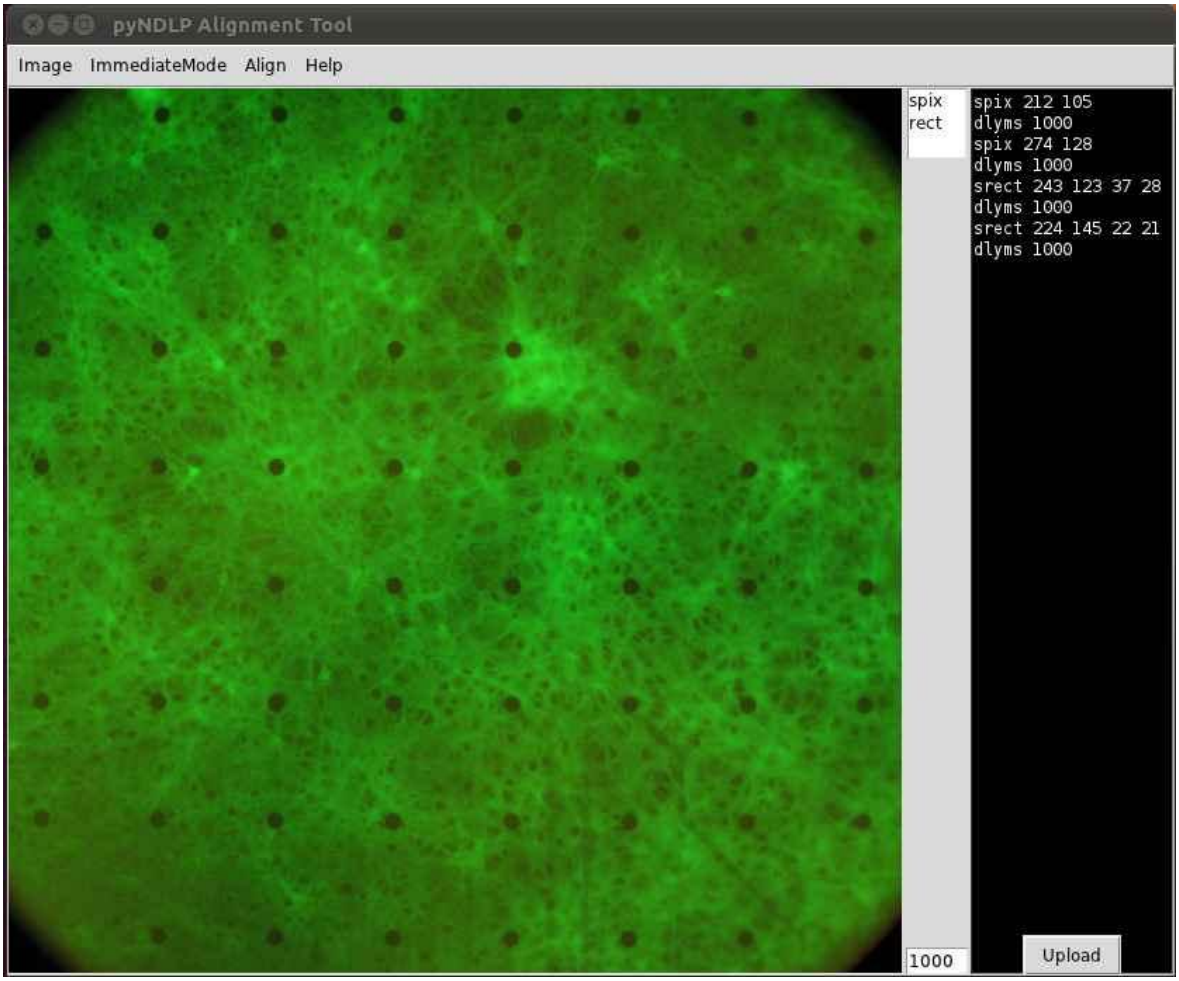

Figure 4-3. Graphical user interface. The MEA layout is shown on the left and the column on the right lists recent commands. After the alignment process, clicking on the image of the MEA will translate this location to DLP coordinates and project a pixel or rectangle to the desired location.

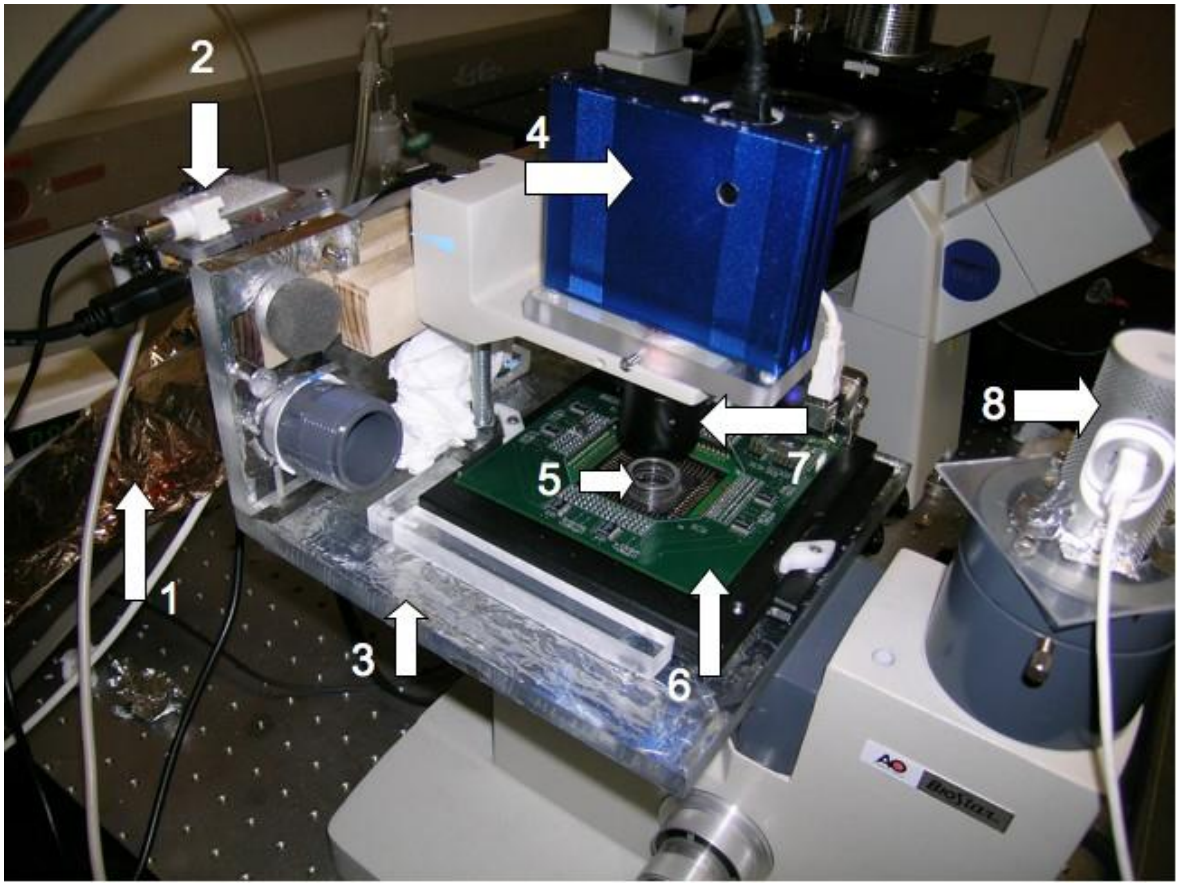

Figure 4-4. Second generation DLP device. This picture shows the entire stimulation and recording setup, with important elements shown with white arrows. (1) Environmental controls regulate air entering the recording box. (2) BeagleBoard computer. (3) Bottom half of the environmental box. The other half fits on top to prevent the escape of air. (4) DLP projector housed in aluminum casing. (5) MEA culture. (6) MEA recording rig. (7) Lens used to demagnify DLP output. (8) Webcam visualizes microscope output for real-time monitoring.

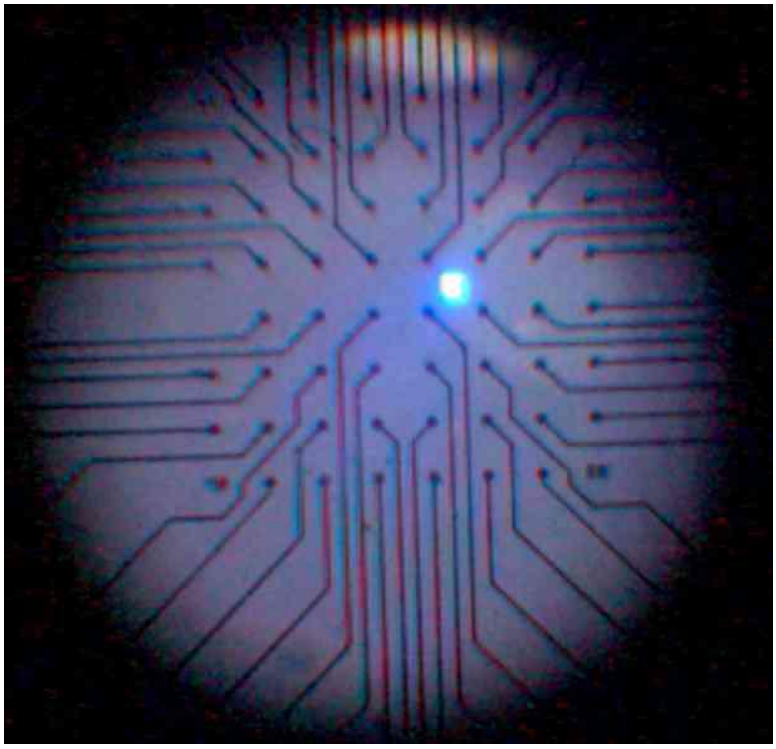

Figure 4-5. DLP generated pixel block projected onto an MEA by the second-generation device. Here the presentation of a block is seen via the microscope camera. The block is 4x4 pixels, approximately 40x40 μm.

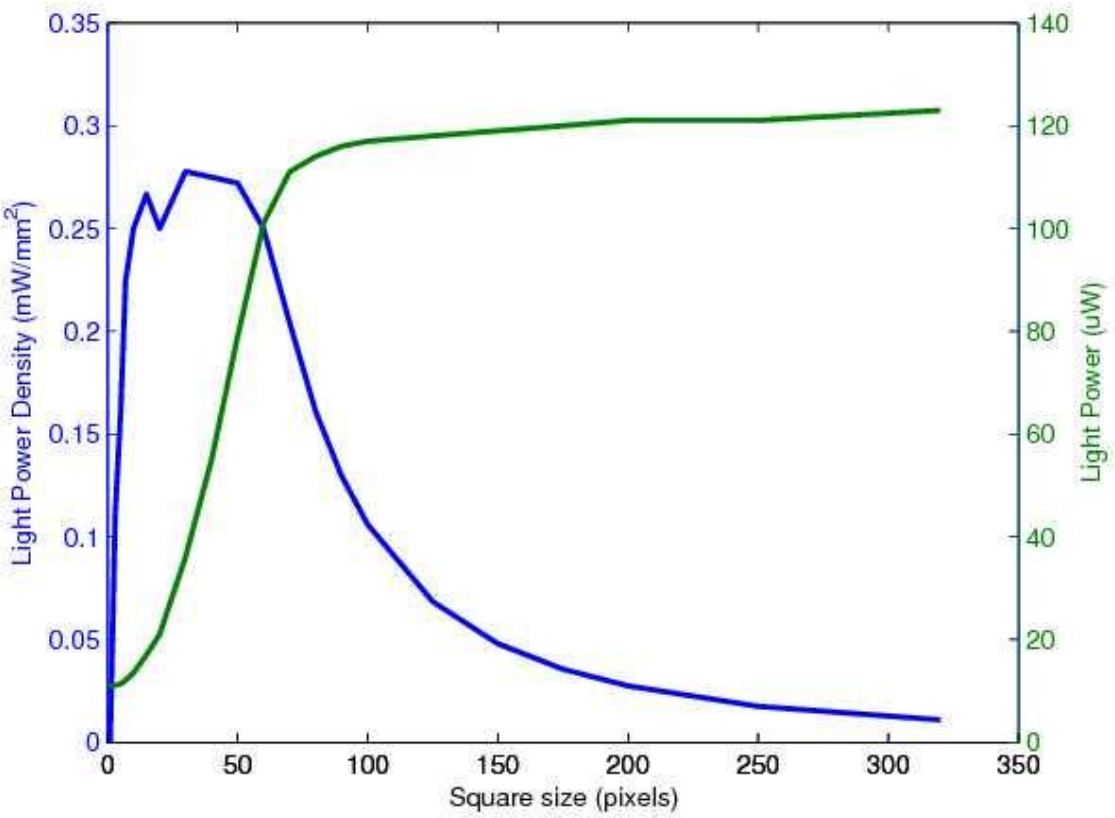

Figure 4-6. Analysis of light power density function for the second generation device. Green curve shows total light power output as pixel square size is increased. A single pixel showed no noticeable power difference over background. Blue curve shows light power density, where each pixel was equal to 10 square micrometers. Light power density peaks at 0.27 mW/mm^2 at a 30 pixel (300 µm) square. Squares of 10 to 60 pixels (100-600 µm) show optimal power density.

CHAPTER 5
DLP EXPERIMENTS

To characterize and test the second-generation system, our first aim was to demonstrate basic feasibility by showing that illumination could successfully evoke activity. Our second aim was to determine the amount of light in terms of surface area and duration needed to elicit a response from the network, and characterize that response. Finally, we tested the ability of the system to reproduce burst suppression investigated earlier with bath LED application. For this experiment, we employed random site, high frequency light presentations to attempt suppression of network bursting activity.

There were three experiments that were performed using the DLP to control neural activity in ChR2/YFP expressing cultures on MEAs. Experiment 5-1 divided the network up into four quadrants and determined whether a unique response could be produced by photostimulation of each quadrant. The second experiment (Experiment 5-2) parametrically manipulated the spot size (block size in pixels) and duration of each photostimulus to determine optimum block and duration parameters and characterize the response. Finally, Experiment 5-3 reproduced high-frequency random site photostimulation manipulating block size and duration.

Experiment 5-1: Quadrant Analysis

Large quadrant based photostimulation was employed to determine whether a response could be evoked with the light intensities of the second-generation projector, and also to examine whether photostimulation at each quadrant would produce distinctly different output patterns. Each quadrant was stimulated 20 times in blocks with the order of quadrants randomized. The durations used for quadrant

photostimulation were 50, 100, 250, and 1000 ms. The time between stimulations was based on the culture's intrinsic (spontaneous) burst rates which were 31.2 ± 22.2 bursts per minute and a mean burst duration of 135 ± 101 ms. The age of each culture was 14 days at the time of this experiment (n=2).

Results

Quadrants were arbitrarily labeled for clarity with the top left quadrant as 1, the top right as quadrant 2, bottom left as 3, and the bottom right as 4. First a visual analysis of the quadrant response was performed. After each quadrant was stimulated 20 times, the culture-wide response was averaged over all stimulations. A PSTH was then created for each trial. An example of the evoked activity during photostimulation at each quadrant is shown in Figure 5-1 (the stimulated quadrant is shaded in the figure). Quadrants were stimulated 20 times for 1 second and the average histogram was taken, using 20 ms bin size. Photostimulation of quadrants 2, 3, and 4 produced a clear increase in activity relative to the responses in these quadrants during trials in which other quadrants were stimulated, while photostimulation of quadrant 1 produced a very small increase in activity.

Because the area we are stimulating for each quadrant is so large, induced activity typically propagated into a burst. Therefore, to determine if activity in the photostimulated quadrant was increased, we must compare it not only to natural activity, but also to bursts that began elsewhere in the culture. This was done in Figure 5-2, where the white column represents the spike rate of a quadrant during natural activity, the grey column represents the spike rate of a quadrant while a different

quadrant was being stimulated, and the black column represents the spike rate of a quadrant when that quadrant was being stimulated.

According to this metric, if the DLP caused a substantial increase in response on the stimulated quadrant, the column representing stimulated activity (black) should be larger than both the column for unstimulated (grey) and natural activity (white). Conversely, if network-wide activity is primarily bursts and the DLP has had no spatial effect on activity, than unstimulated (grey column) will be equal to or larger than stimulated activity (black column).

Spike rates for all four quadrants increased above natural activity, even when that column was not being stimulated (grey). This means that there was substantial network-wide bursting caused by the quadrant stimulation. But during photostimulation (black), spike rates in all four quadrants showed an even further increase in activity relative to unstimulated activity, representing direct spatial activation via DLP.

We applied the cross-trial similarity (CTS) metric to the quadrant analysis, shown in Figure 5-3. This analysis determined the similarity of responses across different trials of the same stimulation. The relative values of this metric are not important, simply the shape of each particular curve. The data from the 50 ms and 1000 ms appears chaotic, and there is not significant change in the mean over time. The 100 ms and 250 ms curves, however, show a very clear upward trend in the early phase and level off after about 100 ms. This would indicate that a stimulation of at least 100 ms is necessary to produce highly similar responses. Why the 1000 ms curve does not increase during this period is unclear.

We then applied a support vector machine analysis (SVM) classification algorithm (Cortes and Vapnik, 1995) to the quadrant data that attempted to classify evoked activity by stimulus duration, shown in Figure 5-4. Indeed, we found that quadrants presented at 100 ms and 250 ms had excellent classification percentages above 95% while the 50 ms and 1000 ms produced responses that were more difficult to classify, with the 1000 ms accuracy at 35%. This is compared to a random shuffle control (white bars), whose performance was near 25% representing chance levels across four potential quadrants.

Discussion

This experiment demonstrated that photostimulation from the DLP system can successfully generate activity within the neural network in a spatially controlled manner. We observed significant increases in spike rate in the stimulated quadrant, well above both natural activity and induced activity seen when another quadrant was stimulated.

Analysis of the pattern of evoked activity following stimulation of each quadrant revealed a unique relationship between which quadrant was stimulated and the pattern of spiking produced by the network. This unique relationship between inputs and outputs is known as the separation property, in which input (stimulation) to distinct stimulus locations evoke distinctly different, separable patterns of spiking as output (Dockendorf et al., 2009; Kermany et al., 2010; Pan et al., 2009; Parodi et al., 1998). This is an important property particularly in terms of the formation or retrieval of a neural code (Kermany et al., 2010).

We found that DLP photostimulation produces uniquely discriminable outputs, and that there is a particular range of durations when output responses are reliably more similar. Surprisingly, output discriminability was lower at longer (1000 ms) stimulus

durations. This may be explained by the CTS values that were taken for each stimulus duration, showing that photostimulation of 100 and 250 ms showed a significant increase in cross-trial similarity over time, while the 50 and 1000 ms durations showed no such increase.

The separation property is also evident when considering the process of spontaneous burst generation and propagation. First, a single neuron fires that has a large enough influence on the activity of other neurons to induce further activity. These neurons activate still more neurons, and this continues until a full burst has occurred. The precise spike timing of the propagation of activity through the network is unique to different inputs. This phenomenon has also been observed during burst onset in which a handful of neurons typically lead the activity at the beginning of a burst (Pan et al., 2009; Cohen et al., 2008; Eckmann et al., 2008). During each burst, which neuron or neurons within that pool lead the onset of the burst also partially determines the spatiotemporal pattern of spiking observed across electrodes. Indeed, often a culture will have only a small number of spontaneous burst patterns or motifs that repeat for many hours (Gross et al., 1999; Raichman et al., 2008; Wagenaar et al., 2006) and can be modified via plasticity manipulations such as tetanic pulse trains (Madhavan et al., 2007).

Experiment 5-2: Parametric Spot Size Analysis

In the next experiment, we specifically manipulated the area of stimulation in conjunction with the duration of the stimulus, in order to determine what effects these parameters had on the magnitude of the response. Surface area was manipulated by presenting square blocks composed of 1x1, 3x3, 5x5, and 10x10 pixels to a single location over an electrode where neurons expressing ChR2 were observed. Durations

of 25, 50, 100, 200, 250, and 1000 ms were tested. Twenty stimuli were delivered for each combination of block size and duration. The interval between stimulations was culture-dependent and based on the spontaneous burst rate of the culture (n=3).

Results

The parametric spot size analysis was similar to that of the quadrants. We stimulated a neural population close to one electrode, and watched for an increase in the elicited activity on that electrode. Photostimulation of areas smaller than ~1 mm^2 never produced a network-wide burst, but rather produced only localized responses. We modulated the spot size and light duration to see what effect varying these parameters had on elicited activity. One of the areas that we had most success was a clump of cells directly next to an electrode, pictured in Figure 5-5. This clump expressed high levels of ChR2, as evidenced by the bright green throughout the cell cluster.

This clump of cells was stimulated for 1 second with a 15x15 pixel square (approximately 150 micrometers square). The activity evoked on the electrode near the clump was compared to spontaneous activity before stimulation began, shown in Figure 5-6, where the electrode of interest is shaded. This PSTH makes evident the difference in activity on the one particular electrode, while activity throughout the culture appears to remain unchanged. This was analyzed by taking the average spike rates for the stimulated electrode and for the rest of the culture, during both photostimulation and no stimulation. These data are presented in Figure 5-7, where a clear increase in spike rate is seen on the stimulated electrode. A small increase in culture-wide activity was not above standard error.

Using a 15x15 pixel square, we first modulated the duration that the light was applied, similar to the experiment performed in Chapter 3. The spike rate for 150 ms following each stimulus was binned (5 ms), smoothed, and averaged. Shown in Figure 5-8 is the average single-electrode response to photostimulation for each duration. This response is the electrical recording measured on a single electrode (not a network-wide average). We can see that as the duration of stimuli increased, the elicited response increases markedly. However, the time to onset of activity remains about the same throughout all durations. With this size pixel, time to onset was between 5-10 ms, similar to the results observed during bath light experiments earlier. The results suggest at least 25 ms of light is required to produce a consistent response at this square size. The control (blue line) consisted of 15x15 pixel applied to a different area of the array that had no cell growth. The results from this stimulus indicated little change in the rate of activity consistent with endogenous levels.

We then varied the size of the light spot being applied, and watched how the elicited activity was affected. We stimulated an area with 250 ms light in squares with a width of 10, 5, 3, and 1 pixel. The spike rates during 240 ms following photostimulation were binned into histograms (10 ms bins) and smoothed. The results, shown in Figure 5-9, indicates a significant increase in elicited activity as the area of light being projected is increases. Like duration, pixel size also affected the time of activity onset. As the size of pixel increased, the latency to observe a response from the network decreased.

Control stimulation was administered where a 15x15 spot was projected directly over an electrode on which no spontaneous activity had been observed. This spot was projected 20 times at a duration of 250 ms to ensure that elicited activity was not merely

a heat-based artifact. This artifact is the result of the Becquerel effect (after Henri Becqueral) in which uneven photo excitation of a metal electrode induces differential heating and hence currents (for example, see Cardin et al, 2010) and is generally associated with the high energy levels found with lasers. Of all electrodes that we investigated, none produced any spiking activity detected by our spike detector or observed visually during recording (6 electrodes over 3 cultures, data not shown).

Discussion

We found that modulating pixel duration has a direct effect on the amount of activity produced, while modulating pixel size affects both the amount of activity, and the time to onset of this activity. When modulating duration, you are simply changing the amount of time a photostimulus is applied but the spatial extent of light remains constant. Therefore it is reasonable that whatever neural population is being stimulated will respond to activation after a criterion amount of light application (here about 25 ms), regardless of the total duration. However, while manipulating pixel square size, we are physically changing the total area of neural membranes that was being stimulated. Because ChR2 is expressed throughout the cell including its processes, it is likely that the time to spike is a function of the total area of neural membrane that is being stimulated. The more membrane surface area that is stimulated (larger pixel size), the more ChR2 channels will open, and the faster a cell will depolarize. Conversely, a smaller pixel size will stimulate less neural membrane, causing a slower influx of ions through the ChR2 channels, and a slower time to initiate activity.

Single electrode stimulation using voltage (e.g., 600 mV, 200 s) or current pulses (e.g., 10 A, 200 s) typically generates a burst of activity that propagates throughout the tissue (Wagenaar et al., 2004). Interestingly, application of small-area stimuli generally

did not evoke a network burst. Instead the response was typically limited to the area of photostimulation. Large light area sizes of 1 mm^2 or more were required to induce a network burst. It is unclear why photostimulation of an area equivalent to the functional area of a single electrode produced a localized response, while electrical stimulation of that same electrode will produce a network-wide response. Perhaps one explanation is that, although the intensity of light produced by the DLP system is sufficient to induce spiking in soma, it may be insufficient for the antidromic excitation of action potentials through axons. The effect would be the recruitment of fewer neurons during the stimulus, and therefore the photostimulation would be less likely to evoke a network wide response.

Experiment 5-3: High-frequency Photostimulation

High-frequency stimulation (HFS) for burst suppression is an example of a practical application of this device for experiments in vitro. It has been demonstrated that high frequency electrical stimulation on multiple electrodes in a cyclical manner can reduce bursting in neural cultures (Wagenaar et al., 2005). This stimulation pattern was recreated using bath light application on ChR2-expressing cultures in chapter 3. Here we try a similar technique using a small spot size applied to random locations at high frequencies. For each culture (n=2), we start with 15x15 pixel spot size, which roughly mimics the size of an electrode effective area, with 100 ms duration at 10Hz. The size of the stimulation square was varied, along with stimulus duration and delay, and the resultant burst suppression examined.

Results

In Chapter 3 we were able to achieve significant burst suppression (with burst suppression ratios of up to 3) using high frequency LED stimulation. Because burst

suppression was originally done with distributed electrical stimulation (Wagenaar et al., 2005), we though using photostimulation in a distributed manner would produce even better burst suppression than bath light application. We essentially found that the opposite was true: that bath light application has far better burst suppression capabilities than distributed photostimulation. Figure 5-10 depicts the instantaneous spike rate over time (bin = 100 ms) during spontaneous, random site, and whole array photostimulation paradigms. Figure 5-10A shows the spontaneous activity of the array, where the sharp high-magnitude peaks represent bursts of activity. Figure 5-10B represents distributed photostimulation with a 150x150 μm spot size. During the period demarcated by the blue bar, random photostimulation sites were chosen and presented for 250 ms. There was no delay between stimulations. While the activity during light application appears mildly changed, it is not a significant change, and certainly there was little to no burst suppression. Figure 5-10C depicts the results from whole-array stimulation. During the blue bar, a 4.8x3.2 mm area was illuminated for 100ms and covered the entire array followed by a 100ms delay. Bursts were entirely suppressed during this period.

Burst suppression ratios were calculated for each square size, and are shown in Figure 5-11. Distributed photostimulation with small-square sizes resulted in low burst suppression ratios, while larger square sizes produced progressively higher suppression ratios. Finally, whole-array stimulation of 480x320 pixels produced the maximum amount of burst suppression, preventing bursts for the entirety of the stimulation phase.

Discussion

The results that bath light application is more effective at burst suppression than distributed high-frequency photostimulation were most unexpected. We attribute this to our theory that the DLP is not powerful enough to stimulate axons, but only soma. During electrical stimulation, an electrode stimulates all somas and neural processes around it. Because neural processes are so dense, it is likely that stimulation of a single electrode produces activity in many more neurons than just those surrounding the electrode (what we consider to be its affective area). However, reproducing distributed electrical stimulation using photostimulation block sizes similar to the functional area of an electrode (~150 μm^2) resulted in little to no burst suppression. Why would electrical stimulation have such larger burst suppression effects than photostimulation of the same areas? Again, the theory that the DLP does not have sufficient power density to stimulate activity in axons explains this phenomenon. We consider the effective area of an electrode to be roughly 150 μm^2 around the electrode, but it likely produces activity over a much broader area than that in response to electrical stimulation. DLP photostimulation, on the other hand, likely only produces activity in the somas of that effective area. This is simply not enough activity being produced in order to constantly deplete synaptic resources enough to prevent burst propagation. This level of activity can only be produced by large, network-wide stimulation at a high frequency.

General Discussion

Quadrant analysis was the most basic experiment to show that the DLP could effectively stimulate activity in one area of the MEA. There was a significant increase in the activity of the stimulated quadrant, far greater than changes seen in the activity of the non-stimulated quadrants.

The more interesting results were gained through the parametric spot size analysis, the basic characterization of the device. Through modulation of spot size and light duration, we saw that light duration did affect the number of spikes that were evoked but spot size affected both the amount of elicited activity and the time to onset of that activity. This explains the difference between effective durations between a small spot sizes through the DLP, and bath light application with an LED. An LED produced activity with light durations as small as 5ms, whereas the DLP needed a light application time of at least 25 ms to produce activity. The smaller the pixel size, the longer the light application needs to be in order to produce a response. For maximum spatial and temporal precision, we recommend a 7x7 pixel square presented for a minimum of 25 ms.

The burst suppression study also revealed a few surprises. We found that high-frequency whole-array photostimulation resulted in better burst suppression than random-site distributed stimulation. The proposed mechanism for the burst suppression produced by distributed electrical stimulation is a constant depletion of synaptic resources. Perhaps, because the DLP is only able to evoke activity in soma within the photostimulus area, stimulating a small area does not deplete enough synaptic resources to prevent a burst. However stimulating the entire array causes enough activity, both direct and via propagation, to exhaust synaptic resources and prevent burst propagation.

Through experiments 5-2 and 5-3, we have seen that the neural network responses to DLP-based photostimulation differ greatly from electrical stimulation. An electrical stimulation from a particular electrode will produce a network-wide burst,

whereas a light square applied to the functional area of that electrode will only produce a localized response. We hypothesize that the DLP light may not illuminate with enough energy, based on the small surface area of axons, to stimulate activity in neural processes. It can only stimulate activity in the somas of neurons within the photostimulation area. This hypothesis would be consistent with many of the discrepancies described above between stimulation via electricity and light, and will be tested further in the near future.

According to our light power density studies (Figure 4-6), any light square of over 100 pixels will have a power density below 0.1 mW/mm^2, the minimum light power reported to cause spiking in ChR2 expressing neurons. And yet we saw that robust bursting activity could reliably be elicited with these large square sizes. We believe this discrepancy arises from the difference between single neuron function and neural network function: a network has much more complex dynamics than a single neuron. Studies done to determine minimum spike irradiance for ChR2 involved patch-clamped single-cells (Degenaar et al., 2009), and light was applied directly to that cell via a microLED array until action potentials were reliably produced. Across a network, it may be possible that you do not need to directly cause an action potential to stimulate a burst. Applying a weak photostimulation across the network would raise the resting potential of the majority of excitatory neurons, making it far more likely that an endogenous action potential will trigger another network-wide burst. We believe this explains the discrepancy seen with minimum light power, but more work would be necessary to verify this hypothesis.

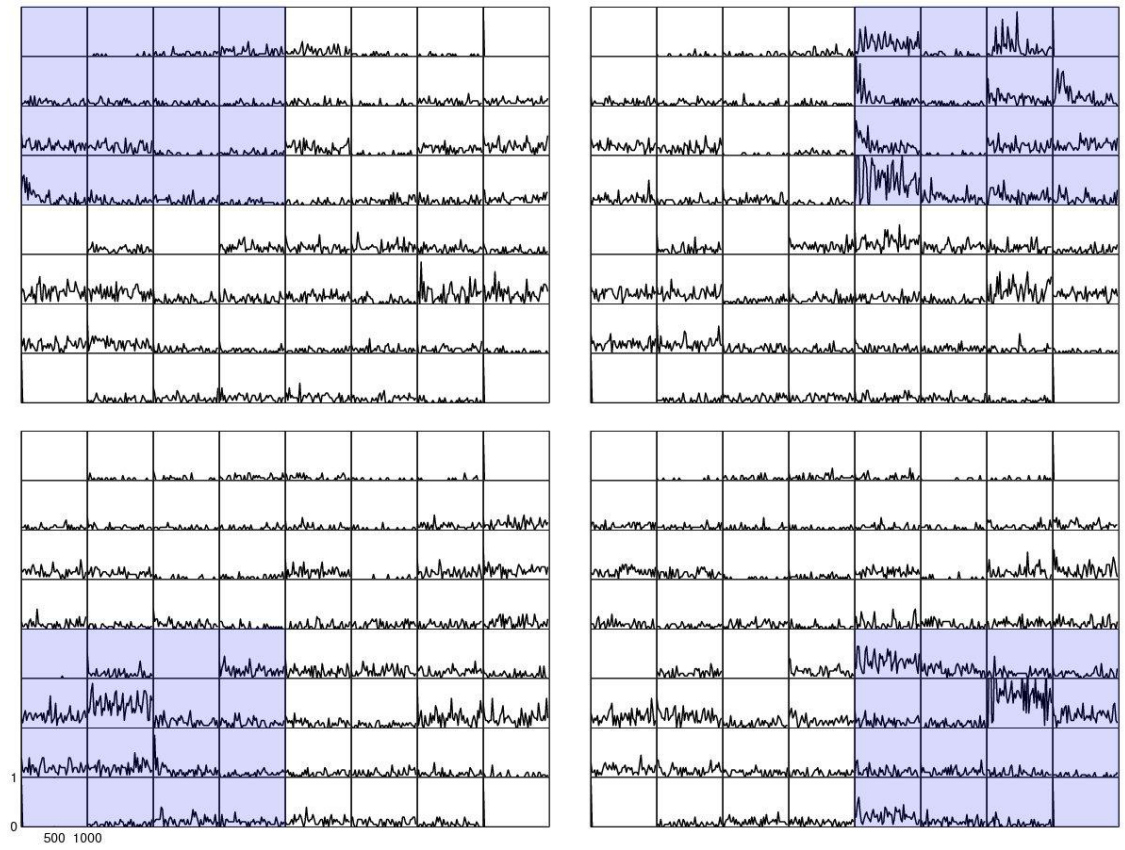

Figure 5-1. Full culture responses to quadrant stimulation. Each quadrant was stimulated 20 times for one second, and the average PSTH was taken over all stimulations using a 20 ms time bin. The shaded area represents the stimulated quadrant. Visual inspection shows that, with the exception quadrant one, the stimulated quadrant showed increased activity compared to when that quadrant was not stimulated.

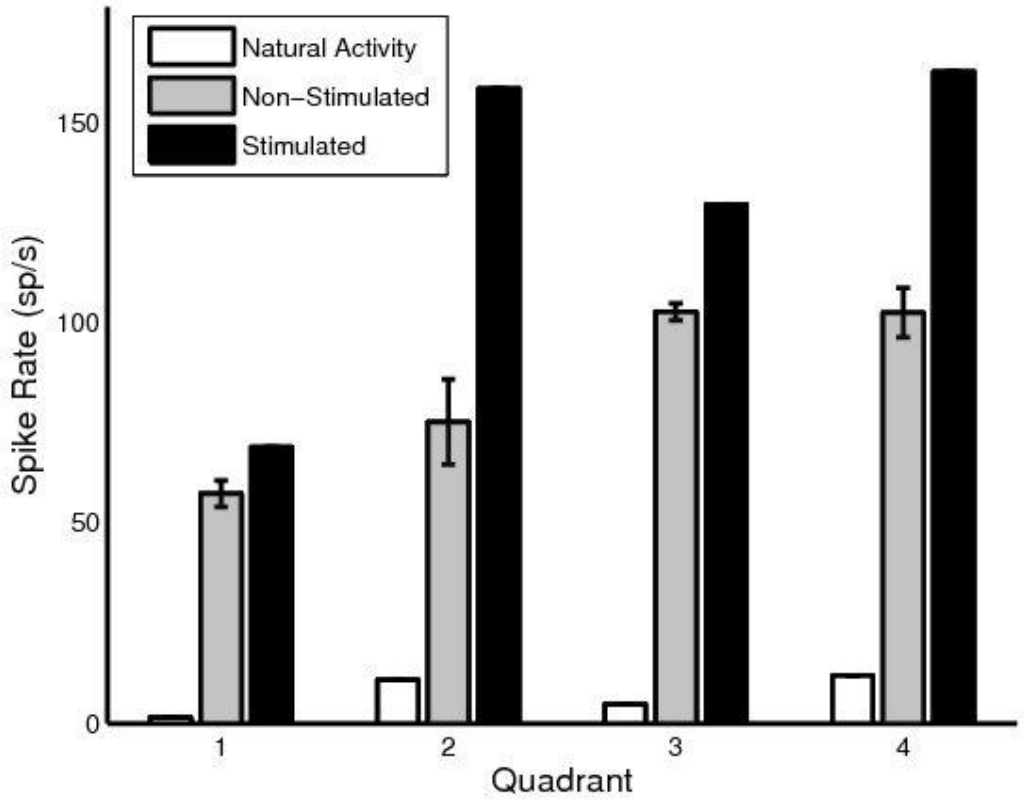

Figure 5-2. Average quadrant response to stimulation. The average spike rate was taken for each quadrant. Then, for each quadrant, the average was taken of the three trials in which that quadrant was not stimulated (white bar), and compared to the one trial in which that quadrant was stimulated (black bar).

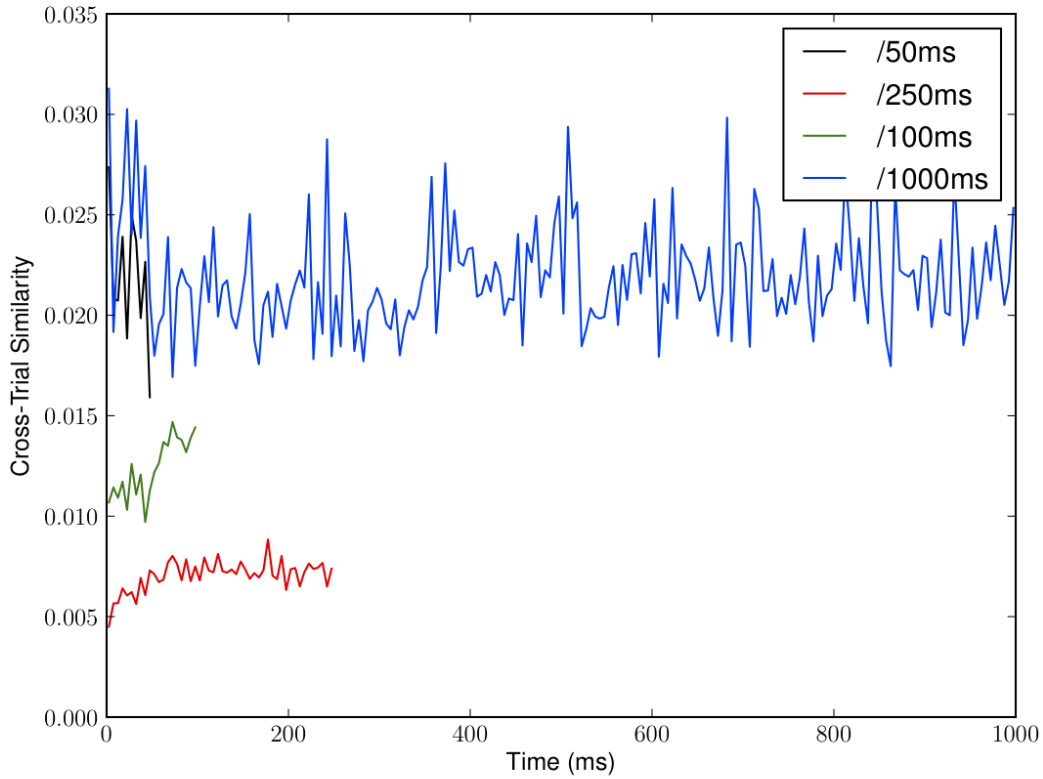

Figure 5-3. Cross-Trial Similarity of quadrant response to stimuli of different durations. Cross-Trial similarity (CTS) is a measure of the similarity of the responses to photostimulation between successive trials, and indicates which regions of time following the photostimulation are the most similar. For the quadrant experiment, the CTS begins to increase approximately 10 to 20 milliseconds following stimulus onset, reaches a peak at 75 ms and remains relatively stable thereafter. This suggests that the latter 75% of the stimulus produced a relatively consistent spatial and temporal response.

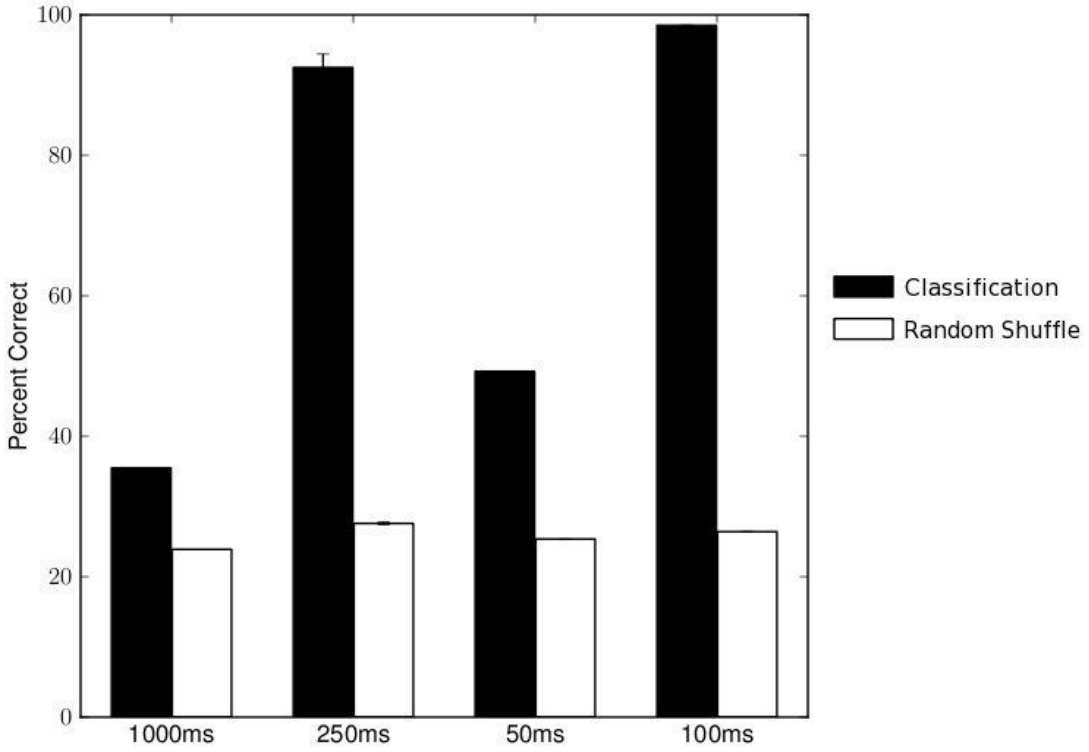

Figure 5-4. Input-Output classification of quadrant response to stimulus of different duration. A support vector machine analysis was used to classify outputs based on the duration of the stimuli as inputs. The mean percent correct classification and classification after trials had been shuffled (control) is shown for each duration. Chance level of performance with four potential classes (Quadrants) is approximately 25%. The discriminability of outputs based on inputs increases up to 250 ms, where performance declined to 35% at long (1000 ms) stimulus durations. This suggests that, like results from electrical stimulation at different electrode locations, stimulating different locations with light produced different and discriminable outputs.

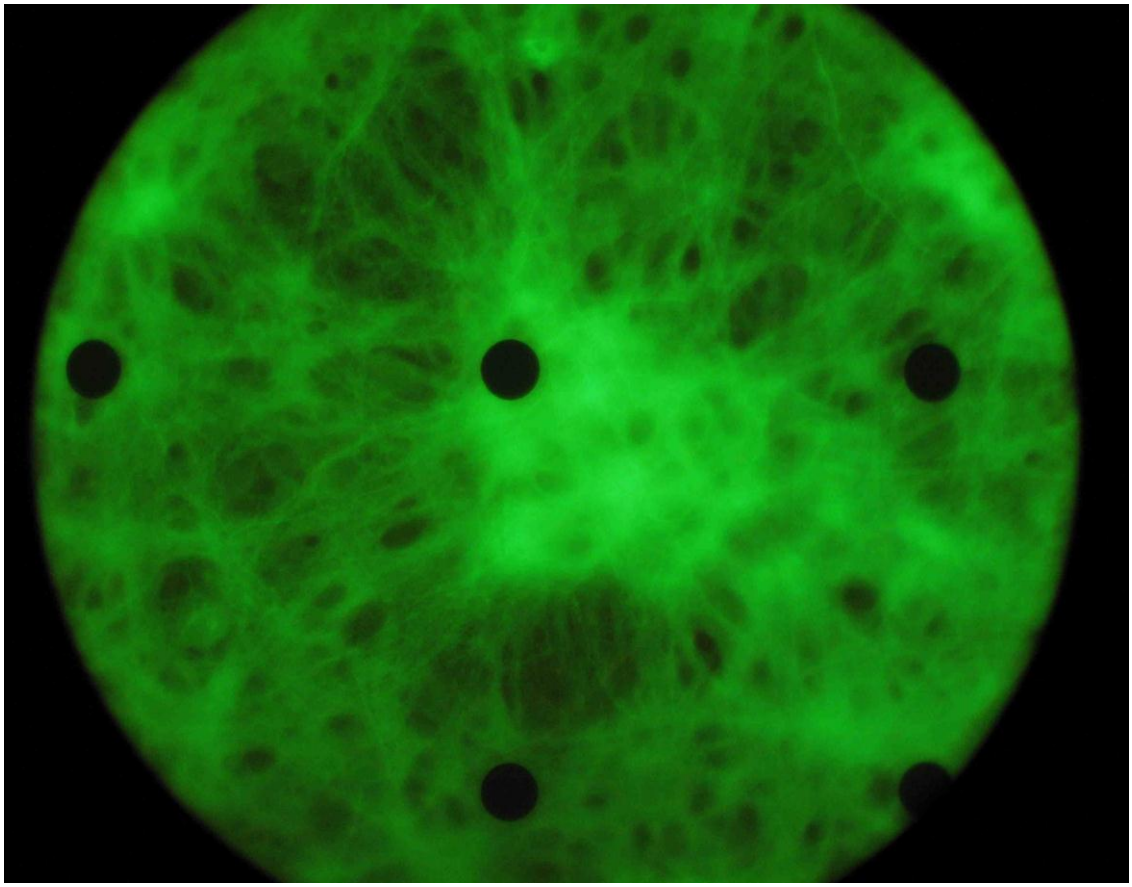

Figure 5-5. Fluorescent clump of cells used for spot size experiments. This group of cells had high levels of ChR2 expression (as can be seen from the strong fluorescence) and was located partially covering an electrode.

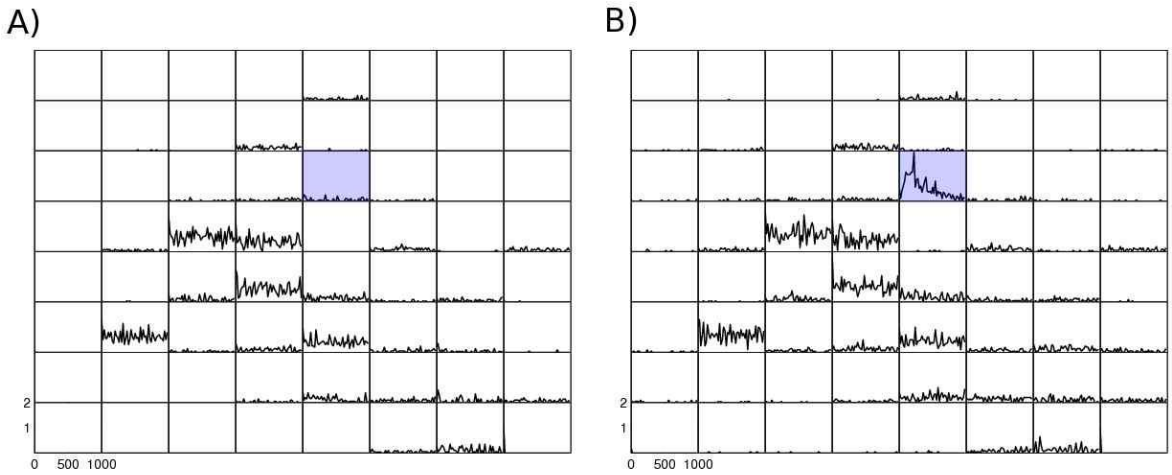

Figure 5-6. PSTH of single electrode optical stimulation. An area of 15 pixels (~150 μm^2) around one electrode (shaded) was stimulated for 1 second (B), and whole-culture activity was compared to that of no photostimulation (A). PSTHs are of 1 second with 20ms bin size. A clear increase in activity is seen on the stimulated electrode, with no noticeable increase in activity through the rest of the culture.

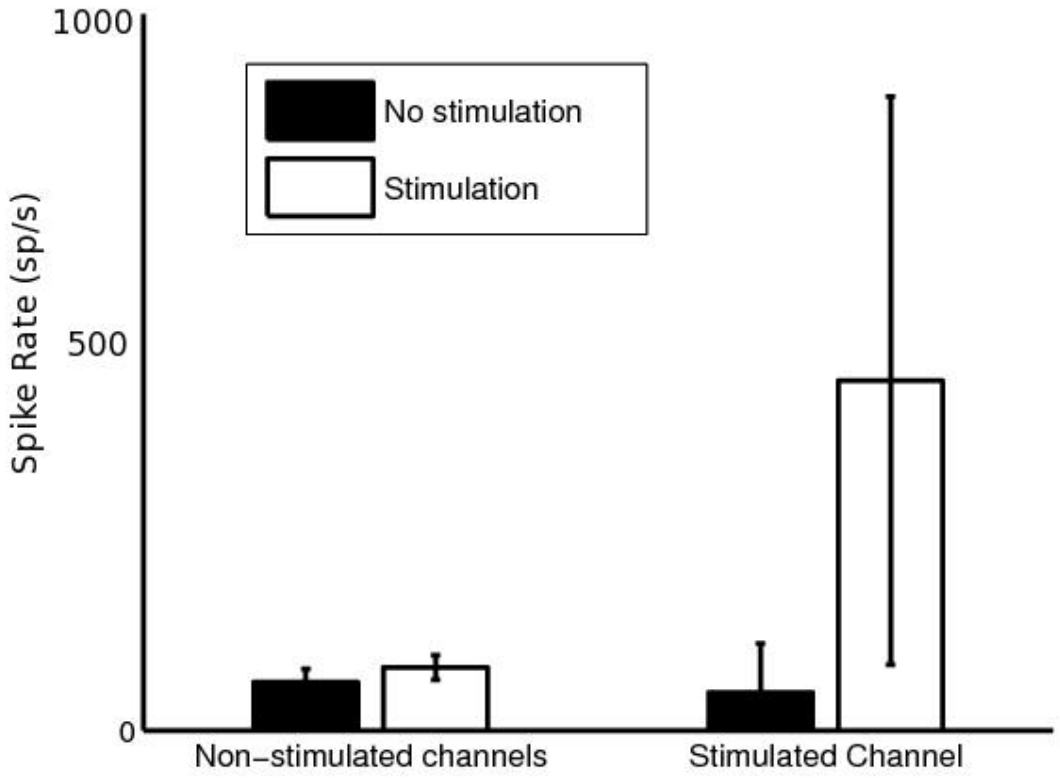

Figure 5-7. Average response to single electrode optical stimulation. Average response was taken for both the stimulated channel, and all non-stimulated channels averaged together. Again, a clear increase in the activity of the stimulated channel is seen, while no significant change is seen through the rest of the culture.

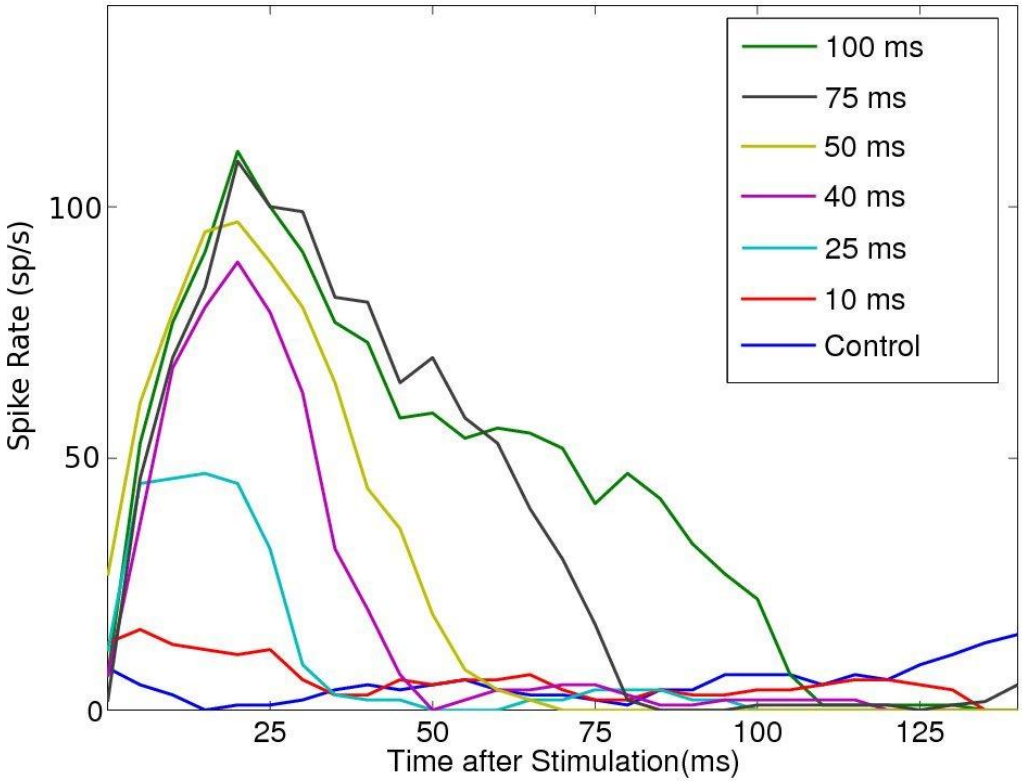

Figure 5-8. Single electrode response as stimulus duration was modulated. A 15x15 pixel (150x150 μm) square was presented at the same spot (clump of cells shown in Figure 5-5) at durations from 10 to 100 ms. Each evoked response was binned (10 ms bin width) and averaged over the 20 stimulations on a single electrode. As duration increased, the amount of activity that is evoked increases significantly, but the time to onset remained the same. For the control, a 15x15 square was projected for 100 ms onto an empty area of the culture that contained no cells and expressed no GFP. This control was to confirm that the elicited activity was not an artifact of the DLP light, and showed no elicited activity. The activity seen in the control represents baseline endogenous activity on that particular electrode. This data was taken from a single electrode on a single dish during photostimulation.

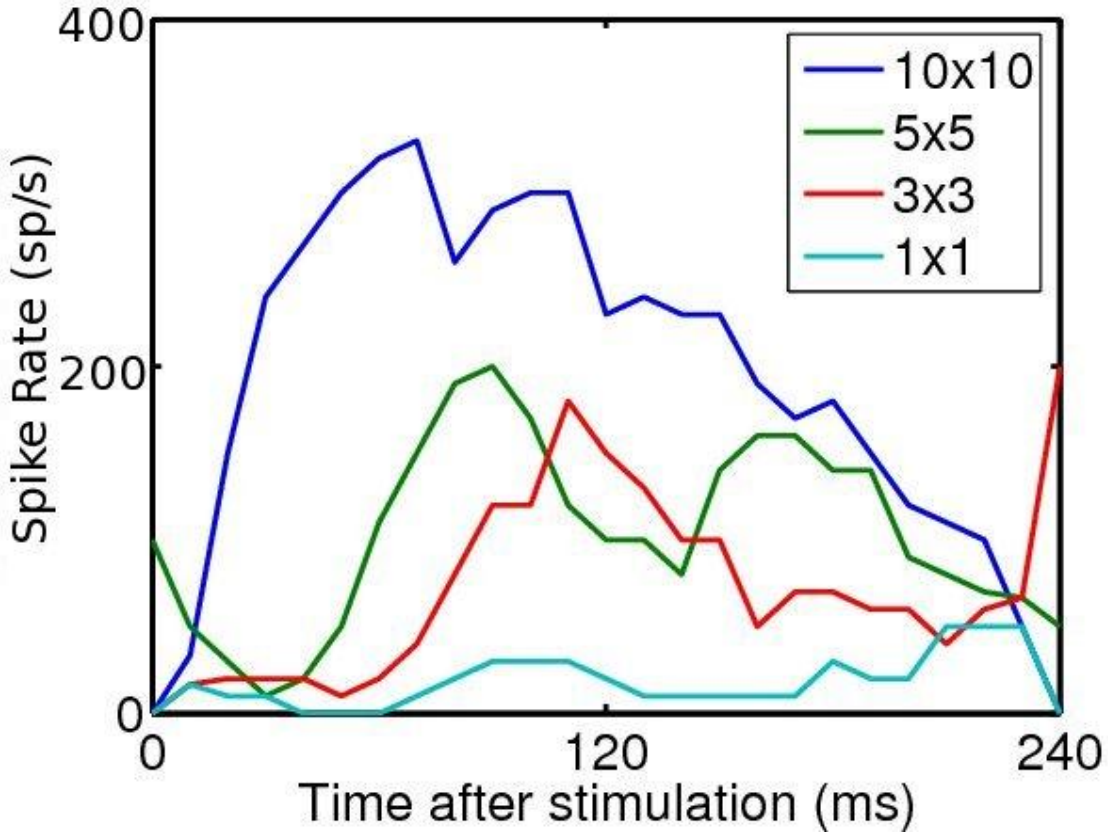

Figure 5-9. Single electrode response as stimulus size was modulated. Response from a single electrode on a single dish as it was photostimulated. Curves represent 240 ms during a fixed 250 ms light pulse of different pixel block sizes. As the size of the square is increased, the evoked response increases and latency to the onset becomes shorter. (Curves have been smoothed via the moving average method)

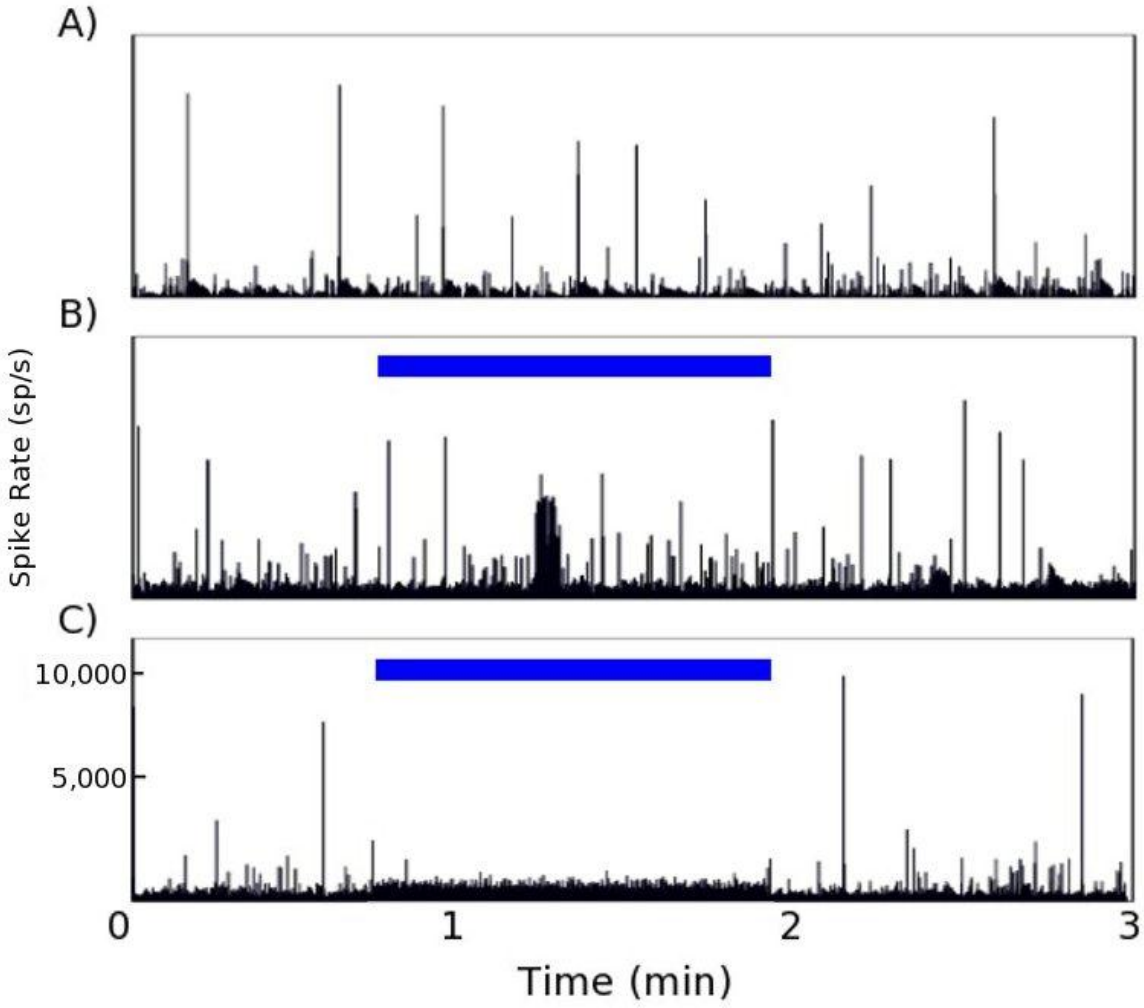

Figure 5-10. Burst suppression with varying sizes of photostimulation block. A) Spike histogram of natural activity over the entire array, using 100ms time bins. Large spikes represent bursts. B) Random-site photostimulation (250ms duration, 4 Hz) with a 15 pixel block size was presented for 80 seconds (highlighted with a blue bar). The photostimulation did not have significant burst suppression effects. C) Whole-array photostimulation (100ms duration, 5 Hz) was presented at the blue bar. Bursting activity was suppressed for the duration of the light presentation.

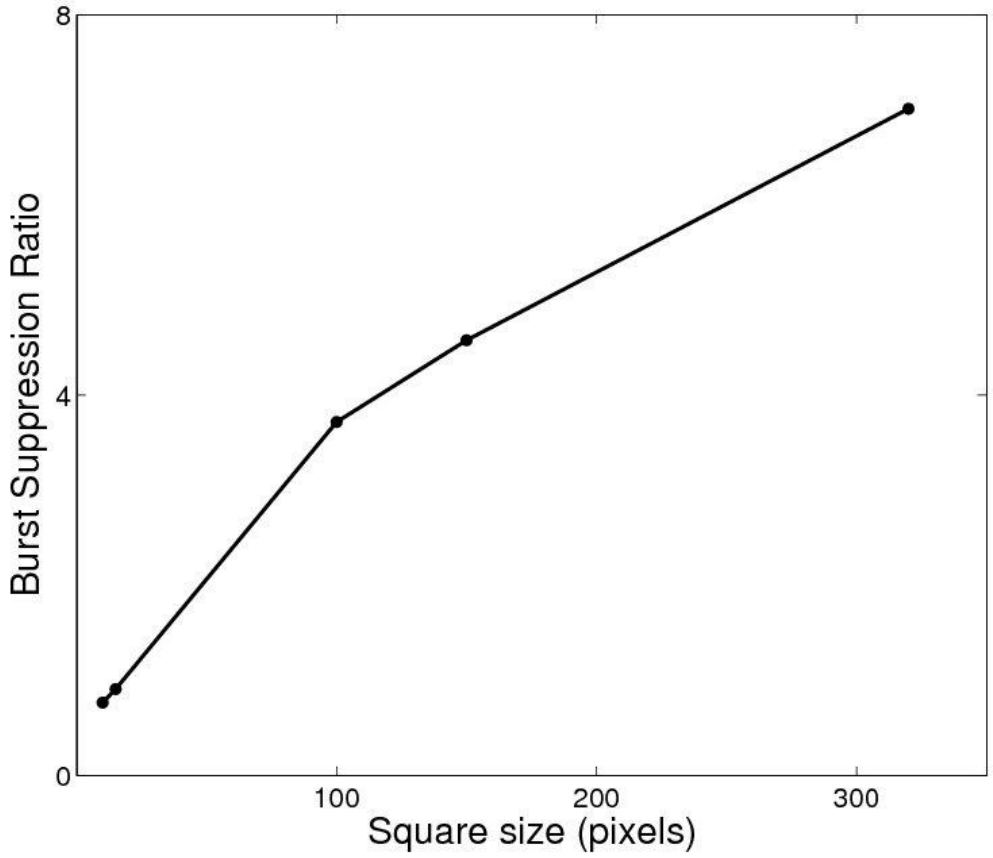

Figure 5-11. Burst suppression ratios for distributed photostimulation using different square sizes. We expected high-frequency, random-site distributed photostimulation with a smaller pixel size to show superior burst suppression, however we saw the opposite. Maximum burst suppression was observed when the whole array was stimulated at once. The final point represents whole-array stimulation, a size of 480x320 pixels (n=1).

CHAPTER 6
CONCLUSIONS

Discussion

For the past several decades, the field of neuroscience has been constrained by insufficient stimulation methods. While the ability to record neural activity as increased in both complexity and precision, the stimulation side of experimentation has never been sufficient. Lack of specificity, lack of control, and stimulation artifacts are but a few of the problems that have prevented researchers from better understanding the neural network. The introduction of optogenetics has provided a new and unique method for stimulating neural activity that bypasses many of the problems with conventional electrical stimulation. The use of genetic targeting methods provides an unprecedented level of specificity to determine which neural populations are being stimulated. It is safe for use both in live animals, using fiberoptics, and in cultures for more traditional neuroscience research. Additionally, because the stimulation and recording method differ, there is no stimulation artifact, which allows examination of the extremely high-precision spike timing immediately after stimulation. One significant hurdle to the area of optogenetics is a light application device that is as precise spatially as it is temporally, in order to control neural populations with single-neuron precision. There have been several attempts to create such a system, but all have had significant shortcomings. We feel that we have created such a system.

The device demonstrated here is incredibly versatile. We have created a multi-color light application system capable of 10 μm spot size, and sub microsecond precision. This allows unprecedented control over neural populations in both the space and time domain. The experiments shown in Chapter 5 are a very simple

demonstration of the capabilities of the device. Indeed, the possibilities available with the system are literally infinite: one can stimulate any neuron or group of neurons for any length of time in any order. This is a significant step toward total control of neural populations, and will doubtless be of interest to any neuroscience research team.

Future Work

This device can be used to further study many of the problems currently being investigated in neuroscience. A popular area of study using MEAs has been plasticity, particularly spike-time dependent plasticity (STDP) (Jimbo et al., 1999; Maeda et al., 1998; Ruaro et al., 2005; Shahaf and Marom , 2001; Tateno and Jimbo, 1999). These experiments generally stimulate two or more sites in rapid succession. In the past, the stimulation artifact has made these experiments particularly difficult. Our device will eliminate this problem, as well as providing additional control to stimulate neural populations not located directly over an electrode. MEA studies using hippocampal slices (Egert et al., 1998; Egert et al., 2002; Heuschkel et al., 2002; Novak and Wheeler, 1988; Oka et al., 1999) would be improved by allowing stimulation of small hippocampal pathways that do not lie directly on an electrode. Essentially, any experiments currently performed using electrical stimulation will be improved with our system through increased specificity and lack of stimulation artifact.

While our system provides a monumental improvement over current electric stimulation technology, there are still improvements that can be made to the current device. The biggest issue is the light power afforded by the current DLP projector. Our device's optimal projection parameters are a 7x7 pixel light area, projected for at least 25 ms. This is sufficient for our present studies, and is a great advantage over electrical stimulation methods, but a brighter light source within the DLP would provide greater

spatial and temporal precision. Our current lens assembly was obtained from a microscope, and is far larger than necessary. A proper casing could be constructed that housed a small lens within it. Additionally, the casing could hold the whole processor assembly, greatly increasing the portability and appearance of the device. The work shown within this dissertation only utilized the blue light mode, but genetic methods and discovery of new opsins will surely render the other color modes useful. Additionally, it may be possible to have specialty DLP devices manufactured containing LEDs of any color. The image resolution could easily be increased by passing the output of the DLP through another lens, if for example one wished to stimulate singe neural processes smaller than an entire soma. The user interface is currently slightly bulky, and could be improved to create a more user-friendly system. The existing software only allows a single shape, either square or rectangle, to be applied at any one time. In the future we would allow multiple types of shapes, including circles and hollow rectangles that could be applied simultaneously. All of these improvements would help this become a fully capable and autonomous optical stimulation device that researchers can easily program to any light application pattern that they see fit.

There are some experiments that could be done in the near future that would further demonstrate the potential of the device. These primarily consist of using cultures expressing Halo and the red light inhibitory capability of the system. For example, we could inhibit activity in certain quadrants with red light while allowing activity to propagate throughout the culture outside of the red light. We could shine a thin line of red light, an inhibitory “barrier” that would prevent burst transmission from one side of the barrier to the other. Determining the minimum width of barrier that

completely prevented cross-propagation would be a worthwhile endeavor. We could then form a small break in that barrier that would allow activity to propagate from one side to the other only through that channel. By placing this channel over an electrode, we could directly examine all activity that passed through the channel. We could form complex patterns of inhibition, and choose where and how we want activity to propagate. This would essentially accomplish the same goal as using lithography for patterned cell growth (Khademhosseini et al., 2004; Miller et al., 2006; Suh et al., 2004), a field that has experienced many challenges and difficulties. Finally, cultures expressing both ChR2 and Halo would show the full potential of the device, by allowing complete control to stimulate or inhibit activity of individual neurons at will.

It is clear that we are only beginning to understand the possibilities of optogenetics. This new technology has vastly changed the way neuroscientists can design experiments, and will surely continue to evolve throughout the next several years. The work presented here is simply a piece of the larger puzzle; a tool to allow more precise and focused investigation of neural systems. We feel that the results presented in this dissertation serve as a simple demonstration of the power of which the device is capable.

LIST OF REFERENCES

Abilez, O.J., Wong, J., Prakash, R., Deisseroth, K., Zarins, C.K., and Kuhl, E. (2011). Multiscale computational models for optogenetic control of cardiac function. Biophys J *101*, 1326-334.

Adamantidis, A.R., Zhang, F., Aravanis, A.M., Deisseroth, K., and de Lecea, L. (2007). Neural substrates of awakening probed with optogenetic control of hypocretin neurons. Nature *450*, 420-24.

Adesnik, H., and Scanziani, M. (2010). Lateral competition for cortical space by layer-specific horizontal circuits. Nature *464*, 1155-11560.

Akemann, W., Mutoh, H., Perron, A., Rossier, J., and Knöpfel, T. (2010). Imaging brain electric signals with genetically targeted voltage-sensitive fluorescent proteins. Nat Methods *7*, 643-49.

Albensi, B.C., Ata, G., Schmidt, E., Waterman, J.D., and Janigro, D. (2004). Activation of long-term synaptic plasticity causes suppression of epileptiform activity in rat hippocampal slices. Brain Res *998*, 56-64.

Alilain, W.J., Li, X., Horn, K.P., Dhingra, R., Dick, T.E., Herlitze, S., and Silver, J. (2008). Light-induced rescue of breathing after spinal cord injury. J Neurosci *28*, 11862-870.

Andrasfalvy, B.K., Zemelman, B.V., Tang, J., and Vaziri, A. (2010). Two-photon single-cell optogenetic control of neuronal activity by sculpted light. Proc Natl Acad Sci U S A *107*, 11981-86.

Aravanis, A.M., Wang, L.P., Zhang, F., Meltzer, L.A., Mogri, M.Z., Schneider, M.B., and Deisseroth, K. (2007). An optical neural interface: in vivo control of rodent motor cortex with integrated fiberoptic and optogenetic technology. J Neural Eng *4*, S143-156.

Arenkiel, B.R., Peca, J., Davison, I.G., Feliciano, C., Deisseroth, K., Augustine, G.J., Ehlers, M.D., and Feng, G. (2007). In vivo light-induced activation of neural circuitry in transgenic mice expressing channelrhodopsin-2. Neuron *54*, 205-218.

Arrenberg, A.B., Stainier, D.Y., Baier, H., and Huisken, J. (2010). Optogenetic control of cardiac function. Science *330*, 971-74.

Audouy, S., and Hoekstra, D. (2001). Cationic lipid-mediated transfection in vitro and in vivo. Mol Membr Biol. *18*, 129-143.

Ayling, O.G., Harrison, T.C., Boyd, J.D., Goroshkov, A., and Murphy, T.H. (2009). Automated light-based mapping of motor cortex by photoactivation of channelrhodopsin-2 transgenic mice. Nat Methods *6*, 219-224.

Bakkum, D.J., Chao, Z.C., and Potter, S.M. (2008). Spatio-temporal electrical stimuli shape behavior of an embodied cortical network in a goal-directed learning task. J Neural Eng *5*, 310-323.

Bamann, C., Gueta, R., Kleinlogel, S., Nagel, G., and Bamberg, E. (2010). Structural guidance of the photocycle of channelrhodopsin-2 by an interhelical hydrogen bond. Biochemistry *49*, 267-278.

Banghart, M., Borges, K., Isacoff, E., Trauner, D., and Kramer, R.H. (2004). Light-activated ion channels for remote control of neuronal firing. Nat Neurosci *7*, 1381-86.

Batista, C.A., Lopes, S.R., Viana, R.L., and Batista, A.M. (2010). Delayed feedback control of bursting synchronization in a scale-free neuronal network. Neural Netw *23*, 114-124.

Benabid, A.L., Minotti, L., Koudsié, A., de Saint Martin, A., and Hirsch, E. (2002). Antiepileptic effect of high-frequency stimulation of the subthalamic nucleus (corpus luysi) in a case of medically intractable epilepsy caused by focal dysplasia: a 30-month follow-up: technical case report. Neurosurgery *50*, 1385-391.

Benavides, J.M., and Webb, R.H. (2005). Optical characterization of ultrabright LEDs. Appl Opt *44*, 4000-03.

Berdondini, L., van der Wal, P.D., Guenat, O., de Rooij, N.F., Koudelka-Hep, M., Seitz, P., Kaufmann, R., Metzler, P., Blanc, N., and Rohr, S. (2005). High-density electrode array for imaging in vitro electrophysiological activity. Biosens Bioelectron *21*, 167-174.

Berndt, A., Yizhar, O., Gunaydin, L.A., Hegemann, P., and Deisseroth, K. (2009). Bi-stable neural state switches. Nat Neurosci *12*, 229-234.

Bi, A., Cui, J., Ma, Y.P., Olshevskaya, E., Pu, M., Dizhoor, A.M., and Pan, Z.H. (2006). Ectopic expression of a microbial-type rhodopsin restores visual responses in mice with photoreceptor degeneration. Neuron *50*, 23-33.

Blankenship, A.G., and Feller, M.B. (2010). Mechanisms underlying spontaneous patterned activity in developing neural circuits. Nat Rev Neurosci *11*, 18-29.

Blaurock, A.E., Stoeckenius, W., Oesterhelt, D., and Scherfhof, G.L. (1976). Structure of the cell envelope of Halobacterium halobium. J Cell Biol *71*, 1-22.

Boyden, E.S., Zhang, F., Bamberg, E., Nagel, G., and Deisseroth, K. (2005). Millisecond-timescale, genetically targeted optical control of neural activity. Nat Neurosci *8*, 1263-68.

Brenner, M., Kisseberth, W.C., Su, Y., Besnard, F., and Messing, A. (1994). GFAP promoter directs astrocyte-specific expression in transgenic mice. J Neurosci *14*, 1030-37.

Brewer, G.J., Boehler, M.D., Ide, A.N., and Wheeler, B.C. (2009). Chronic electrical stimulation of cultured hippocampal networks increases spontaneous spike rates. J Neurosci Methods *184*, 104-09.

Brown, E.A., Ross, J.D., Blum, R.A., Nam, Y., Wheeler, B.C., and DeWeerth, S.P. (2008). Stimulus-artifact elimination in a multi-electrode system. IEEE Transactions on Biomedical Circuits and Systems *2*, 10-21.

Bruegmann, T., Malan, D., Hesse, M., Beiert, T., Fuegemann, C.J., Fleischmann, B.K., and Sasse, P. (2010). Optogenetic control of heart muscle in vitro and in vivo. Nat Methods *7*, 897-900.

Busskamp, V., Duebel, J., Balya, D., Fradot, M., Viney, T.J., Siegert, S., Groner, A.C., Cabuy, E., Forster, V., et al. (2010). Genetic reactivation of cone photoreceptors restores visual responses in retinitis pigmentosa. Science *329*, 413-17.

Cadotte, A.J., DeMarse, T.B., He, P., and Ding, M. (2008). Causal measures of structure and plasticity in simulated and living neural networks. PLoS ONE *3*, e3355.

Callaway, E.M., and Yuste, R. (2002). Stimulating neurons with light. Curr. Opin. Neurobio. *12*, 587-592.

Campagnola, L., Wang, H., and Zylka, M.J. (2008). Fiber-coupled light-emitting diode for localized photostimulation of neurons expressing channelrhodopsin-2. J Neurosci Methods *169*, 27-33.

Cardin, J.A., Carlén, M., Meletis, K., Knoblich, U., Zhang, F., Deisseroth, K., Tsai, L.H., and Moore, C.I. (2010). Targeted optogenetic stimulation and recording of neurons in vivo using cell-type-specific expression of Channelrhodopsin-2. Nat Protoc *5*, 247-254.

Cardin, Jessica A, Marie Carlen, Konstantinos Meletis, Ulf Knoblich, Feng Zhang, Karl Deisseroth, Li-Huei Tsai, and Christopher I Moore. "Targeted Optogenetic Stimulation and Recording of Neurons in Vivo Using Cell-Type-Specific Expression of Channelrhodopsin-2." *Nat Protoc* 5, no. 2 (2010): doi:10.1038/nprot.2009.228.

Cetin, A., Komai, S., Eliava, M., Seeburg, P.H., and Osten, P. (2006). Stereotaxic gene delivery in the rodent brain. Nat Protoc *1*, 3166-173.

Chhatwal, J.P., Hammack, S.E., Jasnow, A.M., Rainnie, D.G., and Ressler, K.J. (2007). Identification of cell-type-specific promoters within the brain using lentiviral vectors. Gene Ther *14*, 575-583.

Chiappalone, Michela,, Massobrio, Paolo, and Martinoia, Sergio (2008). Network plasticity in cortical assemblies. European Journal of Neuroscience *28*, 221-237.

Chow, B.Y., Han, X., Dobry, A.S., Qian, X., Chuong, A.S., Li, M., Henninger, M.A., Belfort, G.M., Lin, Y., et al. (2010). High-performance genetically targetable optical neural silencing by light-driven proton pumps. Nature *463*, 98-102.

Ciocchi, S., Herry, C., Grenier, F., Wolff, S.B., Letzkus, J.J., Vlachos, I., Ehrlich, I., Sprengel, R., Deisseroth, K., et al. (2010). Encoding of conditioned fear in central amygdala inhibitory circuits. Nature *468*, 277-282.

Cohen, E., Ivenshitz, M., Amor-Baroukh, V., Greenberger, V., and Segal, M. (2008). Determinants of spontaneous activity in networks of cultured hippocampus. Brain Res *1235*, 21-30.

Cortes, C., and Vapnik, V. (1995). Support-vector networks. Machine Learning *20*, 273-297.

Covington, H.E., Lobo, M.K., Maze, I., Vialou, V., Hyman, J.M., Zaman, S., LaPlant, Q., Mouzon, E., Ghose, S., et al. (2010). Antidepressant effect of optogenetic stimulation of the medial prefrontal cortex. J Neurosci *30*, 16082-090.

Crick, F.H. (1979). Thinking about the brain. Sci. Am. *241*, 219-232.

Degenaar, P., Grossman, N., Memon, M.A., Burrone, J., Dawson, M., Drakakis, E., Neil, M., and Nikolic, K. (2009). Optobionic vision--a new genetically enhanced light on retinal prosthesis. J Neural Eng *6*, 035007.

Deisseroth, K. (2011). Optogenetics. Nat. Methods *8*, 26-29.

Deisseroth, K., Feng, G., Majewska, A.K., Miesenböck, G., Ting, A., and Schnitzer, M.J. (2006). Next-generation optical technologies for illuminating genetically targeted brain circuits. J Neurosci *26*, 10380-86.

DeMarse, T.B., and Dockendorf, K.P. (2005). Adaptive flight control with living neuronal networks on microelectrode arrays. Proceedings of the International Journal of Computation and Neural Networks *3*, 1548-551.

Diester, I., Kaufman, M.T., Mogri, M., Pashaie, R., Goo, W., Yizhar, O., Ramakrishnan, C., Deisseroth, K., and Shenoy, K.V. (2011). An optogenetic toolbox designed for primates. Nat Neurosci *14*, 387-397.

Dittgen, T., Nimmerjahn, A., Komai, S., Licznerski, P., Waters, J., Margrie, T.W., Helmchen, F., Denk, W., Brecht, M., and Osten, P. (2004). Lentivirus-based genetic manipulations of cortical neurons and their optical and electrophysiological monitoring in vivo. Proc Natl Acad Sci U S A *101*, 18206-211.

Dockendorf, K.P., Park, I., He, P., Príncipe, J.C., and DeMarse, T.B. (2009). Liquid state machines and cultured cortical networks: the separation property. Biosystems *95*, 90-97.

Dong, J.Y., Fan, P.D., and Frizzell, R.A. (1996). Quantitative analysis of the packaging capacity of recombinant adeno-associated virus. Hum Gene Ther *7*, 2101-112.

Dottori, M., Tay, C., and Hughes, S.M. (2011). Neural development in human embryonic stem cells-applications of lentiviral vectors. J Cell Biochem *112*, 1955-962.

Douglass, A.D., Kraves, S., Deisseroth, K., Schier, A.F., and Engert, F. (2008). Escape behavior elicited by single, channelrhodopsin-2-evoked spikes in zebrafish somatosensory neurons. Curr Biol *18*, 1133-37.

Durand, D.M., and Bikson, M. (2001). Suppression and control of epileptiform activity by electrical stimulation: A review. Proceedings of the IEEE *89*, 1065-082.

Eckmann, Jacobi, Marom, Moses, and Zbinden (2008). Leader neurons in population bursts of 2D living neural networks. New Journal of Physics *10*

Egert, U., Heck, D., and Aertsen, A. (2002). Two-dimensional monitoring of spiking networks in acute brain slices. Exp Brain Res *142*, 268-274.

Egert, U., Schlosshauer, B., Fennrich, S., Nisch, W., Fejtl, M., Knott, T., Muller, T., and Hammerle, H. (1998). A novel organotypic long-term culture of the rat hippocampus on substrate-integrated multielectrode arrays. Brain Res Brain Res Protoc *2*, 229-242.

Eytan, D.,.B.N.A.M.S. (2003). Selective Adaptation in Networks of Cortical Neurons. Journal of Neuroscience *23*, 9349-356.

Farah, N., Reutsky, I., and Shoham, S. (2007). Patterned optical activation of retinal ganglion cells. Conf Proc IEEE Eng Med Biol Soc *2007*, 6369-371.

Feldbauer, K., Zimmermann, D., Pintschovius, V., Spitz, J., Bamann, C., and Bamberg, E. (2009). Channelrhodopsin-2 is a leaky proton pump. Proc Natl Acad Sci U S A *106*, 12317-322.

Fortin, D.L., Banghart, M.R., Dunn, T.W., Borges, K., Wagenaar, D.A., Gaudry, Q., Karakossian, M.H., Otis, T.S., Kristan, W.B., et al. (2008). Photochemical control of endogenous ion channels and cellular excitability. Nat Methods *5*, 331-38.

Gandolfo, M., Maccione, A., Tedesco, M., Martinoia, S., and Berdondini, L. (2010). Tracking burst patterns in hippocampal cultures with high-density CMOS-MEAs. J Neural Eng *7*, 056001.

Golan, L., Reutsky, I., Farah, N., and Shoham, S. (2009). Design and characteristics of holographic neural photo-stimulation systems. J Neural Eng *6*, 066004.

Gourine, A.V., Kasymov, V., Marina, N., Tang, F., Figueiredo, M.F., Lane, S., Teschemacher, A.G., Spyer, K.M., Deisseroth, K., and Kasparov, S. (2010). Astrocytes control breathing through pH-dependent release of ATP. Science *329*, 571-75.

Gradinaru, V., Mogri, M., Thompson, K.R., Henderson, J.M., and Deisseroth, K. (2009). Optical deconstruction of parkinsonian neural circuitry. Science *324*, 354-59.

Gradinaru, V., Thompson, K.R., and Deisseroth, K. (2008). eNpHR: a Natronomonas halorhodopsin enhanced for optogenetic applications. Brain Cell Biol *36*, 129-139.

Gradinaru, V., Thompson, K.R., Zhang, F., Mogri, M., Kay, K., Schneider, M.B., and Deisseroth, K. (2007). Targeting and readout strategies for fast optical neural control in vitro and in vivo. J Neurosci *27*, 14231-38.

Gradinaru, V., Zhang, F., Ramakrishnan, C., Mattis, J., Prakash, R., Diester, I., Goshen, I., Thompson, K.R., and Deisseroth, K. (2010). Molecular and cellular approaches for diversifying and extending optogenetics. Cell *141*, 154-165.

Gross, G.W., Harsch, A., Rhoades, B.K., and Goepel, W. (1997). Odor, drug, and toxin analysis with neruonal networks in vitro: extracellular array recording of network responses. Biosensors & Bioelectronics *12*, 373-393.

Gross, G.W., Kowalski, J.M., and Rhoades, B.K. (1999). Spontaneous and evoked oscillations in cultured mammalian neural networks. In Oscillations in Neural Systems, D. Levine, B. Brown, and T. Shirey, eds. (New York: Erlbaum Associates).

Grossman, N., Poher, V., Grubb, M.S., Kennedy, G.T., Nikolic, K., McGovern, B., Palmini, R.B., Gong, Z., Drakakis, E.M., et al. (2010). Multi-site optical excitation using ChR2 and micro-LED array. J Neural Eng *7*, 16004.

Gunaydin, L.A., Yizhar, O., Berndt, A., Sohal, V.S., Deisseroth, K., and Hegemann, P. (2010). Ultrafast optogenetic control. Nat Neurosci *13*, 387-392.

Halassa, M.M., Siegle, J.H., Ritt, J.T., Ting, J.T., Feng, G., and Moore, C.I. (2011). Selective optical drive of thalamic reticular nucleus generates thalamic bursts and cortical spindles. Nat Neurosci *14*, 1118-120.

Han, X., and Boyden, E.S. (2007). Multiple-color optical activation, silencing, and desynchronization of neural activity, with single-spike temporal resolution. PLoS ONE *2*, e299.

Han, X., Qian, X., Bernstein, J.G., Zhou, H.H., Franzesi, G.T., Stern, P., Bronson, R.T., Graybiel, A.M., Desimone, R., and Boyden, E.S. (2009). Millisecond-timescale optical control of neural dynamics in the nonhuman primate brain. Neuron *62*, 191-98.

Haubensak, W., Kunwar, P.S., Cai, H., Ciocchi, S., Wall, N.R., Ponnusamy, R., Biag, J., Dong, H.W., Deisseroth, K., et al. (2010). Genetic dissection of an amygdala microcircuit that gates conditioned fear. Nature *468*, 270-76.

Huber, D., Petreanu, L., Ghitani, N., Ranade, S., Hromádka, T., Mainen, Z., and Svoboda, K. (2008). Sparse optical microstimulation in barrel cortex drives learned behaviour in freely moving mice. Nature *451*, 61-64.

Imfeld, K., Neukom, S., Maccione, A., Bornat, Y., Martinoia, S., Farine, P.A., Koudelka-Hep, M., and Berdondini, L. (2008). Large-scale, high-resolution data acquisition system for extracellular recording of electrophysiological activity. IEEE Trans Biomed Eng *55*, 2064-073.

Ishizuka, T., Kakuda, M., Araki, R., and Yawo, H. (2006). Kinetic evaluation of photosensitivity in genetically engineered neurons expressing green algae light-gated channels. Neurosci Res *54*, 85-94.

Iwai, Y., Honda, S., Ozeki, H., Hashimoto, M., and Hirase, H. (2011). A simple head-mountable LED device for chronic stimulation of optogenetic molecules in freely moving mice. Neurosci Res *70*, 124-27.

Jakobsson, J., Ericson, C., Jansson, M., Björk, E., and Lundberg, C. (2003). Targeted transgene expression in rat brain using lentiviral vectors. J Neurosci Res *73*, 876-885.

Jerome, J., Roehring, R.C., Armstrong, W.E., Spain, W.J., and Heck, D.H. (2011). Parallel optical control of spatiotemporal neuronal spike activity using high-speed digital light processing. Frontiers in Systems Neuroscience *5*, 1-13.

Jia, Z., Valiunas, V., Lu, Z., Bien, H., Liu, H., Wang, H.Z., Rosati, B., Brink, P.R., Cohen, I.S., and Entcheva, E. (2011). Stimulating cardiac muscle by light: cardiac optogenetics by cell delivery. Circ Arrhythm Electrophysiol *4*, 753-760.

Jimbo, Y., Kasai, N., Torimitsu, K., Tateno, T., and Robinson, H.P. (2003). A system for MEA-based multisite stimulation. IEEE Trans Biomed Eng *50*, 241-48.

Jimbo, Y., Kawana, A., Parodi, P., and Torre, V. (2000). The dynamics of a neuronal culture of dissociated cortical neurons of neonatal rats. Biol Cybern *83*, 1-20.

Jimbo, Y., Robinson, H.P., and Kawana, A. (1998). Strengthening of synchronized activity by tetanic stimulation in cortical cultures: application of planar electrode arrays. IEEE Trans Biomed Eng *45*, 1297-1304.

Jimbo, Y., Tateno, T., and Robinson, H.P. (1999). Simultaneous induction of pathway-specific potentiation and depression in networks of cortical neurons. Biophys J *76*, 670-78.

Jones, R. (2011). Plasticity: Don't get too excited!. Nat Rev Neurosci *12*, 6.

Kamioka, H., Maeda, E., Jimbo, Y., Robinson, H.P., and Kawana, A. (1996). Spontaneous periodic synchronized bursting during formation of mature patterns of connections in cortical cultures. Neurosci Lett *206*, 109-112.

Kaplitt, M.G., Feigin, A., Tang, C., Fitzsimons, H.L., Mattis, P., Lawlor, P.A., Bland, R.J., Young, D., Strybing, K., et al. (2007). Safety and tolerability of gene therapy with an adeno-associated virus (AAV) borne GAD gene for Parkinson's disease: an open label, phase I trial. Lancet *369*, 2097-2105.

Kerchner, G.A., and Nicoll, R.A. (2008). Silent synapses and the emergence of a postsynaptic mechanism for LTP. Nat Rev Neurosci *9*, 813-825.

Kermany, E., Gal, A., Lyakhov, V., Meir, R., Marom, S., and Eytan, D. (2010). Tradeoffs and constraints on neural representation in networks of cortical neurons. J Neurosci *30*, 9588-596.

Khademhosseini, A., Suh, K.Y., Yang, J.M., Eng, G., Yeh, J., Levenberg, S., and Langer, R. (2004). Layer-by-layer deposition of hyaluronic acid and poly-L-lysine for patterned cell co-cultures. Biomaterials *25*, 3583-592.

Khosravani, H., Carlen, P.L., and Velazquez, J.L. (2003). The control of seizure-like activity in the rat hippocampal slice. Biophys J *84*, 687-695.

Kravitz, A.V., Freeze, B.S., Parker, P.R., Kay, K., Thwin, M.T., Deisseroth, K., and Kreitzer, A.C. (2010). Regulation of parkinsonian motor behaviours by optogenetic control of basal ganglia circuitry. Nature *466*, 622-26.

Kumar, M., Keller, B., Makalou, N., and Sutton, R.E. (2001). Systematic determination of the packaging limit of lentiviral vectors. Hum Gene Ther *12*, 1893-1905.

Lanyi, J.K., and Oesterhelt, D. (1982). Identification of the retinal-binding protein in halorhodopsin. J Biol Chem *257*, 2674-77.

Lee, J.H., Durand, R., Gradinaru, V., Zhang, F., Goshen, I., Kim, D.S., Fenno, L.E., Ramakrishnan, C., and Deisseroth, K. (2010). Global and local fMRI signals driven by neurons defined optogenetically by type and wiring. Nature *465*, 788-792.

Leifer, A.M., Fang-Yen, C., Gershow, M., Alkema, M.J., and Samuel, A.D. (2011). Optogenetic manipulation of neural activity in freely moving Caenorhabditis elegans. Nat Methods *8*, 147-152.

Li, X., Gutierrez, D.V., Hanson, M.G., Han, J., Mark, M.D., Chiel, H., Hegemann, P., Landmesser, L.T., and Herlitze, S. (2005). Fast noninvasive activation and inhibition of neural and network activity by vertebrate rhodopsin and green algae channelrhodopsin. Proc Natl Acad Sci U S A *102*, 17816-821.

Lobo, M.K., Covington, H.E., Chaudhury, D., Friedman, A.K., Sun, H., Damez-Werno, D., Dietz, D.M., Zaman, S., Koo, J.W., et al. (2010). Cell type-specific loss of BDNF signaling mimics optogenetic control of cocaine reward. Science *330*, 385-390.

Losonczy, A., and Magee, J.C. (2006). Integrative properties of radial oblique dendrites in hippocampal CA1 pyramidal neurons. Neuron *50*, 291-307.

Luo, L., Callaway, E.M., and Svoboda, K. (2008). Genetic Dissection of Neural Circuits. Neuron *57*, 634-660.

Madhavan, R., Chao, Z.C., Wagenaar, D.A., Bakkum, D.J., and Potter, S.M. (2006). Multi-site Stimulation Quiets Network-wide Spontaneous Bursts and Enhances Functional Plasticity in Cultured Cortical Networks. Conf Proc IEEE Eng Med Biol Soc *1*, 1593-96.

Maeda, E., Kuroda, Y., Robinson, H.P.C., and Kawana, A. (1998). Modification of parallel activity elicited by propogating bursts in developing networks of rat cortical neurones. European Journal of Neuroscience *10*, 488-496.

Maeda, E., Robinson, H.P., and Kawana, A. (1995). The mechanisms of generation and propagation of synchronized bursting in developing networks of cortical neurons. J Neurosci *15*, 6834-845.

Massobrio, P., and Martinoia, S. (2008). Modelling small-patterned neuronal networks coupled to microelectrode arrays. J Neural Eng *5*, 350-59.

Matsuno-Yagi, A., and Mukohata, Y. (1977). Two possible roles of bacteriorhodopsin; a comparative study of strains of Halobacterium halobium differing in pigmentation. Biochem Biophys Res Commun *78*, 237-243.

McIntyre, C.C., and Grill, W.M. (2001). Finite element analysis of the current-density and electric field generated by metal microelectrodes. Ann Biomed Eng *29*, 227-235.

Miller, J.S., Béthencourt, M.I., Hahn, M., Lee, T.R., and West, J.L. (2006). Laser-scanning lithography (LSL) for the soft lithographic patterning of cell-adhesive self-assembled monolayers. Biotechnol Bioeng *93*, 1060-68.

Mongillo, G., Barak, O., and Tsodyks, M. (2008). Synaptic Theory of Working Memory. Science *319*, 1543-46.

Mutoh, H., Perron, A., Akemann, W., Iwamoto, Y., and Knöpfel, T. (2011). Optogenetic monitoring of membrane potentials. Exp Physiol *96*, 13-18.

Nagel, G., Brauner, M., Liewald, J.F., Adeishvili, N., Bamberg, E., and Gottschalk, A. (2005). Light activation of channelrhodopsin-2 in excitable cells of Caenorhabditis elegans triggers rapid behavioral responses. Curr Biol *15*, 2279-284.

Nagel, G., Szellas, T., Huhn, W., Kateriya, S., Adeishvili, N., Berthold, P., Ollig, D., Hegemann, P., and Bamberg, E. (2003). Channelrhodopsin-2, a directly light-gated cation-selective membrane channel. Proc Natl Acad Sci U S A *100*, 13940-45.

Nam, Y., Brown, E. A., Ross, J. D., Blum, R. A., Wheeler, B. C., & DeWeerth, S. P. (2009). A retrofitted neural recording system with a novel stimulation IC to monitor early neural responses from a stimulating electrode. *J Neurosci Methods*, *178*(1), 99-102.

Nathanson, J.L., Jappelli, R., Scheeff, E.D., Manning, G., Obata, K., Brenner, S., and Callaway, E.M. (2009). Short Promoters in Viral Vectors Drive Selective Expression in Mammalian Inhibitory Neurons, but do not Restrict Activity to Specific Inhibitory Cell-Types. Front Neural Circuits *3*, 19.

Novak, J.L., and Wheeler, B.C. (1988). Multisite hippocampal slice recording and stimulation using a 32 element microelectrode array. J Neurosci Methods *23*, 149-159.

Nowak, L.G., and Bullier, J. (1998). Axons, but not cell bodies, are activated by electrical stimulation in cortical gray matter. I. Evidence from chronaxie measurements. Exp Brain Res *118*, 477-488.

Oesterhelt, D., and Stoeckenius, W. (1971). Rhodopsin-like protein from the purple membrane of Halobacterium halobium. Nat New Biol *233*, 149-152.

Oesterhelt, D., and Stoeckenius, W. (1973). Functions of a New Photoreceptor Membrane. Proc. Nat. Acad. Sci. *70*, 2853-57.

Oka, H., Shimono, K., Ogawa, R., Sugihara, H., and Taketani, M. (1999). A new planar multielectrode array for extracellular recording: application to hippocampal acute slice. J Neurosci Methods *93*, 61-67.

Pan, L., Song, X., Xiang, G., Wong, A., Xing, W., and Cheng, J. (2009). First-spike rank order as a reliable indicator of burst initiation and its relation with early-to-fire neurons. IEEE Trans Biomed Eng *56*, 1673-682.

Papagiakoumou, E., Anselmi, F., Bègue, A., de Sars, V., Glückstad, J., Isacoff, E.Y., and Emiliani, V. (2010). Scanless two-photon excitation of channelrhodopsin-2. Nat Methods *7*, 848-854.

Parodi, P., Jimbo, Y., Kawana, A., Macrí, D., and Torre, V. (1998). Segmentation of the response of a neuronal network into clusters with similar activity. Biosystems *48*, 171-78.

Peled, A. (2011). Optogenetic neuronal control in schizophrenia. Med Hypotheses *76*, 914-921.

Persi, E., Horn, D., Volman, V., Segev, R., and Ben-Jacob, E. (2004). Modeling of synchronized bursting events: the importance on inhomogeneity. Neural Comput *16*, 2577-595.

Petreanu, L., Huber, D., Sobczyk, A., and Svoboda, K. (2007). Channelrhodopsin-2-assisted circuit mapping of long-range callosal projections. Nat Neurosci *10*, 663-68.

Petreanu, L., Mao, T., Sternson, S.M., and Svoboda, K. (2009). The subcellular organization of neocortical excitatory connections. Nature *457*, 1142-45.

Pettit, D.L., Helms, M.C., Lee, P., Augustine, G.J., and Hall, W.C. (1999). Local excitatory circuits in the intermediate gray layer of the superior colliculus. J Neurophysiol *81*, 1424-26.

Pinato, G., Parodi, P., Bisso, A., Macrì, D., Kawana, A., Jimbo, Y., and Torre, V. (1999). Properties of the evoked spatio-temporal electrical activity in neuronal assemblies. Rev Neurosci *10*, 279-290.

Pine, J. (1980). Recording action potentials from cultured neurons with extracellular microcircuit electrodes. J Neurosci Methods *2*, 19-31.

Potter, S.M., Lukina, N., Longmuir, K.J., and Wu, Y. (2001). Multi-site two-photon imaging of neurons on multi-electrode arrays. SPIE Proceedings *4262*, 104-110.

Racker, E., and Stoeckenius, W. (1974). Reconstitution of purple membrane vesicles catalyzing light-driven proton uptake and adenosine triphosphate formation. J Biol Chem *249*, 662-63.

Raichman, N., and Ben-Jacob, E. (2008). Identifying repeating motifs in the activation of synchronized bursts in cultured neuronal networks. J Neurosci Methods *170*, 96-110.

Rattay, F., and Aberham, M. (1993). Modeling axon membranes for functional electrical stimulation. IEEE Trans Biomed Eng *40*, 1201-09.

Rickgauer, J.P., and Tank, D.W. (2009). Two-photon excitation of channelrhodopsin-2 at saturation. Proc Natl Acad Sci U S A *106*, 15025-030.

Rolls, A., Colas, D., Adamantidis, A., Carter, M., Lanre-Amos, T., Heller, H.C., and de Lecea, L. (2011). Optogenetic disruption of sleep continuity impairs memory consolidation. Proc Natl Acad Sci U S A *108*, 13305-310.

Rosenblum, M., and Pikovsky, A. (2004). Delayed feedback control of collective synchrony: an approach to suppression of pathological brain rhythms. Phys Rev E Stat Nonlin Soft Matter Phys *70*, 041904.

Ruaro, M.E., Bonifazi, P., and Torre, V. (2005). Toward the neurocomputer: image processing and pattern recognition with neuronal cultures. IEEE Trans Biomed Eng *52*, 371-383.

Schobert, B., and Lanyi, J.K. (1982). Halorhodopsin is a light-driven chloride pump. J Biol Chem *257*, 10306-313.

Schoenenberger, P., Grunditz, A., Rose, T., and Oertner, T.G. (2008). Optimizing the spatial resolution of Channelrhodopsin-2 activation. Brain Cell Biol *36*, 119-127.

Shahaf, G., and Marom, S. (2001). Learning in networks of cortical neurons. Journal of Neuroscience *21*, 8782-88.

Shimogori, T., and Ogawa, M. (2008). Gene application with in utero electroporation in mouse embryonic brain. Dev Growth Differ *50*, 499-506.

Shoham, S., O'Connor, D.H., Sarkisov, D.V., and Wang, S.S. (2005). Rapid neurotransmitter uncaging in spatially defined patterns. Nat Methods *2*, 837-843.

Sohal, V.S., Zhang, F., Yizhar, O., and Deisseroth, K. (2009). Parvalbumin neurons and gamma rhythms enhance cortical circuit performance. Nature *459*, 698-702.

Soudais, C., Skander, N., and Kremer, E.J. (2004). Long-term in vivo transduction of neurons throughout the rat CNS using novel helper-dependent CAV-2 vectors. FASEB J *18*, 391-93.

Stirman, J.N., Crane, M.M., Husson, S.J., Wabnig, S., Schultheis, C., Gottschalk, A., and Lu, H. (2011). Real-time multimodal optical control of neurons and muscles in freely behaving Caenorhabditis elegans. Nat Methods *8*, 153-58.

Streit, J., Tscherter, A., Heuschke, M.O., and Renaud, P. (2001). The generation of rhythmic activity in dissociated cultures of rat spinal cord. European Journal of Neuroscience *14*, 191-202.

Streit, J., Tsherter, A., and Darbon, P. (2006). Rhythm generation in spinal cultures: Is it the neuron or the network? In Advances in Network Electrophysiology Using Multi-Electrode Arrays (New York: Springer).

Stroh, A., Tsai, H.C., Ping Wang, L., Zhang, F., Kressel, J., Aravanis, A., Santhanam, N., Deisseroth, K., Konnerth, A., and Schneider, M.B. (2010). Tracking stem cell differentiation in the setting of automated optogenetic stimulation. Stem Cells *29*, 78-88.

Suh, K.Y., Seong, J., Khademhosseini, A., Laibinis, P.E., and Langer, R. (2004). A simple soft lithographic route to fabrication of poly(ethylene glycol) microstructures for protein and cell patterning. Biomaterials *25*, 557-563.

Szobota, S., Gorostiza, P., Del Bene, F., Wyart, C., Fortin, D.L., Kolstad, K.D., Tulyathan, O., Volgraf, M., Numano, R., et al. (2007). Remote control of neuronal activity with a light-gated glutamate receptor. Neuron *54*, 535-545.

Tabak, J., and Latham, P.E. (2003). Analysis of spontaneous bursting activity in random neural networks. Neuroreport *14*, 1445-49.

Tateno, T., and Jimbo, Y. (1999). Activity-dependent enhancement in the reliability of correlated spike timings in cultured cortical neurons. Biol Cybern *80*, 45-55.

Thomas, C.A. (1972). A miniature microelectrode array to monitor the bioelectric activity of cultured cells. Exp. Cell Res. *74*, 61-66.

Tsai, H.C., Zhang, F., Adamantidis, A., Stuber, G.D., Bonci, A., de Lecea, L., and Deisseroth, K. (2009). Phasic firing in dopaminergic neurons is sufficient for behavioral conditioning. Science *324*, 1080-84.

Tye, K.M., Prakash, R., Kim, S.Y., Fenno, L.E., Grosenick, L., Zarabi, H., Thompson, K.R., Gradinaru, V., Ramakrishnan, C., and Deisseroth, K. (2011). Amygdala circuitry mediating reversible and bidirectional control of anxiety. Nature *471*, 358-362.

Tønnesen, J., Parish, C.L., Sørensen, A.T., Andersson, A., Lundberg, C., Deisseroth, K., Arenas, E., Lindvall, O., and Kokaia, M. (2011). Functional integration of grafted neural stem cell-derived dopaminergic neurons monitored by optogenetics in an in vitro Parkinson model. PLoS ONE *6*, e17560.

Tønnesen, J., Sørensen, A.T., Deisseroth, K., Lundberg, C., and Kokaia, M. (2009). Optogenetic control of epileptiform activity. Proc Natl Acad Sci U S A *106*, 12162-67.

van den Pol, A.N., Acuna-Goycolea, C., Clark, K.R., and Ghosh, P.K. (2004). Physiological properties of hypothalamic MCH neurons identified with selective expression of reporter gene after recombinant virus infection. Neuron *42*, 635-652.

van Pelt, J., Vajda, I., Wolters, P.S., Corner, M.A., and Ramakers, G.J. (2005). Dynamics and plasticity in developing neuronal networks in vitro. Prog Brain Res *147*, 173-188.

van Pelt, J., Wolters, P.S., Corner, M.A., Rutten, W.L., and Ramakers, G.J. (2004). Long-term characterization of firing dynamics of spontaneous bursts in cultured neural networks. IEEE Trans Biomed Eng *51*, 2051-062.

Vercueil, L., Benazzouz, A., Deransart, C., Bressand, K., Marescaux, C., Depaulis, A., and Benabid, A.L. (1998). High-frequency stimulation of the sub-thalamic nucleus suppresses absence seizures in the rat: comparison with neurotoxic lesions. Epilepsy Res *31*, 39-46.

Volgraf, M., Gorostiza, P., Numano, R., Kramer, R.H., Isacoff, E.Y., and Trauner, D. (2006). Allosteric control of an ionotropic glutamate receptor with an optical switch. Nat Chem Biol *2*, 47-52.

Wagenaar, D.A., Madhavan, R., Pine, J., and Potter, S.M. (2005). Controlling bursting in cortical cultures with closed-loop multi-electrode stimulation. J Neurosci *25*, 680-88.

Wagenaar, D.A., Nadasdy, Z., and Potter, S.M. (2006a). Persistent dynamic attractors in activity patterns of cultured neuronal networks. Phys Rev E Stat Nonlin Soft Matter Phys *73*, 051907.

Wagenaar, D.A., Pine, J., and Potter, S.M. (2004). Effective parameters for stimulation of dissociated cultures using multi-electrode arrays. J Neurosci Methods *138*, 27-37.

Wagenaar, D.A., Pine, J., and Potter, S.M. (2006). An extremely rich repertoire of bursting patterns during the development of cortical cultures. BMC Neurosci *7*, 11.

Wang, H., Peca, J., Matsuzaki, M., Matsuzaki, K., Noguchi, J., Qiu, L., Wang, D., Zhang, F., Boyden, E., et al. (2007). High-speed mapping of synaptic connectivity using photostimulation in Channelrhodopsin-2 transgenic mice. Proc Natl Acad Sci U S A *104*, 8143-48.

Wang, S., Szobota, S., Wang, Y., Volgraf, M., Liu, Z., Sun, C., Trauner, D., Isacoff, E.Y., and Zhang, X. (2007a). All optical interface for parallel, remote, and spatiotemporal control of neuronal activity. Nano Lett *7*, 3859-863.

Weick, J.P., Johnson, M.A., Skroch, S.P., Williams, J.C., Deisseroth, K., and Zhang, S.C. (2010). Functional control of transplantable human ESC-derived neurons via optogenetic targeting. Stem Cells *28*, 2008-016.

Wen, L., Wang, H., Tanimoto, S., Egawa, R., Matsuzaka, Y., Mushiake, H., Ishizuka, T., and Yawo, H. (2010). Opto-current-clamp actuation of cortical neurons using a strategically designed channelrhodopsin. PLoS ONE *5*, e12893.

Witten, I.B., Lin, S.C., Brodsky, M., Prakash, R., Diester, I., Anikeeva, P., Gradinaru, V., Ramakrishnan, C., and Deisseroth, K. (2010). Cholinergic interneurons control local circuit activity and cocaine conditioning. Science *330*, 1677-681.

Yizhar, O., Fenno, L.E., Davidson, T.J., Mogri, M., and Deisseroth, K. (2011). Optogenetics in neural systems. Neuron *71*, 9-34.

Yoshimura, Y., Dantzker, J.L., and Callaway, E.M. (2005). Excitatory cortical neurons form fine-scale functional networks. Nature *433*, 868-873.

Zemelman, B.V., Nesnas, N., Lee, G.A., and Miesenbock, G. (2003). Photochemical gating of heterologous ion channels: remote control over genetically designated populations of neurons. Proc Natl Acad Sci U S A *100*, 1352-57.

Zhang, F., Wang, L.P., Boyden, E.S., and Deisseroth, K. (2006). Channelrhodopsin-2 and optical control of excitable cells. Nat Methods *3*, 785-792.

Zhang, F., Wang, L.P., Brauner, M., Liewald, J.F., Kay, K., Watzke, N., Wood, P.G., Bamberg, E., Nagel, G., et al. (2007). Multimodal fast optical interrogation of neural circuitry. Nature *446*, 633-39.

Zhang, J., Laiwalla, F., Kim, J.A., Urabe, H., Van Wagenen, R., Song, Y.K., Connors, B.W., Zhang, F., Deisseroth, K., and Nurmikko, A.V. (2009). Integrated device for optical stimulation and spatiotemporal electrical recording of neural activity in light-sensitized brain tissue. J Neural Eng *6*, 055007.

Zhang, Y., Ivanova, E., Bi, A., and Pan, Z.H. (2009a). Ectopic expression of multiple microbial rhodopsins restores ON and OFF light responses in retinas with photoreceptor degeneration. J Neurosci *29*, 9186-196.

Zhao, S., Cunha, C., Zhang, F., Liu, Q., Gloss, B., Deisseroth, K., Augustine, G.J., and Feng, G. (2008). Improved expression of halorhodopsin for light-induced silencing of neuronal activity. Brain Cell Biol *36*, 141-154.

Zrenner, E. (2002). Will retinal implants restore vision? Science *295*, 1022-26.

BIOGRAPHICAL SKETCH

Perry Thomas Twyford was born in 1985 in Anchorage, Alaska to his parents, Stefani and Loren Twyford. At age 4 his family moved to Aberdeen, Scotland where he attended an American school for 3 years. In 1992, his family relocated to Houston, Texas, where the rest of his childhood was spent. Perry graduated from Cinco Ranch High School in 2003 and moved to Cleveland, Ohio. There he earned a BS in Biomedical Engineering from Case Western Reserve University, with a focus in polymer biomaterials. Perry moved with his wife-to-be to Gainesville, Florida, where he enrolled in the Ph.D. program in Biomedical Engineering at the University of Florida, under the supervision of Dr. Thomas DeMarse. He was married to his wife, Julie, in September 2010, had his son, Jack, in August 2011, and received his doctoral degree in December 2011.